Temperature dependence of the electrical conductivity in the quark-gluon plasma.

Amato, Alessandro

Swansea University
Prifysgol Abertawe

Temperature Dependence of the Electrical Conductivity in the Quark-Gluon Plasma

Alessandro Amato

Submitted to Swansea University in fulfilment
of the requirements for the degree of Doctor of Philosophy

2014

Alessandro Amato: *Temperature Dependence of the Electrical Conductivity in the Quark-Gluon Plasma*

SUPERVISORS:
Prof. Simon Hands
Prof. Chris Allton

DATE OF SUBMISSION:
October 27, 2014

ABSTRACT

The heavy-ion collision experiments at RHIC and CERN have presented the opportunity to study the properties of strongly interacting matter under extreme conditions. These have been subject to intensive theoretical investigation and, in this thesis, we will study the transport properties of QCD matter [1–6].

The transport coefficients known as shear and bulk viscosities as well as the electrical conductivity have been studied with perturbative methods to full leading order in the strong coupling α_s [7, 8]. However, these results are in tension with phenomenological observations, which hints to the fact that, in the range of temperatures reached in the experiments, the medium created is strongly interacting and non-perturbative methods need to be employed.

It is this highly desirable to perform a first principles calculation of the transport coefficients of QCD at a temperature of a few hundreds MeV. In this work, we employ lattice QCD simulations to study, for the first time, the temperature dependence of the electrical conductivity and the charge diffusion coefficient in the range of temperatures between $100 - 350\,\mathrm{MeV}$.

In order to achieve this, we use an anisotropic lattice action with $2+1$ flavors of clover fermions [9, 10]. The use of a finer lattice spacing for the time direction provides a better temporal resolution of the correlation functions without increasing the computational cost significantly and it represents one of the novelties of this work.

We study the conserved vector current correlator both in the light and strange quark sectors at different temperatures. We compare their behaviour with the free theory and with the zero temperature case and look for thermal effects. A Bayesian approach called Maximum Entropy Method (MEM) is used to extract the electromagnetic spectral functions from these correlators. This is a non-trivial task since it involves an analytical continuation of the correlation functions from Euclidean to real times.

The electrical conductivity is obtained from the spectral functions via the so-called Kubo relations, whose derivation is reviewed. A detailed study of the systematic uncertainties that the MEM introduces on the final observable is presented and discussed.

The fluctuations of conserved quantities, like baryon number, isospin and electrical charge, are then studied using stochastic techniques. In

particular, the electrical charge susceptibility will allow for the first lattice determination of the charge diffusion coefficient for light quarks.

CONTENTS

ACKNOWLEDGMENTS

Foremost, I would like to thank my supervisor Prof. Simon Hands for the encouragement and advice he has provided during these years.

I would also like to express my gratitude to my collaborators and advisors Prof. Chris Allton and Prof. Gert Aarts for making a great research environment, answering all my questions and the thorough proofreading of this thesis.

I acknowledge the financial support of Swansea University and the European Union Grant Agreement 238353 (ITN STRONGnet), as well as the computing resources provided by HPC Wales, UKQCD, PRACE and DiRAC.

Many thanks go to the staff of the physics department at Swansea University. In particular: Prof. Biagio Lucini for his friendliness and approachability, without him I would have never had the opportunity to study in Swansea; Dr. Pietro Giudice, whose support has been invaluable on both an academic and a personal level; Dr. Benjamin Jäger for helping me with the thesis. I also thank Prof. Gunnar Bali for giving me the chance of doing research at Regensburg University.

All of the students on the 5th and 6th floors of Vivian tower have contributed to make my PhD an unforgettable experience and I am grateful to them: Wynne, Niall, Dan and Benjo, who started with me; Ed and Sam, who shared the office with me for many years; Vlad, who has been a great office mate and has very kindly proofread this thesis; Lorenzo and Roberto, with whom I climbed almost every possible wall in South Wales and for the many "pause lunghe", which have got me going over the years.

Finally, I want to deeply thank my family: my sister, for taking care of my parents; my dad and mum, for caring no matter how far away I was; and Steve for his infinite support and for making me feel at home during all these years.

DECLARATION

This work has not previously been accepted and is not being concurrently submitted for any degree.

Under the supervision of Prof. Simon Hands I have produced this thesis through my endeavour alone. Sources are acknowledged explicitly by references linking to an appended bibliography.

I give consent for my thesis to be available for photocopying and inter-library loan, and for the title and summary to be made available to outside organisations.

Swansea, October 27, 2014

Alessandro Amato

PUBLICATIONS

The work in this thesis have already appeared in the following publications:

G. Aarts, C. Allton, A. Amato, P. Giudice, S. Hands, and J.-I. Skullerud, *Electrical conductivity and diffusion coefficient of the quark-gluon plasma across the deconfinement transition with* $2+1$ *dynamical flavours* , In preparation.

A. Amato, G. Aarts, C. Allton, P. Giudice, S. Hands, and J.-I. Skullerud, *Electrical conductivity of the quark-gluon plasma across the deconfinement transition*, Phys. Rev. Lett. **111**, 172001 (2013), arXiv:1307.6763.

A. Amato, G. Aarts, C. Allton, P. Giudice, S. Hands, and J.-I. Skullerud, *Transport Coefficients of the QGP*, Proceedings of the 31st International Symposium on Lattice Field Theory, arXiv:1310.7466.

P. Giudice, G. Aarts, A. Amato, C. Allton, S. Hands, and J.-I. Skullerud, *Electric charge susceptibility in* $2+1$ *flavour QCD on an anisotropic lattice*, Proceedings of the 31st International Symposium on Lattice Field Theory, arXiv:1309.6253.

C. Allton, G. Aarts, A. Amato, W. Evans, P. Giudice, S. Hands, A. Kelly, S. Kim *et al, Quark-gluon plasma phenomenology from the lattice*, Strangeness in Quark Matter SQM 2013, arXiv:1310.5135.

1 INTRODUCTION

Quantum ChromoDynamics (QCD), is a non-Abelian gauge theory that describes the interactions which govern the dynamics of quarks and gluons. In nature there are six different flavors of quark: up, down, charm, strange, top, and bottom. They represent the fermionic content of QCD and carry electric, weak and strong charge. The quantum number associated with the latter is called color and it comes in $N_c = 3$ different states. The gluons are the bosonic carriers of such force, but since they posses a color quantum number themselves, they interact with each other as well.

In order to describe this rich dynamics, we will introduce in this chapter the fundamental tools of the Quantum Theory of Fields (QFT) and in particular we will describe the Lattice Gauge Theory (LGT) formalism as a non-perturbative regularization of QCD. The starting point will be the path integral formalism for a scalar theory and we will then review the Euclidean formulation of QFT, followed by its discretization on a hyper-cubic lattice. The same scheme will be followed for the introduction of non-Abelian gauge theories, which will then bring us to the formulation of QCD on a lattice. A more detailed treatment can of course be found in a variety of textbooks and reviews [11–15].

Everywhere in this thesis, we employ natural units $\hbar = c = 1$ as well as Einstein's summation convention on repeated indices.

1.1 PATH INTEGRAL FORMALISM

In this Section we will introduce the path integral formulation of QFT. The imaginary time formalism is then introduced and the resulting Euclidean field theory will be defined on a discretized space-time, in the form of a lattice. These concepts will be illustrated using a scalar field theory.

In one spatial dimension, the quantum mechanical transition amplitude for one particle is written as:

$$\langle x', t' | x, t \rangle = \langle x' | \exp\left[-iH(t' - t)\right] | x \rangle , \tag{1}$$

where the infinitesimal generator for the time translation is the Hamiltonian H and is composed of a kinetic and a potential term:

$$H = \frac{p^2}{2m} + V(x) \equiv H_0 + V\,, \tag{2}$$

where V is time-independent and is only a function of the spatial coordinate x. We can divide the temporal interval in Eq. (1) into two parts $[t, t_1]$ and $[t_1, t']$. Since H is time independent, the exponential in Eq. (1) trivially follows algebraic rules and decomposes into a product of exponentials:

$$e^{-iHT} \equiv e^{-iH(T-\Delta t)} e^{-iH\Delta t}\,, \tag{3}$$

with $T = (t' - t)$ and $\Delta t = (t_1 - t)$. We can insert a complete set of coordinate eigenstates,

$$\mathbb{1} = \int dx_1\, |x_1\rangle\langle x_1|\,, \tag{4}$$

between the two exponentials of Eq. (3), which can then be used to rewrite Eq. (1) as:

$$\langle x', t'|x, t\rangle = \int \mathrm{d}x_1\, \langle x'|e^{-iH(T-\Delta t)}|x_1\rangle\langle x_1|e^{-iH\Delta t}|x\rangle. \tag{5}$$

Now we can divide T into n equal parts, $T = n\Delta t$ and insert the resolution of the identity a further $(n-1)$ times, obtaining:

$$\begin{aligned}\langle x', t'|x, t\rangle = \int \mathrm{d}x_1 \ldots \mathrm{d}x_{n-1}\ \langle x'|e^{-iH\Delta t}|x_{n-1}\rangle \times \\ \times \langle x_{n-1}|e^{-iH\Delta t}|x_{n-2}\rangle \ldots \langle x_1|e^{-iH\Delta t}|x\rangle\,,\end{aligned} \tag{6}$$

where we identify $x \equiv x_0$ and $x' \equiv x_n$. In each of the matrix elements above, we want to separate the contribution from the kinetic and the potential part of the Hamiltonian in Eq. (2). In order to use the first order approximation of the Baker-Campbell-Hausdorff formula, we need to have $\Delta t \ll 1$ so that:

$$\begin{aligned}&\langle x_{k+1}|e^{-iH\Delta t}|x_k\rangle \approx \\ &\quad \langle x_{k+1}|e^{-iH_0\Delta t}e^{-iV\Delta t}|x_k\rangle = \langle x_{k+1}|e^{-iH_0\Delta t}|x_k\rangle\, e^{-iV(x_k)\Delta t}\,,\end{aligned} \tag{7}$$

where we used the fact that V is a function of only the space coordinates. The other matrix element can be calculated by inserting a complete set of momentum eigenstates and performing the Fourier transform. The result is:

$$\langle x_{k+1}|e^{-iH\Delta t}|x_k\rangle \approx \sqrt{\frac{m}{2\pi i\Delta t}}\, \exp\left\{i\Delta t\left[\frac{m}{2}\left(\frac{x_{k+1}-x_k}{\Delta t}\right)^2 - V(x_k)\right]\right\}.$$

(8)

Reiterating this operation for every matrix element, we obtain for the amplitude (1) the final form:

$$\langle x'|e^{-iHT}|x\rangle = \left(\frac{m}{2\pi i\Delta t}\right)^{\frac{n}{2}} \int \mathrm{d}x_1 \dots \mathrm{d}x_{n-1} \prod_{k=0}^{n-1} e^{i\Delta t\left[\frac{m}{2}\left(\frac{x_{k+1}-x_k}{\Delta t}\right)^2 - V(x_k)\right]}. \tag{9}$$

If we set the number n of intervals to diverge and take the limit $\Delta t \to 0$, then the exponent in Eq. (9) becomes:

$$\begin{aligned}\sum_{k=0}^{n-1} \Delta t \left[\frac{m}{2}\left(\frac{x_{k+1}-x_k}{\Delta t}\right)^2 - V(x_k)\right] &\xrightarrow{\Delta t\to 0} \int_0^T dt \left[\frac{m}{2}\left(\frac{\mathrm{d}x}{\mathrm{d}t}\right)^2 - V(x)\right] \\ &= \int_0^T dt\, L(x,\dot{x}) \equiv S[x(t)]\,, \end{aligned} \tag{10}$$

which is nothing but the classical action for the path $x(t)$ from x to x' with $x_k = x(k\Delta t)$. The integration over the x_k is then interpreted as an exploration of all possible paths of the system. The measure for the path integral is defined as:

$$\mathscr{D}[x] = \mathrm{const} \prod_t \mathrm{d}x(t) \equiv \lim_{\Delta t\to 0} \left(\frac{m}{2\pi i\Delta t}\right)^{n/2} \mathrm{d}x_1 \dots \mathrm{d}x_{n-1}\,. \tag{11}$$

The amplitude in Eq. (1) can then be cast, using the definitions above, into the compact form:

$$\langle x'|e^{-iHT}|x\rangle = \int \mathscr{D}[x]\ e^{iS[x]}\,, \tag{12}$$

which is an integral over all possible paths, starting at x' and ending at x, weighted by the classical action. It can also be immediately generalised for N_d-dimensional paths $x_i(t)$ with $i = 1, \dots, N_d$.

In the framework of QFT, where relativistic effects are taken into account, the focus is placed on the field $\phi(x)$, function of a space-time vector $x = (t, \mathbf{x})$, which can be interpreted as a combination of creation and destruction operators, in a certain basis. Much information about the physics of the system is then contained in objects called Green functions:

$$G(x_1, x_2, \dots, x_n) = \langle 0|\phi(x_1)\phi(x_2)\dots\phi(x_n)|0\rangle\,. \tag{13}$$

These are vacuum expectation value of a product of n fields at different space-time points. The path integral formalism can be developed in this context as well, but a formal derivation, like the one given above,

is out of the scope of this thesis. The result, though, is conceptually equivalent, so that we can simply translate variables $x_i(t)$ into fields $\phi(\vec{x}, t)$, in such a way that the integration measure becomes:

$$\prod_{t,i} \mathrm{d}x_i(t) \longleftrightarrow \prod_{t,\mathbf{x}} \mathrm{d}\phi(\mathbf{x}, t) \equiv \mathscr{D}[\phi]\,. \tag{14}$$

The Green functions in Eq. (13) are then represented as functional integrals carried out over all the field configurations

$$\langle 0|\phi(x_1)\phi(x_2)\dots\phi(x_n)|0\rangle = \frac{1}{Z}\int \mathscr{D}[\phi]\;\phi(x_1)\phi(x_2)\dots\phi(x_n)\,e^{iS[\phi]}\,, \tag{15}$$

with the normalization

$$Z = \int \mathscr{D}[\phi]\;e^{iS[\phi]}. \tag{16}$$

The field configurations are again weighted by the exponential of the classical action S, which can be written as an integral over a Lagrangian density:

$$S \equiv S[\phi] = \int \mathrm{d}t\,\mathrm{d}\mathbf{x}\,\mathscr{L}(t, \mathbf{x})\,. \tag{17}$$

The form of $\mathscr{L}$ dictates all the possible allowed interactions among the fields. For example:

$$\mathscr{L} = \frac{1}{2}(\partial_\mu\phi)(\partial^\mu\phi) - \frac{1}{2}m_0^2\phi^2 - \frac{1}{4!}\lambda_0\phi^4\,, \tag{18}$$

describes the so-called $\lambda\phi^4$ theory. Note that in Eq. (15) the weight is represented by an oscillating exponential. This turns out to be problematic at a practical level, when convergence of the integrals in Eq. (15) is questioned. In the following, we will make use of an imaginary time prescription to address this problem.

1.2 EUCLIDEAN FUNCTIONAL INTEGRAL

In this section we will introduce the so-called Euclidean correlator G_E, which will be of central interest throughout the whole thesis. Let us consider an operator O, which can create or annihilate states and/or measure a certain quantity. A Euclidean correlation function is defined as:

$$G_E(\tau) = \langle O(\tau)O(0)\rangle_\beta \equiv \frac{1}{Z_\beta}\,\mathrm{Tr}\left[e^{-(\beta-\tau)H}\,O\,e^{-\tau H}\,O\right]\,, \tag{19}$$

where the normalization Z_β is given by:

$$Z_\beta \equiv \mathrm{Tr}\,e^{-\beta H}\,. \tag{20}$$

Here H is as usual the Hamiltonian operator, and the trace is evaluated over a complete set of eigenstates. The parameters τ and β are real and non-negative and denote a Euclidean time distance. Note that τ is the actual separation we are interested in, while β can be regarded as a maximal allowed extension. Later we will show that β represents the inverse of the physical temperature.

We need to choose an orthonormal basis in order to perform the trace and, for convenience, we use here the eigenstates of H. We can regard the spectrum $|n\rangle$ of H as discrete, so that the secular equation reads:

$$H\,|n\rangle = E_n\,|n\rangle\ ,$$

where the integer subscript n labels the eigenvalues, which can be ordered according to $E_0 \leq E_1 \leq E_2 \ldots$. The correlator in Eq. (19) can then be evaluated by inserting the identity $\mathbb{1} = \sum_n |n\rangle\,\langle n|$ between the two operators:

$$\begin{aligned}\langle O(\tau)O(0)\rangle_\beta &= \frac{1}{Z_\beta}\sum_{n,m}\langle m|\,e^{-(\beta-\tau)H}O\,|n\rangle\,\langle n|\,e^{-\tau H}O\,|m\rangle \\ &= \frac{1}{Z_\beta}\sum_{n,m}|\langle m|\,O\,|n\rangle|^2\,e^{-(\beta-\tau)E_m}e^{-\tau E_n}\,. \end{aligned} \tag{21}$$

Now the normalization Z_β, defined in Eq. (20), can be easily written as $\sum_n e^{-\beta E_n}$, so that in both numerator and denominator we can pull out a factor $e^{-\beta E_0}$, obtaining:

$$\langle O(\tau)O(0)\rangle_\beta = \frac{\sum_{n,m}|\langle m|\,O\,|n\rangle|^2\;e^{-(\beta-\tau)\,\Delta E_m}\,e^{-\tau\,\Delta E_n}}{1+e^{-\beta\,\Delta E_1}+e^{-\beta\,\Delta E_2}+\ldots}\,, \tag{22}$$

where we defined $\Delta E_n \equiv E_n - E_0$. Then it is apparent that the Euclidean correlator depends only on the energy differences with respect to the vacuum. We can then renormalize the latter to $E_0 \equiv 0$ and drop the notation ΔE_n in what follows.

Let us now explore what happens in the limit where $\beta \to \infty$. If the vacuum is non-degenerate, i.e. $\Delta E_i > 0$ for $i > 0$, then the denominator is equal to 1. In the numerator, all the terms with $E_m \neq 0$ vanish, so that we are left with the expression:

$$\lim_{\beta\to\infty}\langle O(\tau)O(0)\rangle_\beta = \sum_n|\langle 0|\,O\,|n\rangle|^2\;e^{-\tau\,E_n}\,. \tag{23}$$

This formula can be used to extract physical information from the Euclidean correlator. For example, suppose that $O = O_\pi$ is the operator that creates a pion with zero momentum. Then $|\langle 0|\,O_\pi\,|n\rangle|^2$ will vanish for all the Fock states which do not have the quantum numbers of a pion at rest. Moreover, if we take τ to be large, then Eq. (23) can be

used to extract the lowest energy level, i.e. the mass of the pion, from the exponential behaviour of the Euclidean correlator.

In the previous section, we introduced the path integral formalism as a formal tool to evaluate the Green functions in Eq. (13). We would like to show here that, with some modifications, the path integral can be applied to the Euclidean correlators in Eq. (19) as well. We start by recalling that, in the Heisenberg picture, the operators evolve in time according to:

$$O(t) = e^{itH}\, O(0)\, e^{-itH}\,. \tag{24}$$

The Euclidean correlators in Eq. (19) can then be viewed as a two-point Green function (see Eq. (13) with $n = 2$) analytically continued to imaginary times, i.e. with the substitution

$$t = -i\tau\,, \tag{25}$$

and the addition of an extra imaginary time transporter $e^{-\beta H}$, which projects to the vacuum in the limit $\beta \to \infty$. The transformation in Eq. (25) is called *Wick rotation*, and it changes the Minkowski metric to a Euclidean one, according to:

$$-ds^2 = -dt^2 + dx_1^2 + dx_2^2 + dx_3^2 \;\to\; d\tau^2 + dx_1^2 + dx_2^2 + dx_3^2\,. \tag{26}$$

This observation allows us to use the formula in Eq. (15) to evaluate G_E as:

$$\begin{aligned} G_E((\tau_1, \mathbf{x}_1), \ldots, (\tau_n, \mathbf{x}_n)) &= G((-i\tau_1, \mathbf{x}_1), \ldots, (-i\tau_n, \mathbf{x}_n)) \\ &= \frac{1}{Z} \int \mathscr{D}[\phi]\; \phi(x_1) \ldots \phi(x_n)\, e^{-S_E[\phi]}\,, \end{aligned} \tag{27}$$

with

$$Z = \int \mathscr{D}[\phi]\; e^{-S_E[\phi]}\,. \tag{28}$$

S_E denotes here the Euclidean action:

$$\begin{aligned} S_E[\phi] &= \int \mathrm{d}\tau\, \mathrm{d}\mathbf{x}\; L_E\left[\phi(\tau, \mathbf{x}), \partial_\mu \phi(\tau, \mathbf{x})\right] \\ &= \int \mathrm{d}\tau\, \mathrm{d}\mathbf{x}\; \left[\frac{1}{2}\left(\frac{d\phi}{d\tau}\right)^2 + \frac{1}{2}(\nabla\phi)^2 + \frac{1}{2}m^2\phi^2 + \frac{1}{4!}\lambda\phi^4\right] \\ &= \int \mathrm{d}x\; \left[\frac{1}{2}(\partial_\mu\phi)^2 + \frac{1}{2}m^2\phi^2 + \frac{1}{4!}\lambda\phi^4\right], \end{aligned} \tag{29}$$

which is a positive definite quantity. In chapter 3, we will return to this topic and the correspondence between real-time and imaginary-time correlators will be further explored.

From now on we shall remain in the Euclidean space and suppress the subscript E. Note that in Eq. (27) each field configuration is now weighted by an exponentially decaying factor e^{-S}, which is a better behaved object than the one appearing in Eq. (15). In the following, this will allow to draw a formal comparison with the framework and tools generally used in statistical mechanics, making it possible to use its well-known numerical algorithms to simulate the theory.

1.3 NON-ZERO TEMPERATURE

The central topic of this thesis will be the study of how certain properties of QCD depend on the temperature. In this section we will briefly review how the temperature can be introduced in the discussion above.

In thermodynamics, the canonical ensemble represents all the available states of a system in thermal equilibrium with a heat bath of temperature T. It is described by the partition function $Z(T)$, which, in the quantum mechanical case, assumes the form:

$$Z(T) = \mathrm{Tr}\, e^{-\frac{H}{k_B T}} = \mathrm{Tr}\, e^{-\beta H}, \tag{30}$$

where H is the Hamiltonian of the system and β denotes the inverse temperature. In the following, we will use units where Boltzmann constant $k_B \equiv 1$, so that the temperature is given in units of energy or mass. One immediately realises that Eq. (30) is identical to Eq. (20), introduced in the previous section. This means that we can express the partition function via the path integral formalism of Eq. (28):

$$Z(T) = \int \mathscr{D}[\phi]\, e^{-S_E[\phi]}, \tag{31}$$

where this time the integration is carried out without taking the limit $\beta \to \infty$, but on a finite Euclidean temporal interval:

$$S_E[\phi] = \int_0^\beta \mathrm{d}\tau \int_{\mathbb{R}^3} \mathrm{d}\mathbf{x}\, L_E\left[\phi(\tau,\mathbf{x}), \partial_\mu \phi(\tau,\mathbf{x})\right]. \tag{32}$$

From this equation we can identify the Euclidean time extent β with the inverse of the temperature:

$$\text{Euclidean Time Extent} = \beta = \frac{1}{T}, \tag{33}$$

which means that in the previous section, by taking the limit $\beta \to \infty$ we were effectively measuring the Green functions at zero temperature. We will see in the next section other important consequences of having a finite temporal extent β.

These simple but fundamental steps are the basic ingredients necessary to introduce the temperature in a QFT calculation. These concepts will be often used in this thesis and will be illustrated with practical examples.

1.4 FIELD THEORIES ON AN HYPERCUBE

The path integral representation of the Euclidean correlation functions in the form of Eq. (27), despite being formally elegant, is still difficult to approach from a practical point of view, since it involves an infinite number of degrees of freedom. The approach followed here consists in regularizing the theory on a Euclidean hypercubic lattice, where a position is specified by a vector as:

$$x_\mu = a n_\mu, \qquad n_\mu \in \mathbf{Z}. \tag{34}$$

The quantity a is called *lattice spacing* and it represents the minimum allowed distance. The scalar field $\phi(x)$ is now defined on the lattice points x only. The lattice action in Eq. (29) assumes the discretized form:

$$S = \sum_x a^4 \left[\frac{1}{2} \sum_{\mu=1}^{4} (\Delta_\mu \phi(x))^2 + \frac{m_0^2}{2} \phi(x)^2 + \frac{g_0}{4!} \phi(x)^4 \right] . \tag{35}$$

Here we have introduced the following changes:

- derivatives of the field ϕ have naturally been replaced by finite differences:

$$\partial_\mu \phi \longrightarrow \Delta_\mu \phi(x) \equiv \frac{1}{a} \left[\phi(x + a\hat{\mu}) - \phi(x) \right] ; \tag{36}$$

- space-time integrals have now become sums:

$$\int d^4x \quad \longrightarrow \sum_x a^4 ; \tag{37}$$

- the functional integral of Eq. (27) is now equipped with a measure involving only a discrete set of lattice points:

$$\mathscr{D}[\phi] = \prod_x d\phi(x) . \tag{38}$$

Another advantage of formulating the theory on a discretized lattice becomes clear when we switch to momentum space. In fact, the Fourier transform $\phi(p)$ of the field, defined by

$$\phi(p) = \sum_x a^4 \, e^{-ipx} \, \phi(x) , \tag{39}$$

is periodic and the momenta are restricted to the so-called Brillouin zone $p \in (-\pi/a, \pi/a]$. This means that the inverse Fourier transform

$$\phi(x) = \int_{-\pi/a}^{\pi/a} \frac{d^4p}{(2\pi)^4} \, e^{ipx} \, \phi(p) , \tag{40}$$

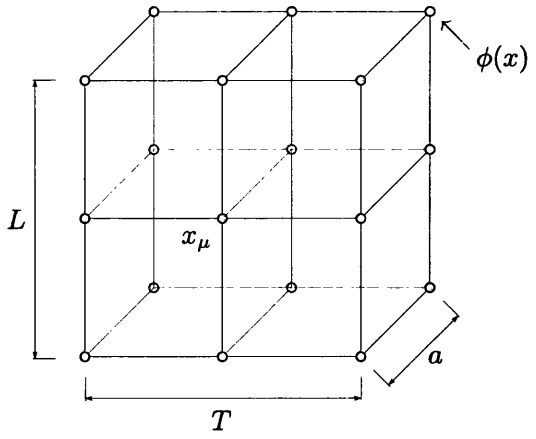

Figure 1: Example of a lattice in $d = 3$ dimensions.

has now an ultraviolet cutoff $|p_\mu| \leq \pi/a$, which acts as a natural regulator of the discretized field theory.

As we mentioned in the end of the previous section, the ultimate aim will be to perform numerical simulations. It is then necessary to restrict ourselves to finite lattices. Let us assume a hypercubic lattice with

$$x_\mu = a n_\mu, \qquad n_\mu = 0, 1, 2, \ldots, L_\mu - 1, \tag{41}$$

where

$$L_\mu = \begin{cases} L_s & \text{for } \mu = 1, 2, 3 \\ L_t & \text{for } \mu = 4, \end{cases} \tag{42}$$

where every spatial direction has a length of $a_s L_s$, while in Euclidean time we have $a_t L_t = \beta$, so that the total volume is $V = (a_s L_s)^3 (a_t L_t)$. Here we have generalized to the case where the lattice spacing in the spatial direction a_s differs from the temporal one a_t.

In a finite volume one has to specify boundary conditions. We will choose periodic b.c., i.e. $\phi(x) = \phi(x + aL\hat{\imath})$, for all the spatial directions. They imply that the momenta are also discretized, according to:

$$p_i = \frac{2\pi}{a} \frac{l_i}{L} \qquad \text{with } l_i = -\frac{L}{2} + 1, \ldots, \frac{L}{2}, \tag{43}$$

and therefore integration over the three-momentum is replaced by finite sums

$$\int \frac{\mathrm{d}^3 p}{(2\pi)^3} \longrightarrow \frac{1}{a^3 L^3} \sum_{l_i}. \tag{44}$$

If we look at the Euclidean correlator in Eq. (19) and taking into account the cyclic properties of the trace, then it is possible to show that if the field ϕ (anti-)commutes, then it must have (anti-)periodic b.c. in the Euclidean time direction:

$$\phi(\tau + T, \mathbf{x}) = \begin{cases} +\phi(\tau, \mathbf{x}) & \text{(Bosons)} \\ -\phi(\tau, \mathbf{x}) & \text{(Fermions)}\,. \end{cases} \tag{45}$$

Similarly to the three-momentum case, the Fourier transform over the time variable yields a discrete set of variables ω_n called *Matsubara frequencies*:

$$\omega_n = \begin{cases} \frac{2\pi}{a_t}\frac{n}{L_t} & \text{(Bosons)} \\ \frac{\pi}{a_t}\frac{2n+1}{L_t} & \text{(Fermions)} \end{cases} \qquad \text{with} \quad n = 0, \ldots, N_t - 1\,. \tag{46}$$

This concludes our construction of a QFT regularized on a finite lattice. We note that, in order to recover the continuum physics, results should in principle be extrapolated by a limiting procedure where the lattice spacing is sent to zero. This should be done in such a way that the physical volume remains unchanged. In practice, one would simulate the theory at smaller and smaller value of the lattice spacing, while accordingly adjusting the extent of the lattice to maintain V constant.

In the previous sections, we have already anticipated how the Euclidean formulation of Quantum Field Theory bears many similarities with the formalism of Statistical Mechanics (SM). First of all, the functional integrals, regularized on a hyper-cubic lattice, have the form of partition functions:

$$\int \mathscr{D}[\phi]\, e^{-S[\phi]} \quad \longleftrightarrow \quad \sum e^{-\beta H}\,,$$

where we have seen in the previous section how the action has the same role that the Hamiltonian function has in the SM case:

$$S[\phi] \quad \longleftrightarrow \quad \beta H\,.$$

Finally in Eq. (23), we noticed how the mass of a bound states can be extracted by looking at the exponential decay of an ad-hoc correlation functions in the large Euclidean time:

$$G(\tau) \sim e^{-m\tau} \quad \longleftrightarrow \quad G(x) \sim e^{-|x|/\xi}\,,$$

which is the analogous of the inverse ξ^{-1} of the correlation length of a statistical ensemble. This formal analogy allows us to use well-established methods of statistical mechanics in field theory and vice versa.

1.5 LATTICE FORMULATION OF QCD

A gauge theory is a field theory that is invariant under a local transformation. Such transformations may be a continuous function of several parameters and in general need not commute. Those groups that contain non-commuting elements are generally called non-Abelian. Since QCD belongs to the class of non-Abelian gauge theories, we will review some of their basic properties in this section. As it is customary, we will start from the continuum formulation, in order to then apply the discretization procedure already outlined in the previous section for a scalar theory. The topics here exposed can be found in a number of textbooks [16–20], to which we refer for a more detailed treatment. We are interested in the Euclidean space, which is where the equations of this section will be formulated. The Lorentz index μ is then Euclidean, i.e., we do not distinguish between covariant and contravariant indices. The metric tensor is trivial $g_{\mu\nu} = \mathrm{diag}\{1,1,1,1\}$ and $\mu = 1,2,3,4$ simply labels the different components.

The fermionic content of QCD is represented by massive quarks, described by 4-spinor Dirac fields $\overline{\psi}^c_\alpha(x)$ and $\psi^c_\alpha(x)$. The space-time position is denoted by x, which is a shorthand for $\{x^\mu\}$ with $\mu = 1,2,3,4$, the Dirac index by $\alpha = 1,2,3,4$ and the color quantum number is labeled by $c = 1,\ldots,N_c$, where the meaning of N_c will be clarified below.

The action is bilinear in the fermion fields and reads:

$$\begin{aligned} S_\psi &= \int \mathrm{d}^4x \left[\overline{\psi}(x)\left(\not{\partial} + m\right)\psi(x)\right] \\ &= \int \mathrm{d}^4x \left[\overline{\psi}^a_\alpha(x)\left(\partial_\mu \gamma^\mu_{\alpha\beta}\delta_{ab} + m\delta_{\alpha\beta}\delta_{ab}\right)\psi^b_\beta(x)\right] \end{aligned} \tag{47}$$

where γ^μ are the so-called Dirac matrices in Euclidean space (see Appendix A.1 for their explicit form) satisfying the anti-commutation relation:

$$\{\gamma_\mu, \gamma_\nu\} = 2\delta_{\mu\nu}\,. \tag{48}$$

This theory has a global symmetry $SU(N_c)$, the special group of unitary $N_c \times N_c$ matrices, with unit determinant. A matrix $\Lambda \in SU(N_c)$ will act on the color index c of the fermion fields ψ^c as (in matrix notation):

$$\begin{aligned} \psi' &= \Lambda\,\psi \\ \overline{\psi}' &= \overline{\psi}\,\Lambda^\dagger \end{aligned} \qquad \Lambda \in SU(N_c)\,, \tag{49}$$

and the action in Eq. (47) is invariant under such a transformation.

The transformation in Eq. (49) is then promoted to be a local one, so that the matrix $\Lambda \to \Lambda(x)$ acquires a space-time index x and the transformation becomes:

$$\begin{aligned} \psi'(x) &= \Lambda(x)\,\psi(x) \\ \overline{\psi}'(x) &= \overline{\psi}(x)\,\Lambda^{\dagger}(x) \end{aligned} \qquad \Lambda \in SU(N_c)\,, \tag{50}$$

In order to keep the action in Eq. (47) invariant under Eq. (50), the ordinary derivative ∂_μ must be replaced by a covariant one D_μ:

$$\partial_\mu \longrightarrow D_\mu = \partial_\mu + iA_\mu(x) \tag{51}$$

where A_μ is called the gauge field. It belongs to the algebra $\mathfrak{su}(N_c)$ of the gauge group, hence it is a Hermitian traceless matrix. A_μ transforms according to:

$$A_\mu(x) \to A'_\mu(x) = \Lambda(x)A_\mu(x)\Lambda(x)^{\dagger} + i(\partial_\mu\Lambda(x))\Lambda(x)^{\dagger}\,, \tag{52}$$

from which the transformation rule for the covariant derivative can be deduced:

$$D'_\mu\psi'(x) = \Lambda(x)D_\mu\psi(x). \tag{53}$$

When we replace $\partial_\mu \to D_\mu$ in Eq. (47), the action becomes invariant under local gauge transformations:

$$\begin{aligned} S_\psi &= \int \mathrm{d}^4x\,\left[\overline{\psi}(x)\,(\not{D} + m)\,\psi(x)\right] \\ &= \int \mathrm{d}^4x\,\left[\overline{\psi}(x)\,(\not{\partial} + m)\,\psi(x) + i\overline{\psi}(x)\,\gamma^\mu A_\mu\,\psi(x)\right]\,, \end{aligned} \tag{54}$$

where, in the last term, we can see how the field A_μ mediates the interactions between the quarks. Since $A_\mu \in \mathfrak{su}(N_c)$, then it can be rewritten as a combination of $N_c^2 - 1$ generators T^a of the group:

$$\left(A_\mu(x)\right)_{ij} = g_s \sum_{a=1}^{N^2-1} A_{\mu,a}(x)T^a_{ij}\,, \tag{55}$$

where g_s is called the coupling constant of the theory. The T^a satisfy commutation relations proper to the group:

$$[T_a, T_b] = if_{abc}T_c, \qquad \mathrm{Tr}\,(T_aT_b) = \frac{1}{2}\delta_{ab} \tag{56}$$

where f_{abc} are the structure constants of the group itself. The gluon field is then identified with the $N_c^2 - 1$ components $A_{\mu,a}$.

Another reason to require the substitution in Eq. (51) can be found in the evaluation of $\psi(x + \mathrm{d}x) - \psi(x)$. The gauge transformation matrix depends on x and the difference between $\Lambda(x + \mathrm{d}x)$ and $\Lambda(x)$ must be

taken into account. This is obtained by the introduction of a parallel transporter that maps the vectorial space V_x, related to the vector $\psi(x)$ into the one V_{x+dx} of $\psi(x+dx)$. Let us call $\mathscr{C}_{yx}$ a curve between two space-time points x and y. This can be associated to a $SU(N_c)$ matrix, that defines a mapping from V_x to V_y and transforms under Eq. (50) as:

$$U\left(\mathscr{C}_{y,x}\right) \to U'\left(\mathscr{C}_{y,x}\right) = \Lambda(y) U\left(\mathscr{C}_{y,x}\right) \Lambda(x)^{\dagger}. \tag{57}$$

Using the parallel transporter operator $U(\mathscr{C}_{x+dx,x})$ on a straight path from x to $x+dx$, the covariant differential can be written as:

$$D\psi(x) = \psi(x+dx) - U\left(\mathscr{C}_{x+dx,x}\right)\psi(x). \tag{58}$$

As the path $\mathscr{C}_{x+dx,x}$ is infinitesimal the operator $U(\mathscr{C}_{x+dx,x})$ is a matrix close to the identity:

$$U\left(\mathscr{C}_{x+dx,x}\right) = \mathbb{1} + iA_\mu(x)dx^\mu, \tag{59}$$

which is then consistent with the definition Eq. (51). For a finite path $\mathscr{C}_{x,y}$, we can obtain U by exponentiation:

$$U(\mathscr{C}_{x,y}) = \exp \int_{\mathscr{C}_{x,y}} iA_\mu(x)dx^\mu. \tag{60}$$

In order to make the gluon field A_μ dynamical, we must introduce another term in the action. This has to be invariant under the transformations in Eq. (52) and it must be a functional of only the gauge fields and its derivatives. A good candidate is the commutator of two covariant derivatives, which we will call the field strength $F_{\mu\nu}$

$$F_{\mu\nu} \equiv -i\left[D_\mu, D_\nu\right] = \partial_\mu A_\nu(x) - \partial_\nu A_\mu(x) + i\left[A_\mu(x), A_\nu(x)\right] \tag{61}$$

From a geometrical point of view, this tensor is related to the parallel transport of a vector around an infinitesimal parallelogram $\mathscr{C}_{xx}$:

$$U\left(\mathscr{C}_{xx}\right) = \mathbb{1} + iF_{\mu\nu}(x)dx^\mu dy^\nu, \tag{62}$$

from which we can deduce that F gauge-transforms under Eq. (52) as $F'_{\mu\nu} = \Lambda(x)F_{\mu\nu}(x)\Lambda(x)^{\dagger}$. If we make explicit the generators T^a of $SU(N_c)$ we can factorize the field strength tensor as:

$$F_{\mu\nu}(x)_{ij} = \sum_{a=1}^{N^2-1} F_{\mu\nu,a}(x)T^a_{ij} \tag{63}$$

where each component $F_{\mu\nu,a}$ is:

$$F_{\mu\nu,a} = \partial_\mu A_{\nu,a} - \partial_\nu A_{\mu,a} - f_{abc}A^b_\mu A^c_\nu. \tag{64}$$

The so-called Yang-Mills action is then defined in terms of the field strength as:

$$S_{\rm YM} = \frac{1}{4}\int {\rm d}^4x (F^a_{\mu\nu})^2. \tag{65}$$

It contains terms quadratic in A_μ and its derivatives plus quartic and cubic terms that account for the self-interaction of A_μ, which is one of the peculiarities of the non-Abelian gauge theory.

The QCD action is then obtained by putting together Eq. (54) and Eq. (65)

$$S_{\rm QCD} = S_\psi + S_{\rm YM}\,. \tag{66}$$

In order to define the Euclidean theory and its path integral evaluation in QCD, we need first to introduce the Grassmann variables. These are complex totally anti-commuting fields, which are defined by the algebra of elements η_i and $\bar\eta_i$, which obey:

$$\{\eta_i, \eta_j\} = 0 \tag{67}$$
$$\{\eta_i, \bar\eta_j\} = 0 \tag{68}$$
$$\{\bar\eta_i, \bar\eta_j\} = 0. \tag{69}$$

In this algebra we can formally introduce an integration procedure defined by:

$$\int d\eta_i\ (a + b\eta_i) = b \tag{70}$$

for arbitrary complex numbers a, b. We can then reinterpret the quantum field $\overline{\psi}, \psi$ in Eq. (54), as Grassmann variables at every space-time point. The fermionic path integrals are then represented as integrals over fermionic and anti-fermionic Grassmanian field configurations:

$$\mathscr{D}[\psi]\,\mathscr{D}[\bar\psi] = \prod_x \prod_{\alpha=1}^{4} d\psi_\alpha(x)\, d\bar\psi_\alpha(x). \tag{71}$$

The quantum expectation value of any observable $O[\bar\psi, \psi, A_\mu]$ in QCD is then evaluated as:

$$\langle O\rangle = \frac{1}{Z}\int \mathscr{D}[\bar\psi, \psi, A_\mu]\ O[\bar\psi, \psi, A_\mu]\ e^{-S_{\rm QCD}}\,. \tag{72}$$

Since S_ψ is bilinear in the fermionic fields, we can rewrite it in the form:

$$S_\psi = \int d^4x\ \bar\psi(x) D[A_\mu]\psi(x)\,, \tag{73}$$

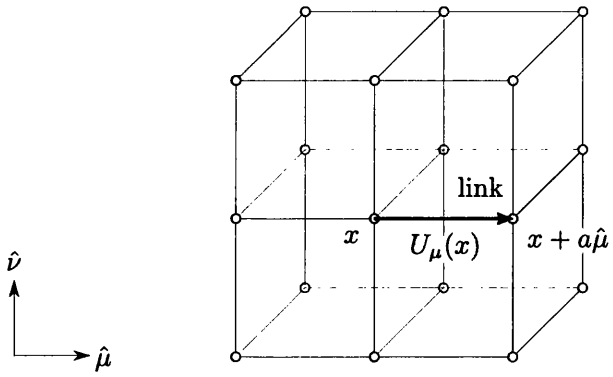

Figure 2: Representation of a link variable, which represents the gauge parallel transporter on the smallest possible path on a lattice.

where D is the so-called Dirac operator:

$$D[A_\mu] = \gamma_\mu D^\mu + m\,. \tag{74}$$

We can then use the Grassmann integration rules of Eq. (70) to formally evaluate the functional integral:

$$\int \mathscr{D}[\bar{\psi}, \psi]\; e^{-\int d^4x\, \bar{\psi}(x) D[A_\mu] \psi(x)} = \det D[A_\mu]\,, \tag{75}$$

which is called the fermion determinant. We will see in the next section how we can put the QCD action on a lattice. Even then, D will be represented by a huge matrix and the evaluation of its determinant will remain a non-trivial task.

We now want to define the gauge theory outlined in the previous pages on a lattice. A local gauge transformation is now defined on the site x of the lattice:

$$\psi(x) \to \psi'(x) = \Lambda(x)\psi(x)\;. \tag{76}$$

In order to define in a meaningful way finite differences of nearest-neighbour fermionic fields, we need the smallest parallel transporter that exists on a lattice. This is called a *link* and it is a group-valued object connecting each site with its nearest-neighbour, as we can see in Fig. (2). We will denote by $U_\mu(x)$ the link connecting the site x with its neighbour $x + a\hat{\mu}$ in the direction $\hat{\mu}$. The link variables transform according to:

$$U_\mu(x) \longrightarrow \Lambda(x)\, U_\mu(x)\, \Lambda^\dagger(x + a\hat{\mu})\,. \tag{77}$$

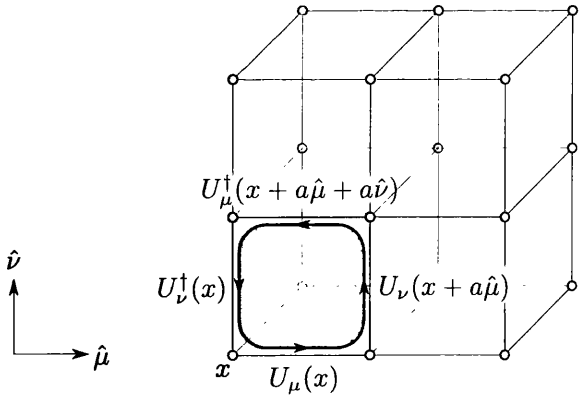

Figure 3: Plaquette $U_{\mu\nu}(x)$ located at the four vertices $x, x + \hat{\mu}a, x + \hat{\mu}a + \hat{\nu}a$ and $x + \hat{\nu}a$.

In the lattice formulation, the gluonic content of the theory is represented by the links, rather than the gauge potential A_μ (the two are related via the relation Eq. (59)). This is a substantial difference, since the A_μ is an element of the $\mathfrak{su}(N_c)$ algebra, while the link $U \in SU(N_c)$.

In order to describe the dynamics of the link variables, we need a discretized version of the Yang-Mills action (65). Therefore we need to find a candidate for the tensor $F_{\mu\nu}$ on the lattice, where the smallest closed path is represented by a square of side a delimited by 4 links. The parallel transporter around such elementary loop is called the plaquette variable and it is the ordered product of the link variables around it. In Fig. 3 it is displayed a plaquette $U_{\mu\nu}(x)$ located in x oriented along the directions $\hat{\mu}$ and $\hat{\nu}$. The lattice gauge action

$$S_{\mathrm{GW}} = \beta \sum_x \sum_{\mu,\nu} \left[1 - \frac{1}{N_c} \mathrm{Re}\,\mathrm{Tr}\, U_{\mu\nu}(x) \right] \tag{78}$$

was introduced in 1974 by Wilson [21] and features a sum over all the possible plaquettes $U_{\mu\nu}(x)$ contained in the lattice volume with just one orientation. The action Eq. (78) is manifestly gauge invariant by construction.

If we write down the dependence of the link variable on the gauge filed $A_\mu(x)$ using Eq. (59), we obtain:

$$U_\mu(x) \equiv e^{iaA_\mu(x)} \,. \tag{79}$$

When we then substitute this expression in the action Eq. (78) (for a rigorous derivation see e.g. [15]) the result is:

$$S_{\mathrm{GW}} = -\frac{\beta}{4N_c} \sum_x a^4 \mathrm{Tr}\, F_{\mu\nu}(x) F^{\mu\nu}(x) + O\left(a^2\right) \,. \tag{80}$$

This proves that, when the lattice spacing vanishes $a \to 0$, $S_{\rm GW}$ coincides with the Yang-Mills action of Eq. (65) if we identify

$$\beta = \frac{2N_c}{g_s^2}\,. \tag{81}$$

For the quantum theory we have to specify how to do functional integrals. In Eq. (72), the functional integral over $A_\mu(x)$ is replaced by a group-integral over all the link variables $U_\mu(x)$:

$$\mathscr{D}[A_\mu] \longrightarrow \prod_{x,\nu} \mathrm{d}U_\mu(x)\,, \tag{82}$$

where the integration is carried via the so-called Haar measure. It has the following defining properties:

- It must be gauge invariant

$$\mathrm{d}U_\mu(x) = \mathrm{d}U'_\mu(x) = \mathrm{d}(\Lambda(x)\,U_\mu(x)\,\Lambda^\dagger(x+a\hat{\mu}))\,, \tag{83}$$

- It must be invariant under left and right multiplication by another group element $V \in SU(N_c)$

$$\mathrm{d}U = \mathrm{d}(VU) = \mathrm{d}(UV)\,, \tag{84}$$

- it is normalized to unity:

$$\int dU = 1\,. \tag{85}$$

The expectation value of any observable O is then written as:

$$\langle A\rangle = \frac{1}{Z}\int \prod_{x,\mu} \mathrm{d}U_\mu(x) O\, e^{-S_{\rm GW}}\,, \tag{86}$$

Note that the choice for the gauge action is not unique and a different gauge action will produce different discretization effects.

In Eq. (54), we wrote the fermionic part of the QCD action. This can be discretized by replacing the covariant derivative with a finite difference of neighbouring fields:

$$D_\mu\psi(x) \to \frac{U_\mu(n)\psi(x+\hat{\mu}) - U^\dagger_\mu(x-\hat{\mu})\psi(x-\hat{\mu})}{2a}\,. \tag{87}$$

where the parallel transporter $U_\mu(n)$ is inserted according to Eq. (58) in order to ensure gauge invariance. The so-called "naïve" fermionic action is defined by

$$\begin{aligned} S^N_\psi =& a^4 \sum_x m_0\,\overline{\psi}(x)\psi(x) + \\ & a^4 \sum_x \overline{\psi}(x)\frac{\gamma_\mu}{2a}\left[U_\mu(x)\psi(x+\hat{\mu}) - U^\dagger_\mu(x-\hat{\mu})\psi(x-\hat{\mu})\right] \qquad (88)\\ =& a^4 \sum_{x,y} \overline{\psi}(x) D(x,y)\psi(y)\,, \qquad (89) \end{aligned}$$

where $D(x,y)$ is the discretized version of the Dirac operator introduced in the continuum case in Eq. (74). It has the form:

$$D(x,y) = m_0\,\delta_{x,y} + \frac{\gamma_\mu}{2a}\left[U_\mu(x)\delta_{x+\hat{\mu},y} - U_\mu^\dagger(x-\hat{\mu})\delta_{x-\hat{\mu},y}\right]. \tag{90}$$

When the lattice spacing is sent to zero, the continuum action is recovered modulo a discretization error of order $O(a^2)$.

In momentum space, the Dirac operator Eq. (90) becomes:

$$\widetilde{D}(q,p) = \widetilde{D}(p)\delta(p-q), \tag{91}$$

with

$$\widetilde{D}(p) = m_0 + \frac{\mathrm{i}}{a}\gamma_\mu \sin(p_\mu a). \tag{92}$$

In the massless limit, one would expect it to vanish only at $p = 0$, but in addition to this, there are 15 other solutions located at

$$p = (\pi/a,0,0,0),(0,\pi/a,0,0),\ldots,(\pi/a,\pi/a,\pi/a,\pi/a) \tag{93}$$

This is known as the *fermion doubling problem* and the unwanted poles in Eq. (93) are called the *doublers*. In order to cure this, Wilson introduced in [21] an additional two-derivative term D^Δ to the naïve Dirac operator of Eq. (90):

$$D^\Delta = \sum_{\mu=1}^{4} \frac{U_\mu(x)\,\delta_{x+\hat{\mu},y} - 2\,\delta_{x,y} + U_\mu^\dagger(x-\hat{\mu})\,\delta_{x-\hat{\mu},y}}{2a}. \tag{94}$$

In momentum-space, the Dirac operator with this addition becomes:

$$\widetilde{D}_{\mathrm{W}}(p) = m_0 + \frac{\mathrm{i}}{a}\gamma_\mu \sin(p_\mu a) + \frac{1}{a}\sum_{\mu=1}^{4}\left[1-\cos(p_\mu a)\right]. \tag{95}$$

By comparison with Eq. (92), the last term is the newly added one. It becomes irrelevant in the limit $a \to 0$ and for $pa \ll 1$, but in the region $p \sim 1/a$ removes the additional doublers. In this new form, the action takes the name of *Wilson fermion action* S_{W} and in coordinate space is given by:

$$S_{\mathrm{W}} = -a^4 \sum_{x,y} \overline{\psi}(x) D_{\mathrm{W}}(x,y)\psi(y) \tag{96}$$

with

$$\begin{aligned} D_{\mathrm{W}}(x,y) = &-\left(m + \frac{4}{a}\right)\delta_{x,y} \\ &+ \left(\frac{1-\gamma_\mu}{2a}\right) U_\mu(x)\,\delta_{x+\hat{\mu},y} \\ &+ \left(\frac{1+\gamma_\mu}{2a}\right) U_\mu^\dagger(x-\hat{\mu})\,\delta_{x-\hat{\mu},y}. \end{aligned} \tag{97}$$

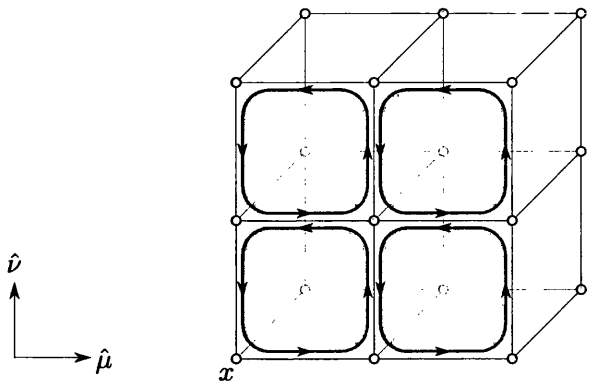

Figure 4: Pictorial representation of the clover-leaf $Q_{\mu\nu}$.

For the Wilson action, discretization effects enter at the level $\mathcal{O}(a)$ in contrast to the naïve and the gauge action. Symanzik [22, 23] has shown that the leading discretization effects can be removed by adding an appropriate counter-term to the action. By applying Symanzik's formalism to Wilson fermions, Sheikholeslami and Wohlert [24] have added a 5-dimension operator to the Wilson action:

$$S_{\mathrm{SW}} = S_{\mathrm{W}} + c_{\mathrm{SW}}\, a^5 \sum_x \sum_{\mu<\nu} \frac{1}{2}\, \overline{\psi}(x)\, \sigma_{\mu\nu} \widehat{F}_{\mu\nu}\, \psi(x)\,, \tag{98}$$

which requires the tuning of the parameter c_{SW} to remove leading lattice artefacts, e.g. in perturbation theory [25], this has been estimated as $c_{\mathrm{SW}} = 1 + 0.36533(4)g^2 + O(g^4)$. In Eq. (98) $\widehat{F}_{\mu\nu}$ is the lattice field strength tensor:

$$\widehat{F}_{\mu\nu}(n) = -\frac{\mathrm{i}}{8a^2}\left(Q_{\mu\nu}(n) - Q_{\nu\mu}(n)\right)\,, \tag{99}$$

can be constructed from the so-called *"clover leaves"*

$$Q_{\mu\nu}(n) = P_{\mu\nu}(n) + P_{\mu\nu}(n-\hat{\mu}) + P_{\mu\nu}(n-\hat{\nu}) + P_{\mu\nu}(n-\hat{\mu}-\hat{\nu}), \tag{100}$$

where each consists of four plaquettes as shown in Fig. 4. In this thesis, we will use a generalization of this action for anisotropic lattices, which will be described in detail in chapter 5.

1.6 NUMERICAL SIMULATIONS

In the previous sections we have seen how it is possible to define QCD on a finite dimensional lattice, so that we can write down the partition function as:

$$Z_{\mathrm{QCD}} = \int \prod_{n,\mu} \mathrm{d}U_\mu(n)\, (\det D_{\mathrm{W}}[U])^{N_f}\, e^{-S_{\mathrm{GW}}[U]}\,, \tag{101}$$

where the determinant of the Dirac operator D_W comes from the integration of the fermionic degrees of freedom, N_f is the number of quark flavours and the integral is carried out over the group manifold $SU(N_c)$.

Even if the integration variables are finite, the configuration space is still too large to permit direct evaluation. This is the reason why these integrations are carried out by means of statistical tools. The Monte Carlo method consists in sampling the space U of possible configuration by generating an ensemble $\{U_i\}_{i=1}^N$. It is particularly advantageous in those cases where integrals have a high number of dimensions, which in our case exceeds $\mathcal{O}(10^7)$.

A numerical evaluation of the integrals is then achievable by means of so-called *importance sampling*. The huge sum appearing in Eq. (101) is approximated by a comparatively small subset of configurations, which are sampled according to the weight factor:

$$W = \frac{1}{Z} \left(\det D[U]\right)^{N_f} e^{-S_G[U]} . \tag{102}$$

From a practical point of view, one starts from some arbitrary configuration and then constructs a stochastic sequence that relax to the equilibrium distribution defined by Eq. (102). This is done with a so-called homogeneous *Markov chain*, where the configurations U_i are generated sequentially

$$U_0 \to U_1 \to U_2 \to \dots \tag{103}$$

where i labels the configuration in the order it appears in the chain. The change of a field configuration to a new one is called an "update" or a Monte Carlo step.

A number of algorithms are available to construct such a chain. In this work, we mainly use a global update step based on the concept of the *Hybrid Monte Carlo* algorithm, which combines *Molecular Dynamics* with the Monte Carlo algorithm, see e.g. [26] for more details.

A numerical estimate for the operator O can then be obtained from a set of N configuration by evaluating its mean and variance:

$$\bar{O} = \frac{1}{N} \sum_{i=1}^{N} O_i , \qquad \text{var}\,[O] = \frac{1}{N-1} \sum_{i=1}^{N} \left(O_i - \bar{O}\right)^2 , \tag{104}$$

where O_i corresponds to a measure obtained from the i-th Monte Carlo-generated configuration. This average value $\bar{O}$ is a random variable itself and it comes with an intrinsic statistical uncertainty, which will vanish in the limit where the total number of available configurations N becomes very large. This error can be estimated by evaluating the variance var $[\bar{O}]$, which for uncorrelated O_i is:

$$\text{var}\,[\bar{O}] = \frac{1}{N} \text{var}\,[O]^2 . \tag{105}$$

The statistical error is then defined as the square-root of Eq. (105) and it decreases like $N^{-1/2}$ with the number N of uncorrelated configurations. The statistical analysis of fitted or derived quantities is then achieved by the well-known Jackknife procedure, see e.g. [27–29] for more details.

This concludes our brief introduction to the lattice regularization of QCD. In the next chapter we will review some of the main properties and symmetries of QCD, making contact with the experimental point of view.

2

THE QUARK-GLUON PLASMA

2.1 INTRODUCTION

In this thesis, we will study the state of matter above a temperature $T = T_c \approx 100 - 200\text{MeV}$, which is equivalent to about 150000 times the core temperature of the Sun. This phase is called the Quark-Gluon Plasma (QGP), since the color charge is transported by quasiparticles carrying either quark or gluon quantum numbers. In the past few years, much effort has been devoted to the understanding of the dynamical and static properties of the QGP. In this thesis, the transport properties of the QGP will be studied, and in particular, the electrical conductivity, which is of great interest to the understanding of the output of the heavy-ion collision experiments at RHIC and CERN.

At the moment, the theoretical interpretation of these experiments consists of a hydrodynamical description of the evolution of the fireball [30–33]. This turns out to be a very useful tool and it relies upon an early thermalization of the QGP medium. In this context, QCD has the important role of giving a description of the QGP at a microscopic level, providing the low energy parameters which are used in the hydrodynamic equations, known as the transport coefficients.

The question of which of the available theoretical frameworks in QCD is the most appropriate for these calculations is resolved by the experimental results for the shear viscosity to entropy ratio η/s, which is found to be smaller than for any other known system [32]. From the point of view of kinetic theory, this means that we are dealing with strongly interacting matter. As a consequence, perturbative calculations show poor convergence in the regimes that we are interested in (see [8, 34] for perturbative results and [35] for a review).

The use of lattice QCD, as a non-perturbative tool to address this problem, presents its own issues. In fact, it is formulated on an Euclidean space-time, meaning that the transport coefficients can be accessed only upon analytic continuation to real times. Nevertheless, it has recently produced a handful of results [3, 36–41], where the study of the systematic uncertainties takes a central role.

In this chapter we will introduce the basic notions about the QGP, starting from its building blocks, namely the properties of QCD at non-

zero temperature. In the latter case, emphasis is put on lattice QCD results for thermodynamics. Finally, a brief introduction to heavy-ion collision experiments is provided.

2.2 QUARKS, GLUONS AND QCD

From the earliest of times, philosophers and then scientists have attempted to explain the world around them by giving a description of matter in terms of forces acting upon more elementary constituents. The very word "atom" comes from the ancient Greek ἄτομος - àtomos, meaning indivisible - and was introduced from the fifth century B.C. by Leucippus, Democritus, and Epicurus, reflecting their purely speculative beliefs that matter was not a continuous entity, but rather made up of discrete units. This paradigm has survived across the centuries and today, our latest model suggests that nucleons are not elementary entities, but bound states of quarks, spin 1/2 particles, which interact by the exchange of gluons, the bosonic carriers of the color force. The latter gives the name to the theory describing them, Quantum Chromodynamics (QCD), whose formulation has been outlined in section 1.5.

Gluons (like photons in QED) have no mass, but since they carry a color charge, they are able to interact with themselves as well, as we have shown in Eq. (64). This additional 'stickiness' is what makes QCD such an interesting and rich theory. In particular, QCD features three very special properties, which we will briefly discuss. First of all, nature confines quarks and gluons inside the hadrons, meaning that the only physical excitations that are allowed are singlets under the gauge group. This feature is called confinement and it implies that, at large distances, the potential between two heavy color charges rises linearly as:

$$V(r) \sim \sigma r\,, \tag{106}$$

where the parameter σ is known as the string tension and has an approximate value of $\sigma \simeq 880\text{MeV/fm} \simeq (420\text{MeV})^2$. This name derives from the fact that the chromoelectric field lines remain concentrated in a region of space called the *fluxtube*. In this picture, one can consider hadrons as little pieces of spinning chromoelectric "string", whose ends are defined by the two quark sources, moving at relativistic speeds. Eq. (106) suggests that an infinite amount of energy is needed to pull apart the two quarks, but this classical picture is bound to fail when relativistic effects appear. In fact, when the energy density is enough, a new $q - \bar{q}$ pair is created, which then breaks the string and becomes a new source for the broken field lines, so that the system can effectively lower its free energy.

On the other hand, experiments performed at SLAC during the 1960s have shown that processes involving high energy electrons scattering off a hadron target were dominated by electromagnetic interactions. This was explained, in 1973 by Gross, Wilczek and Politzer, who found that the coupling constant g of QCD depends on the energy scale q^2 at which the theory is considered. In particular:

$$g^2(q^2) = \frac{16\pi^2}{b\log(q^2/\Lambda^2_{QCD})}, \qquad b = \frac{11N_c}{3} - \frac{2N_f}{3}. \tag{107}$$

If the scale q^2 is large then the coupling is small, so that quarks and gluons are asymptotically free. But when the region of low energy is approached, their interaction becomes strong. Even if the coupling g is dimensionless, the theory dynamically generates a parameter Λ_{QCD} which is the scale at which it becomes non-perturbative. If all the quark masses are set to 0, Λ_{QCD} is also the only dimensionful quantity of QCD, and in this case it only reflects our choice of units. In standard units, $\Lambda_{QCD} \simeq 200\,\text{MeV} \simeq 1\,\text{fm}^{-1}$. Note that hadrons indeed have sizes $r \sim \Lambda^{-1}_{QCD}$.

2.3 SYMMETRIES

Beyond this rich dynamics, which is intimately connected with the non-Abelian nature of the local $SU(3)$ gauge symmetry, there is another factor which makes QCD so peculiar: the pattern of its global symmetries. Quark flavors are usually separated into two sets: the charm, bottom and top are too heavy to be considered a significant factor in the analysis of the system, leaving only the up, down and strange quarks as ones to be included. In the following, N_f will denote the number of quark flavors considered.

When all the quark masses vanish, i.e. in the chiral limit, the left and right-handed fields, defined as

$$\psi_{\text{L,R}} = \frac{1}{2}(1 \pm \gamma_5)\psi, \tag{108}$$

decouple from each other and the Lagrangian becomes invariant under independent flavor transformations of the left-handed and right-handed fields. These transformations are represented by the $U(N_f)_\text{R} \times U(N_f)_\text{L}$ global group:

$$\begin{aligned} &\psi'_{\text{R,L}} = U_{\text{R,L}}\,\psi_{\text{R,L}} \\ \text{with}\quad &U_{\text{R,L}} \equiv \exp\left(i\sum_{j=0}^{N_f^2-1} \alpha^j_{\text{R,L}}\,T_j\right) \in U(N_f)_{\text{R,L}}, \end{aligned} \tag{109}$$

where $\alpha^a_{R,L}$ are the coefficients of the generators T_a. Note that when we discretized the QCD action in section 1.5, the Wilson action of Eq. (96) explicitly breaks chiral symmetry,

$$\{D_W, \gamma_5\} \neq 0. \tag{110}$$

In fact, Nielsen and Ninomiya showed in [42] that any local lattice regularization cannot be free of the doublers of Eq. (93) whilst preserving chiral symmetry. This is known as the *No-Go-Theorem*. One of the most important consequences of Eq. (110) is that the Wilson fermion action generates an additive renormalization for the quark mass m, which then needs to be taken into account during the tuning procedure of the bare parameters.

The chiral group is usually rearranged into the form of unitary vector and axial transformations:

$$U(N_f)_R \times U(N_f)_L \simeq U(N_f)_V \times U(N_f)_A. \tag{111}$$

The two groups are isomorphic with $\alpha_V \equiv (\alpha_R + \alpha_L)/2$, $\alpha_A \equiv (\alpha_R - \alpha_L)/2$. Moreover, we can also decompose the unitary groups in Eq. (111) into the direct product of a special unitary group and a complex phase:

$$U(N_f)_R \times U(N_f)_L \cong SU(N_f)_R \times SU(N_f)_L \times U(1)_R \times U(1)_L \tag{112}$$

$$\cong SU(N_f)_R \times SU(N_f)_L \times U(1)_V \times U(1)_A, \tag{113}$$

where other two $U(1)$ global symmetries appeared. The first one corresponds to the conservation of the baryon number in QCD and it is exact even when the quark masses are taken into account:

$$U(1)_V: \qquad \psi_L \to e^{i\alpha}\psi_L, \quad \psi_R \to e^{i\alpha}\psi_R. \tag{114}$$

The other one is an axial transformation and it acts on the left and right spinors as follows:

$$U(1)_A: \qquad \psi_L \to e^{i\alpha}\psi_L, \quad \psi_R \to e^{-i\alpha}\psi_R. \tag{115}$$

This holds at the classical level only when the quarks are massless but it is broken by quantum corrections. This phenomenon is referred to as an anomaly and the divergence of the $U(1)_A$ current is given by

$$\partial^\mu j^5_\mu = \frac{N_f g^2}{16\pi^2} F^a_{\mu\nu}\tilde{F}^a_{\mu\nu}, \tag{116}$$

where $\tilde{F}^a_{\mu\nu} = \epsilon_{\mu\nu\alpha\beta}F^a_{\alpha\beta}/2$ is the dual of field strength tensor introduced in Eq. (61).

In the real world though, quarks have non-zero masses, which break explicitly the chiral symmetry of Eq. (111). The mass term is:

$$\bar{\psi}^i \, m_i \, \psi^i \equiv \bar{\psi}^i_{\mathrm{R}} \, m_i \, \psi^i_{\mathrm{L}} + \bar{\psi}^i_{\mathrm{L}} \, m_i \, \psi^i_{\mathrm{R}} \, . \tag{117}$$

Nevertheless, if the quarks are grouped into a isospin symmetric point, e.g. $m_u = m_d$ for $N_f = 2$, then the mass term in Eq. (117) preserves an $SU(N_f)_V$ symmetry, while all axial symmetries are explicitly broken. In nature though, quark masses exhibit a strong hierarchy:

$$m_u \simeq m_d \ll m_s \ll m_c \ll m_b \ll m_t \, , \tag{118}$$

so that only an approximate $SU(2)_V$ isospin symmetry remains present.

Despite the explicit breaking described above, the remarkable fact is that chiral symmetry is also spontaneously broken by the ground state of the theory. In fact, at zero temperature and density, the QCD interactions modify the vacuum, making it unstable with respect to the formation of a condensate of tightly bound $q\bar{q}$ pairs:

$$\langle \bar{\psi}\psi \rangle \equiv \langle 0 | \bar{\psi}_{\mathrm{L}} \psi_{\mathrm{R}} + \bar{\psi}_{\mathrm{R}} \psi_{\mathrm{L}} | 0 \rangle \simeq (250\mathrm{MeV})^3 \, , \tag{119}$$

which implies that the condensate pairs ψ_{L} with $\bar{\psi}_{\mathrm{R}}$ and ψ_{R} with $\bar{\psi}_{\mathrm{L}}$. The net effect of this pairing is that a quark, travelling through the vacuum, will flip its chirality at a rate proportional to $\langle \bar{\psi}\psi \rangle$ as if it had a mass. This dynamically generated mass, called constituent mass Σ, accounts for the $30 - 40\%$ of a nucleon's mass, which cannot be exclusively explained by the intrinsic masses m of the constituents. Chiral symmetry breaking χ_{SB} is a very important phenomenon to understand the low energy behaviour of QCD. The breaking pattern $SU(N_f)_{\mathrm{L}} \times SU(N_f)_{\mathrm{R}} \to SU(N_f)_V$ has a great impact on the dynamics at low energy. In fact, the Goldstone theorem shows us that the $N_f^2 - 1$ broken generators give rise to an equivalent number of (approximately) massless excitations. For $N_f = 2$ the latter are represented by the three pions, over which the effective chiral Lagrangian is constructed.

After exploring the symmetries which represent the building blocks of QCD, we can attempt a description from a statistical mechanics viewpoint, i.e. a system where a few global observables can specify the average properties. These can exhibit a fundamentally different behaviour depending on the value of temperature, energy density or net charge, corresponding to different states of matter, with "phase" transitions occurring when the system changes from one state to the other.

2.4 THERMODYNAMICS

In this section we want to explore the behaviour of QCD when the temperature is raised above Λ_{QCD}. According to Eq. (107), when a large

energy scale, such as a high temperature in this case, is introduced into the system, eventually we might expect that the strong coupling constant runs towards zero, following asymptotic freedom, and that quarks and gluons become a plasma of weakly interacting particles carrying a color quantum number [43, 44].

We can gain some insight into this transition by constructing a simple model for the equation of state (EoS). As we said before, at some high temperature we would expect weak interactions inside the medium, so we can approximate its pressure P and energy density ϵ with the expressions valid for non-interacting massless particles:

$$P = d\,\zeta\,\frac{\pi^2}{90}T^4, \tag{120}$$

$$\epsilon = 3P, \tag{121}$$

where ζ accounts for the statistics and d is the number of degrees of freedom. Specifically, ζ is equal to 1 for bosons and 7/8 for fermions, while in a quark-gluon plasma there are $d_q = 4N_fN_c$ quarks and $d_g = 2(N_c^2 - 1)$ gluonic degrees of freedom. If we consider only 2 flavors we obtain $d_{\text{eff}} = d_g + d_q 7/8 = 37$ so that Eq. (120) becomes:

$$P_{\text{QGP}} = \frac{37\pi^2}{90}T^4. \tag{122}$$

On the other hand, when the temperature is small compared to Λ_{QCD}, quarks and gluons remain confined inside the hadrons. In this regime, the Goldstone bosons will be the relevant degrees of freedom and they can be considered to be massless near T_c. Under these assumptions $d = (N_f^2 - 1)$. For $N_f = 2$ we get $d = 3$ and

$$P_{\text{HAD}} = \frac{3\pi^2}{90}T^4. \tag{123}$$

Comparing the two values for the pressure obtained above, a mismatch is observed, because at low T, P_{HAD} is always smaller. Since the system chooses the state with maximum pressure, this would mean that the phase with chiral symmetry breaking is never favored. A simple solution to this problem comes from the bag model, which attempts to take into account non-perturbative effects by assigning a negative vacuum energy and a positive pressure to the vacuum. In this model, quarks can freely move inside a space bounded by the size of the hadron, but cannot travel further because of the pressure applied by the confining vacuum. We start by writing the vacuum energy momentum tensor, which by Lorentz invariance assumes the form $T_{\mu\nu} = Bg_{\mu\nu}$ and

$$\epsilon_{\text{vac}} = -P_{\text{vac}} = +B, \tag{124}$$

the parameter B characterises the model and carries information about the non-perturbative behaviour of QCD. Without going into too much detail, this can be estimated via the so called QCD trace anomaly relation [45]. It characterises the energy of the vacuum, yielding the result $\epsilon_{\text{vac}} \simeq -0.5\ \text{GeV/fm}^3$. The pressure predicted by the bag model intersects P_{HAD} at a critical value T_c for the temperature, where the transition from hadronic matter to free quarks and gluons takes place. We can estimate T_c as:

$$T_c = \left(\frac{45B}{17\pi^2}\right)^{1/4} \simeq 180\ \text{MeV}\,, \tag{125}$$

which is over one trillion kelvin. The two phases are characterized by very different values for the entropy and energy density. An estimate for the latter above and below T_c can be given as:

$$\epsilon_{\text{HAD}} = \lim_{T\to T_c^-} \epsilon(T) = \frac{3\pi^2}{30} T_c^4 \simeq 130\ \text{MeV/fm}^3, \tag{126}$$

$$\epsilon_{\text{QGP}} = \lim_{T\to T_c^+} \epsilon(T) = \frac{37\pi^2}{30} T_c^4 + B \simeq 2000\ \text{MeV/fm}^3\,, \tag{127}$$

where the latent heat of the transition exceeds $1\ \text{GeV/fm}^3$.

We can see that the bag model, though crude, is able to provide useful information about the QCD thermodynamics. Over the years, lattice QCD (LQCD) has become the preferred framework used to carry out more refined calculations (regarding the QCD thermodynamics) [46–51]. This has received a great amount of interest recently, since the deconfined phase of QCD has become reproducible in laboratories, such as those at CERN and RHIC. This has made it possible to deepen our understanding of matter under extreme conditions, allowing for a rich interplay between experiment and theoretical interpretation. The equation of state (EoS) is obtained from the assumption that in the thermodynamic limit, where the three dimensional volume V diverges, the pressure is related to the free energy density $f = -\frac{T}{V}\log Z$ as:

$$p = -\lim_{V\to\infty} f\,. \tag{128}$$

The other observables, such as entropy s and energy ϵ densities, are then reconstructed via thermodynamical relations from the pressure $p(T)$. From the numerical point of view, the partition function $Z = Z(\beta, m)$ is normally only accessible through its derivatives with respect to the bare lattice parameters. One of the most-used methods to reconstruct the pressure p is to perform several simulations at different values of $\{\beta, m\}$ and then apply a careful integration procedure, which goes beyond the scope of this thesis. We show in Fig. 5 the "state of the art" result from the Wuppertal-Budapest collaboration for the energy density ϵ over the transition region.

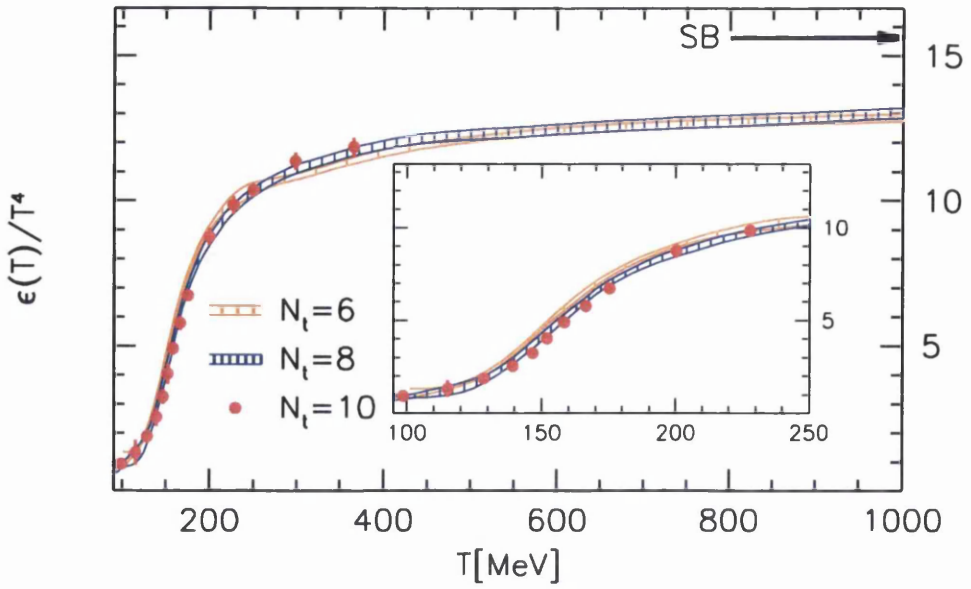

Figure 5: Results for Energy density normalized by T^4 from [49] as a function of the temperature for several lattice spacings. The Stefan-Boltzmann limit $\epsilon_{SB} = 3p_{SB}$ is indicated by an arrow.

2.5 DECONFINING TRANSITION

Another important aspect that LQCD has clarified is the nature of the deconfinement transition. The value of the quark masses, which are the only dimensionful parameters in the QCD lagrangian, have a great impact on the order of the transition. Since the up and down quark masses m_u, m_d are very similar, while the strange quark is much heavier, it has become customary to represent the various phases in a mass diagram where the light quarks are put together on the abscissa, and the strange quark mass is represented by the value of the ordinate. This diagram, called the *Columbia plot* after the institution where it first was introduced [50, 52], is shown in Fig. 6.

The chiral point, where all the quark masses vanish, is represented by the origin in Fig. 6, where the transition is of first order [52]. In this regime, the phase transition is associated with the breaking of the chiral symmetry, driven by a non-zero value for the chiral condensate in Eq. (119), which can be used as an order parameter.

The pure gauge theory is represented by the upper right corner in Fig. 6, where all quark flavors are infinitely heavy and the transition is still first order [53, 54]. In this case, the order parameter is the ex-

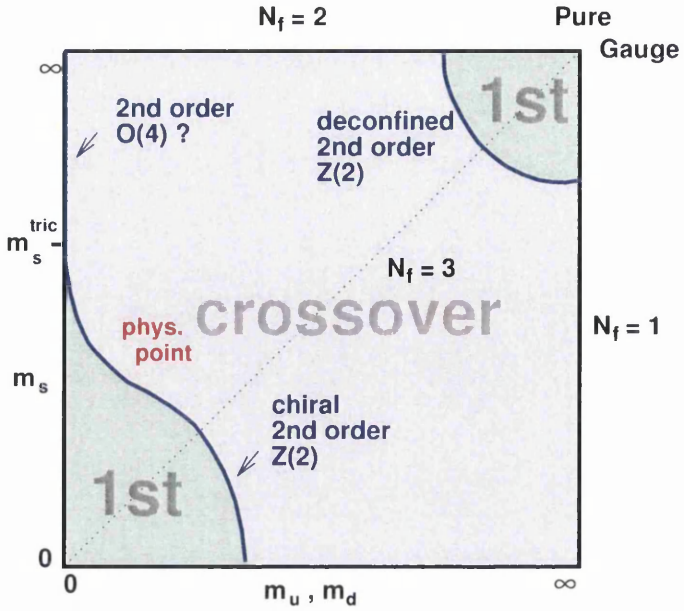

Figure 6: Nature of the deconfining transition as a function of the number of flavors and the value of the quark masses. Plot from [50, 52].

pectation value $\langle L(\mathbf{x})\rangle$ of the Polyakov loop, which is the time ordered product of temporal links at a given spatial position $\mathbf{x}$:

$$L(\mathbf{x}) = \mathrm{Tr} \prod_{\tau=0}^{N_T-1} U_4(\mathbf{x},\tau)\,. \tag{129}$$

This operator vanishes in the confined phase, while it acquires a non-zero value in the deconfined one. Physically, the expectation value of the Polyakov loop can be interpreted as the free energy of an infinitely heavy quark via $\langle L(\mathbf{x})\rangle \sim \exp(-F_Q/T)$. A vanishing $\langle L(\mathbf{x})\rangle$ implies that the free energy diverges or, in other words, the color charges are confined. In fact, the $SU(N_c)$ pure gauge theory admits a global $Z(N_c)$ symmetry and the action does not change when multiplying all time-like links at a given spatial position $\mathbf{x}$ by an element $z = \exp(i2\pi n/N_c)$ of the centre $Z(N_c)$ of the gauge group. This centre symmetry is then broken spontaneously when, in the deconfined region, the Polyakov loop acquires a non-zero expectation value, signalling a phase transition.

The two first-order points described above actually extend into regions bounded by critical lines of second order phase transition. There, the universality class is the one of the $Z(2)$ Ising model. The massless $N_f = 2$ case is located in the upper left corner, where the strange quark is infinitely heavy. Here, the transition is of second order and it lies in the $O(4)$ universality class.

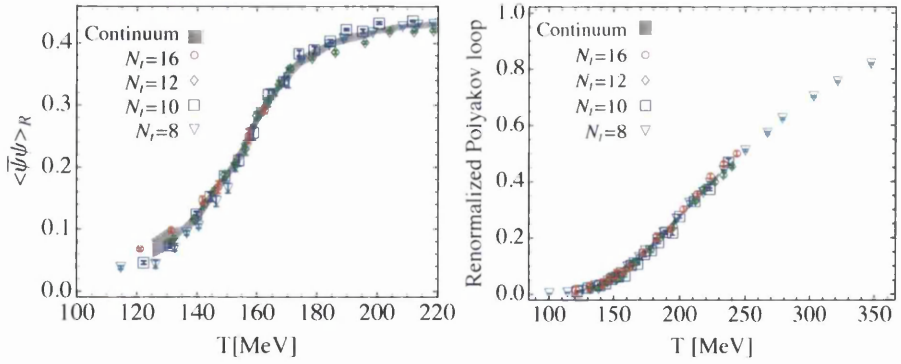

Figure 7: Plots from [48]. Behaviour of the renormalized chiral condensate $\langle\bar{\psi}\psi\rangle_R$ (left) and renormalized Polyakov loop (right) in the transition region. In both figures, the different symbols correspond to different N_t, while the grey band is a continuum estimate. See reference [48] for more details.

At the physical point though, due to the particular values that quark masses assume in nature, the transition has been shown to be a crossover [47]. This means that all observables will have an analytic behaviour with the temperature and might either develop a sharp peak or exhibit a rapid change, so that no proper order parameter exists. Even if no singularity occurs, one might decide to locate T_c either at the peak position or at the inflection point, which are always well defined. Note though that this definition of the transition temperature will be different depending on the observable considered; it is the manifestation of the broad nature of the analytic transition [46, 47, 51]. For this reason, studies of the QCD crossover transition take into consideration the whole behaviour of the studied observable, which is perhaps more informative than T_c and gives a measure of the broadness of the transition. In [48] different observables are studied and the resulting transition temperature lies in a region between 150 and 170 MeV, see Fig. 7 for two examples.

2.6 HEAVY-ION COLLISIONS

The study of QGP, albeit interesting in itself, is relevant to the understanding of two main physical scenarios: the early-universe cosmology and heavy-ion collision experiments (HIC).

In the first case, following Friedmann's solution (Friedmann, 1922) to Einstein's gravitational equations, we know that the Universe experienced an expansion from a singularity at time zero. The solution relates the radius R of the observable universe to its age t (time after the Big Bang) and its temperature T, e.g. before matter cooled down and became non-relativistic, the behaviour was $R \propto T^{-1} \propto t^{\frac{1}{2}}$. We can

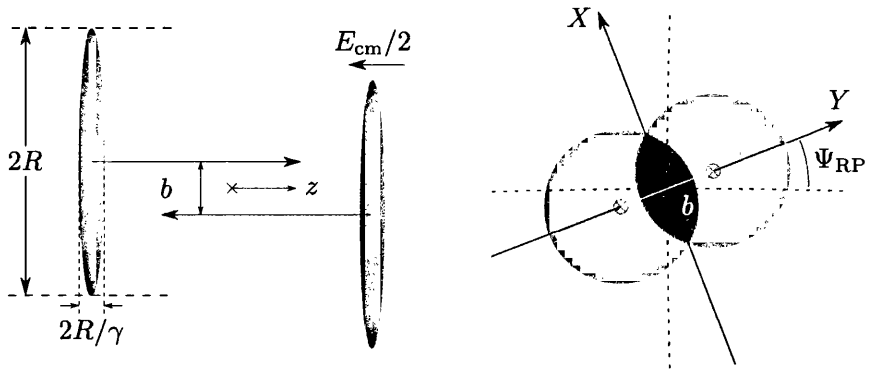

Figure 8: Overview of a heavy-ion event. In the left figure the two nuclei collide along the beam axis usually labelled as z. Due to relativistic energies the nuclei appear length-contracted in the centre of mass frame. The right figure shows a schematic view of the transverse plane. Both the magnitude and direction of the impact parameter b can be determined on an event-by-event basis. X and Y label the reaction plane axes and the dotted lines indicate the lab axis. Ψ_{RP} is known as the reaction plane angle. Note the almond shaped area where the interactions take place.

use this prediction to infer the existence of the QGP between $t \sim 10^{-5}$ and $t \sim 10^{-4}$ seconds. The dynamical properties of the QGP are then important to constrain those cosmological models aiming to describe this part of the evolution of the universe. For example, if the confining transition was first order, it would have been driven by inhomogeneous processes, e.g. growth of hadronic bubbles. This would result in local fluctuations in baryon concentration, with potentially observable consequences in the relative abundances of light elements formed at the nucleosynthesis epoch at $t \sim 10$ minutes [55].

In the HIC experiments, the main topic of this section, a bulk state of hadronic matter is artificially produced in laboratory for a time of the order of 5fm/c. They have been the main "probe" for the study of the QGP since the mid 1970's, at facilities like the Alternating Gradient Synchrotron (AGS) in Brookhaven and the Super Proton Synchrotron (SPS) at CERN. More recent experiments are the Relativistic Heavy Ion Collider (RHIC) at Brookhaven National Laboratory and the Large Hadron Collider (LHC) at CERN. At RHIC, gold (Au) nuclei are the largest used, with a relativistic energy in the centre of mass frame of $E_{cm} \sim 200A$ GeV, where A is the number of nucleons in the nucleus. At LHC, lead (Pb) ions are used, reaching much greater energies of $2.76A$ TeV.

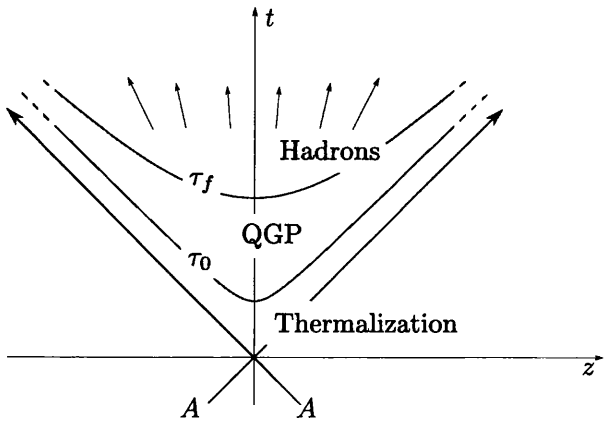

Figure 9: A schematic view of the different stages of a heavy-ion collision event. [56].

In Fig. (8), a schematic way to describe these reactions is provided: the two nuclei of radius R are collided along the axis z. In the centre of mass frame, the nuclei appear as Lorentz-contracted "pancakes" of thickness $2R/\gamma_{\text{cm}}$, where $\gamma_{\text{cm}} = E_{\text{cm}}/2m_N$ is the Lorentz factor. Since the de Broglie wavelength turns out to be much shorter than the size of the nucleus, the impact parameter b, connecting the centre of both nuclei, can be used to characterise the geometry of the collision. In particular, a non-zero value for b implies a highly anisotropic interaction region, see Fig. (8).

Providing a complete description of these collisions is an extremely difficult task. The most successful picture was introduced by Bjorken (Bjorken, 1976) and it takes into account the existence of low energy partons surrounding the nuclei as well as the time dilatation of particle productions. It is outside the scope of this thesis to provide a detailed analysis of the first stages of the collision, since they involve non-equilibrium processes of the underlying non-Abelian gauge theory. We will, however, mention the main features.

At ultra-relativistic energies, when $E_{\text{cm}} > 100$ GeV, the two nuclei pass through each other, leaving behind a highly excited region with a small net baryon number. The different stages of the collision are usually parametrised by the proper time $\tau = \sqrt{t^2 - z^2}$; it turns out that there exists a characteristic proper time τ_0 where the medium has reached local equilibrium, which produces the initial condition for describing the evolution of the system for $\tau > \tau_0$, using some effective model.

In fact, between the time $\tau_0 < \tau < \tau_f$ the system can then be described by relativistic dissipative hydrodynamics, for a detailed review on the topic see e.g. [32, 57]. This theory provides a description of the

flow of the fluid without taking into account its microscopic structure. More precisely, it can be thought as a low-energy effective theory, involving a few parameters, called transport coefficients, which encode the infrared behaviour of the underlying microscopic theory (QCD in our case) and can be computed via first principle calculations. In order to understand the scope of hydrodynamics, it is useful to draw a comparison with thermodynamics. The latter describes a many–body system in global thermal equilibrium, where the so-called intensive quantities (temperature, pressure and chemical potentials) are time–independent and uniform in the volume V of the system. Hydrodynamics can be viewed as a generalisation of this picture towards a state of local equilibrium: the intensive quantities are now allowed to vary in space and time, but they do that so slowly that one can still assume thermal equilibrium to hold locally. Gradients of pressure and temperature naturally lead to flow, with a local fluid velocity which is itself slowly varying in space and time.

The equations of hydrodynamics are built using the conservation laws for the energy, momentum and baryon number

$$\partial_\mu T^{\mu\nu} = 0\,, \tag{130a}$$

$$\partial_\mu J^\mu_B = 0\,, \tag{130b}$$

where $T^{\mu\nu}$ is the energy–momentum tensor, J^μ_B is the density of the baryonic current. These are then coupled to some constitutive equations, which are represented by a gradient expansion involving the transport coefficients mentioned above. For example, when the system is in equilibrium, the spatial components of the energy-momentum tensor are described in terms of the pressure P as $T^{ij} = \delta^{ij}P$. A non-uniform flow field $u(t, v)$ will change this to[1]:

$$T^{ij} = \delta^{ij}P - \eta\left(\partial^i u^j + \partial^j u^i - \frac{2}{3}\delta^{ij}\partial_l u^l\right) - \zeta\delta^{ij}\partial_l u^l + O(\partial^2)\,, \tag{131}$$

where the transport coefficients η and ζ are called the shear and bulk viscosity respectively. These can be determined by a matching procedure with the underlying quantum field theory, i.e. QCD.

The hydrodynamics equations can then describe the time evolution of the system until $\tau \simeq \tau_f$. After this point, the freezout of the medium takes place: initially the number of each species freezes (chemical freezout) and after that the interaction rates drops off and thermal equilibrium is no longer achievable (thermal freezout). After this stage, a typical number of $N \sim O(10^3)$ hadrons are emitted and then detected with

1 We are working in the local rest frame, where $T^{0i} = 0$.

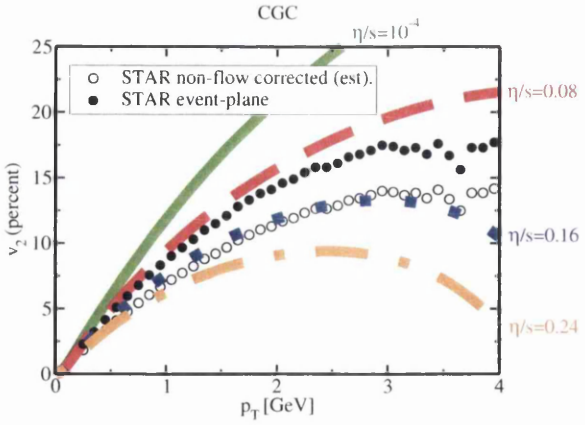

Figure 10: The elliptic flow predicted by viscous hydrodynamics, for different values of the shear viscosity per unit entropy η/s and for the color-glass condensate initial conditions, compared to the measurements by the STAR collaboration at RHIC [31].

a certain distribution along the azimuthal angle ϕ around the beam axis. The distribution is then parametrized by Fourier coefficients:

$$\frac{dN}{d\phi} \propto \left[1 + 2\sum_n v_n \cos(2n\phi)\right]. \tag{132}$$

The second coefficient v_2 is called elliptic flow and plays a key role in unveiling one of the most important observations at RHIC. The observed value for v_2 is unexpectedly large and it represents (in non-central collisions) the response of the system to the initial, anisotropic "almond-shaped" region where the interactions take place. In fact the pressure gradient in the Y direction is larger than in the X direction (see Fig. (8)), so that the nuclear medium expands preferentially along the short axis of the ellipse. We observe that if the mean free path of the particles were bigger than the actual volume where the interactions take place, then the particles would be emitted without any "memory" of what the system looked like, and they would not respond to the initial geometry.

As shown in Fig. (10), using the hydrodynamic calculations mentioned above, it is possible to set some phenomenological bounds on the shear viscosity η of Eq. (131), see e.g. [30, 58, 59]. It was immediately clear that, in order to reproduce the large elliptic flow measured in the experiments, the shear viscosity to entropy density ratio η/s of the formed medium has to be very small compared to any other observed systems [57]. The molecular theory of transport phenomena in dilute gases goes back to Maxwell. In this framework the shear viscosity of a dilute gas is proportional to the particle mean free path.

This supports the idea that the hot quark matter produced at RHIC is actually a strongly-coupled one.

If one takes into account all the systematics involved in the hydrodynamic treatment (see e.g. [32]), then a conservative bound for η/s can be inferred from the RHIC data:

$$\left(\frac{\eta}{s}\right)_{\text{pheno}} \lesssim 0.40 \tag{133}$$

A first-principle calculation of this quantity from QCD has been attempted using several approaches. In [34], a leading-log perturbative prediction has been carried out, yielding the result:

$$\left(\frac{\eta}{s}\right)_{\text{leading log}} = \frac{c}{g^4 \log(1/g)}, \tag{134}$$

where c is a constant and g is the strong coupling constant. At full leading order this amounts to $\eta/s \approx 2.0$ using $\alpha_s = 0.15$ [8]. This result is in tension with the experimental bound given above and it is clear that the perturbative picture is not applicable at the temperatures reached in heavy-ion collisions.

A precise bound for the viscosity was proposed by Kovtun et al. [60] using the formalism of string theory. They argued that

$$\frac{\eta}{s} \geq \frac{1}{4\pi} \simeq 0.08, \tag{135}$$

for all fluids. A fluid which saturates this bound was found in [61], for the $\mathcal{N} = 4$ super-Yang-Mills in the limit of infinite gauge coupling. Such a fluid dissipates the smallest possible amount of energy, and satisfies the laws of fluid dynamics in the largest possible domain: it is called a perfect fluid. The medium produced in the heavy-ion collisions appears to be very close to this limit.

The discussion carried out above is intended to clarify which one of the strong or weak coupling paradigms is more appropriate to describe the QGP at temperatures of a few T_c, which are characteristic of the RHIC and the LHC heavy-ion experiments. A non-perturbative treatment is then needed for a first principles calculation of the transport coefficients and it represents the main topic of this thesis. In particular, we will study the electrical conductivity σ and the diffusion D, which will be described in the next chapter. From a phenomenological point of view, the conductivity plays an important role in the evolution of electromagnetic fields during a heavy-ion collision [62, 63].

In the next chapter, we will introduce the framework of linear response theory, which shows how σ is related to the Euclidean correlator of the electromagnetic current, which is accessible from lattice QCD.

3

KUBO'S FORMULAS

3.1 INTRODUCTION

The very first tool available to physicists in order to interact with the system being studied is the act of "measuring". This amounts to applying a local disturbance using an external force at some space-time point and to measure the response of the system at a later time. One might initially guess that if a small perturbation is applied to the system, its response will be comparatively small as well. This simple intuition can be made more quantitative, and the formalism under which this is done is called *linear response theory*. This powerful tool makes it possible to express the feedback of the system as a convolution of the external perturbation with a response function, computed using equilibrium correlation functions, which do not depend on the strength of the external source.

3.2 LINEAR RESPONSE TO AN EXTERNAL FIELD

We follow here the treatment of [20]. We aim to obtain the effect that a small perturbation, e.g. caused by an external field, has on the ensemble averages of a local observable $O(\mathbf{x}, t)$, to first order in such an external field. The observable under study might be, for example, the local density, the charge current or the local magnetization. The system is described by the following Hamiltonian:

$$H(t) = H_0 + H_{\text{ext}}(t)\,, \tag{136}$$

where H_0 is the time-independent unperturbed Hamiltonian, which describes the system and its interactions, $H_{\text{ext}}(t)$ is the perturbation which couples the original system to the external field. We require it to be weak, so that it can be described perturbatively and also to be adiabatically switched on and off. In the following, we will assume that the unperturbed system has already achieved equilibrium when at $t = t_0$ the perturbation $H_{\text{ext}}(t)$ is turned on.

The expectation value of a physical observable O in the canonical ensemble can be written using the density matrix ρ for the unperturbed system as:

$$\langle O \rangle = \frac{1}{Z_0} \operatorname{Tr} \{\rho O\} = \frac{1}{Z_0} \sum_n \langle n| O |n\rangle e^{-\beta E_n}, \tag{137a}$$

$$\rho = e^{-\beta H_0} = \sum_n |n\rangle \langle n| e^{-\beta E_n}, \tag{137b}$$

where Z_0 is the partition function of the unperturbed system and we have used a complete set of eigenstates $\{|n\rangle\}$ of the Hamiltonian H_0 with eigenenergies $\{E_n\}$. We want to know how the ensemble average of O changes after we turn on the perturbation. To achieve this we need to understand how the density matrix evolves in time or equivalently the time evolution of the eigenstates of the unperturbed Hamiltonian $\{|n(t)\rangle\}$. In other words:

$$\langle O(t) \rangle = \frac{1}{Z_0} \operatorname{Tr} \{\rho(t) O\} = \frac{1}{Z_0} \sum_n \langle n(t)| O |n(t)\rangle e^{-\beta E_n}, \tag{138a}$$

$$\rho(t) = \sum_n |n(t)\rangle\langle n(t)| e^{-\beta E_n}. \tag{138b}$$

The meaning of the equations above is the following. The initial states of the system were distributed according to Eq. (137b). At later times the system is described by the same distribution of states but these are now time-dependent and they have evolved according to the new Hamiltonian. The time dependence of the states $|n(t)\rangle$ is of course governed by the Schrödinger equation:

$$i\partial_t |n(t)\rangle = H |n(t)\rangle . \tag{139}$$

Since $H_{\text{ext}}(t)$ is to be regarded as a small perturbation, it is useful to switch to the so-called interaction picture representation $\{|\hat{n}(t)\rangle\}$. The physical observables $O(t)$ of the coupled system are now time dependent and will evolve according to the Hamiltonian of the isolated system H_0, but the states will follow the external perturbation. Hence the time evolution can be summarised as:

$$|n(t)\rangle = e^{-iH_0 t} |\hat{n}(t)\rangle = e^{-iH_0 t} \hat{U}(t, t_0) |\hat{n}(t_0)\rangle , \tag{140}$$

where by definition $|\hat{n}(t_0)\rangle = e^{iH_0 t_0} |n(t_0)\rangle = |n(t)\rangle$. The evolution operator $\hat{U}$ satisfies the differential equation:

$$i\partial_t \hat{U}(t, t_0) = H_{\text{ext}}(t)\hat{U}(t, t_0), \qquad \hat{U}(t_0, t_0) = 1. \tag{141}$$

which we can expand to linear order in H_{ext} as:

$$\hat{U}(t, t_0) = 1 - i \int_{t_0}^{t} \mathrm{d}t' \, H_{\text{ext}}(t') + O(H_{\text{ext}}^2) . \tag{142}$$

Now inserting Eq. (142) in Eq. (138) we can obtain the expectation value of O to linear order in the perturbation:

$$\begin{aligned}\langle O(t)\rangle &= \langle O\rangle_0 - i\int_{t_0}^{t} \mathrm{d}t' \sum_n \frac{e^{-\beta E_n}}{Z_0} \langle n(t_0)|\,[O(t), H_{\mathrm{ext}}(t')]\,|n(t_0)\rangle \\ &= \langle O\rangle_0 - i\int_{t_0}^{t} \mathrm{d}t' \,\langle [O(t), H_{\mathrm{ext}}(t')]\rangle_0\,, \end{aligned} \tag{143}$$

where the notation $\langle\rangle_0$ stands for an equilibrium average in the unperturbed system described by H_0. Equation (143) turns out to be very useful, since it expresses the non-equilibrium quantity $\langle O(t)\rangle$ as a correlation function in the system in equilibrium.

We can apply these ideas to the case where H_{ext} takes the form:

$$H_{\mathrm{ext}} = \int \mathrm{d}\mathbf{x}\, J(\mathbf{x},t) O(\mathbf{x},t)\,. \tag{144}$$

Inserting Eq. (144) into Eq. (143) we obtain:

$$\delta\langle O(\mathbf{x},t)\rangle = i\int_{t_0}^{t} \mathrm{d}t' \int \mathrm{d}\mathbf{x}'\, J(\mathbf{x}',t')\, \langle [O(\mathbf{x}',t'), O(\mathbf{x},t)]\rangle_0\,. \tag{145}$$

We note that since we assume that the system is in equilibrium, the correlator in Eq. (145) must only depend on $\mathbf{x}-\mathbf{x}'$ and $t-t'$. We can then define the retarded Green function as:

$$G_R(\mathbf{x}-\mathbf{x}';t-t') = -i\theta(t-t')\,\langle [O(\mathbf{x}',t'), O(\mathbf{x},t)]\rangle_0\,, \tag{146}$$

which then can be rewritten in Fourier components:

$$G_R(\mathbf{x}-\mathbf{x}';t-t') = -i\int \frac{\mathrm{d}^3k\,\mathrm{d}\omega}{(2\pi)^4}\, e^{i\mathbf{k}\cdot(\mathbf{x}-\mathbf{x}')-i\omega(t-t')}\, G_R(\omega,\mathbf{k})\,. \tag{147}$$

Using Eq. (146) and letting $t_0 \to -\infty$ and the upper integration time $t\to\infty$, Eq. (145) becomes:

$$\delta\langle O(\mathbf{x},t)\rangle = \int_{-\infty}^{\infty} \mathrm{d}t' \int \mathrm{d}\mathbf{x}'\, J(\mathbf{x}',t') G_R(\mathbf{x}-\mathbf{x}';t-t')\,. \tag{148}$$

It is interesting to express the perturbed observable in frequency and momentum space and to do so we insert Eq. (147) into Eq. (145), obtaining:

$$\delta\langle O(\mathbf{x},t)\rangle = \int \frac{\mathrm{d}^3k\,\mathrm{d}\omega}{(2\pi)^4} e^{i(\mathbf{k}\cdot\mathbf{x}-\omega t)} J(\mathbf{k},\omega) G_R(\mathbf{k},\omega)\,. \tag{149}$$

Eventually, we are left with the compact form:

$$\delta\langle O(\mathbf{k},\omega)\rangle = J(\mathbf{k},\omega) G_R(\mathbf{k},\omega), \tag{150}$$

where the variation in the observable in momentum space is given by the external source times the retarded Green function.

3.3 KUBO FORMULA FOR CONDUCTIVITY

In Sec. 2.6, in the context of the hydrodynamical description of the heavy-ion collisions, we introduced the concept of transport coefficients. These are low energy parameters, bridging the gap between a rigorous first-principle treatment of a problem and a classical effective theory. In this section and for the rest of this thesis, we will focus on a transport coefficient called electrical conductivity σ. We want to calculate σ in the quark-gluon plasma (see Chapter 2), using orthodox lattice QCD simulations, at temperatures relevant to heavy-ion collision experiments, described in Sec. 2.6. Using the Kubo formula, derived in Sec. 3.2 for a generic case, we will show how to relate the calculation of the electrical conductivity to the evaluation of some Green function of the system being considered, which will potentially pave the way to a lattice QCD determination.

Let us then consider a system composed of charged particles in equilibrium. We now apply an external electrical field and we want to have a quantitative description of the current induced in the medium. The electrical conductivity σ is the linear response coefficient that relates the electromagnetic current $\mathbf{J}_{\text{em}}$ at some space-time point $(\mathbf{r},t)$ to the applied electrical field E at $(\mathbf{r}',t')$. In formula:

$$J^{\alpha}_{\text{em}}(\mathbf{r},t) = \int \mathrm{d}t' \int \mathrm{d}\mathbf{r}' \sum_{\beta} \sigma^{\alpha\beta}(\mathbf{r}-\mathbf{r}',t-t')E^{\beta}(\mathbf{r}',t')\,, \tag{151}$$

where the conductivity is represented by a tensor $\sigma^{\alpha\beta}$, depending only only on the combination $\mathbf{r}-\mathbf{r}'$ and $t-t'$. The electromagnetic current $\mathbf{J}_{\text{em}}$ is defined in terms of the current density operator of the charged particles, which in our system composed of electrically charged quarks means:

$$\mathbf{J}_{\text{em}} = q\,\langle \mathbf{J} \rangle\,, \tag{152}$$

where q is the electrical charge and the current density $\mathbf{J}$ is defined as the variation of the Hamiltonian δH due to variation in the vector potential $\delta\mathbf{A}$:

$$\delta H = -q \int \mathrm{d}\mathbf{r}\, \mathbf{J}\cdot\delta\mathbf{A}\,. \tag{153}$$

In terms of the electromagnetic potential, the electric field $\mathbf{E}_{\text{ext}}$ is written as:

$$\mathbf{E}_{\text{ext}}(\mathbf{r},t) = -\nabla_{\mathbf{r}}\phi_{\text{ext}}(\mathbf{r},t) - \partial_t \mathbf{A}_{\text{ext}}(\mathbf{r},t)\,. \tag{154}$$

We can write down the perturbing term H_{ext} in Eq. (136), due to this external electromagnetic field by coupling the charged particles to the scalar and vector potential:

$$H_{\text{ext}} = q\int \mathrm{d}t\,\mathrm{d}\mathbf{r}\,\rho(\mathbf{r},t)\phi_{\text{ext}}(\mathbf{r},t) - q\int \mathrm{d}t\,\mathrm{d}\mathbf{r}\,\mathbf{J}(\mathbf{r},t)\cdot\mathbf{A}_{\text{ext}}(\mathbf{r},t)\,. \tag{155}$$

We can work in a gauge where $\phi_{\text{ext}} = 0$ and drop the first term in Eq. (155), to simplify the expressions. In the following, we will call $\mathbf{A}_0$ the vector potential of the system in equilibrium, so that the total vector potential will be $\mathbf{A} = \mathbf{A}_0 + \mathbf{A}_{\text{ext}}$. We now switch to the frequency domain and therefore we rewrite Eq. (154) in Fourier modes as:

$$\mathbf{A}_{\text{ext}}(\mathbf{r}, \omega) = \frac{\mathbf{E}_{\text{ext}}(\mathbf{r}, \omega)}{i\omega} . \tag{156}$$

The external perturbation in Eq. (155) in frequency domain becomes:

$$H^{\omega}_{\text{ext}} = -\frac{q}{i\omega} \int \mathrm{d}\mathbf{r}\, \mathbf{J}(\mathbf{r}, \omega) \cdot \mathbf{E}_{\text{ext}}(\mathbf{r}, \omega) . \tag{157}$$

Since in Eq. (151) the conductivity tensor is defined through a convolution, its frequency transform is simply:

$$J^{\alpha}_{\text{em}}(\mathbf{r}, \omega) = \int \mathrm{d}\mathbf{r}' \sum_{\beta} \sigma^{\alpha\beta}(\mathbf{r} - \mathbf{r}', \omega) E^{\beta}(\mathbf{r}', \omega) . \tag{158}$$

We can now apply the Kubo's formulas of Eqs. (143) and (145) to obtain the expectation value of the current density $\langle \mathbf{J}_{\text{em}} \rangle$, by replacing O by $\mathbf{J}$ and H_{ext} by Eq. (157). Note that the equilibrium state does not carry any current, so that $\langle \mathbf{J}_0 \rangle_0 = 0$ and $\langle \mathbf{J}_0 \rangle = \delta \langle \mathbf{J}_0 \rangle$. In the frequency domain, using Eq. (150) and writing in components we have:

$$\langle J^{\alpha}(\mathbf{r}, \omega) \rangle = -\frac{q}{i\omega} \int \mathrm{d}\mathbf{r}'\, C^{\alpha\beta}_{\text{R}}(\mathbf{r} - \mathbf{r}', \omega) E^{\beta}_{\text{ext}}(\mathbf{r}', \omega) , \tag{159}$$

which is non-local in space. In Eq. (159) we wrote the retarded Green function for the electromagnetic current as:

$$C^{\alpha\beta}_{\text{R}}(\mathbf{r} - \mathbf{r}', t - t') = -i\theta(t - t') \left\langle \left[J^{\alpha}(\mathbf{r}, t), J^{\beta}(\mathbf{r}', t') \right] \right\rangle_0 . \tag{160}$$

Now comparing Eq. (159) with the definition of the conductivity tensor in Eq. (158) and using Eq. (152), we finally arrive at the Kubo formula for the conductivity:

$$\sigma^{\alpha\beta}(\mathbf{r} - \mathbf{r}', \omega) = \frac{iq^2}{\omega} C^{\alpha\beta}_{\text{R}}(\mathbf{r} - \mathbf{r}', \omega) . \tag{161}$$

Now the DC conductivity is obtained by taking the limit $\mathbf{k} \to 0$ and then $\omega \to 0$ of the real part of σ^{ij}. Moreover, we consider homogeneous translational-invariant systems, i.e. the conductivity tensor is isotropic and therefore diagonal $\sigma^{ij} = \sigma\, \delta^{ij}$. In the end we obtain:

$$\sigma = \frac{1}{3} \operatorname{Re} \sigma^{ii} = q^2 \lim_{\omega \to 0} \lim_{\mathbf{k} \to 0} \frac{\operatorname{Im} \left[C^{ii}_{\text{R}}(\mathbf{k}, \omega) \right]}{3\omega} . \tag{162}$$

This formula will be extensively used in the following chapters and in particular, the combination:

$$\rho^{ii}(\omega) = \lim_{\mathbf{k}\to 0} 2\,\mathrm{Im}\left[C_{\mathrm{R}}^{ii}(\mathbf{k},\omega)\right] \tag{163}$$

takes the name of spectral function, which will be described in the following section. Combining Eqs. (162) and (163), we can obtain the conductivity in terms of the spectral function:

$$\sigma = \frac{q^2}{6}\lim_{\omega\to 0}\frac{\rho^{ii}(\omega)}{\omega}\,. \tag{164}$$

3.4 SPECTRAL FUNCTIONS AND EUCLIDEAN CORRELATORS

The main focus of this thesis is the estimate of spectral functions in QCD starting from imaginary-time correlation functions computed numerically. In the previous section, we showed how the study of the correlation functions for the relevant observables of the system is physically important. They are crucial to analyse the deviations from the mean values, yielding information about the dynamic behaviour of the system near equilibrium [64]. In this section we want to derive some relations between real and imaginary time correlators and to do so let us start by considering an hermitian observable $O(\mathbf{x},t)$, which we can use to build the Wightman correlation functions:

$$G_>(t) \equiv \mathrm{Tr}\,\{\hat{\rho}\,O(t)O(0)\}, \quad G_<(t) \equiv \mathrm{Tr}\,\{\hat{\rho}\,O(0)O(t)\}\,, \tag{165}$$

where the equilibrium density matrix $\hat{\rho} = \frac{1}{Z}e^{-\beta H}$ has already been introduced in Eq. (137) and a hat has been added to avoid confusion with the spectral function. We will now describe some of the properties of these correlators. From the hermiticity of O and the time-translation invariance of $\hat{\rho}$, follow two useful relations:

$$G_<(t) = G_>(-t), \qquad G_>^*(t) = G_>(-t^*)\,. \tag{166}$$

Moreover, from the definition (165) and the form of $\hat{\rho}$, one can deduce the Kubo-Martin-Schwinger (KMS) relation,

$$G_>(t) = G_>(-t - i\beta), \tag{167}$$

which in case of imaginary time direction, implies the periodicity of the correlation function. The commutator $[O(t),O(0)]$ is a physically relevant quantity since it reflects the causality of the theory. In fact, its expectation value,

$$G(t) = i\,\mathrm{Tr}\,\{\hat{\rho}[O(t),O(0)]\} = i(G_>(t) - G_<(t)), \tag{168}$$

vanishes outside the light-cone and by means of Eq. (166), it is straightforward to show that:

$$G(-t) = -G(t), \qquad G^*(t) = G(t^*). \tag{169}$$

As we mentioned in the beginning, we are interested in the Euclidean time correlator, which is accessible from lattice calculation. This is expressed in terms of an analytic continuation (or a Wick rotation) $it \to \tau$ performed on $G_>(t)$:

$$G_E(\tau) = G_>(-i\tau). \tag{170}$$

Using Eq. (167) it can be shown to be periodic:

$$G_E(\beta - \tau) = G_E(\tau)\,, \tag{171}$$

which allows it to be expressed as a Fourier series on the interval $0 \leq \tau < \beta$:

$$G_E(\tau) = \beta \sum_{\ell \in \mathbb{Z}} G_E^{(\ell)}\, e^{-i\omega_\ell \tau} \quad \text{with} \quad G_E^{(\ell)} = \int_0^\beta \mathrm{d}\tau\, e^{i\omega_\ell \tau} G_E(\tau)\,, \tag{172}$$

where $\omega_\ell = \omega_M \cdot \ell = 2\pi\beta\,\ell$ are the Matsubara frequencies introduced in Eq. (46).

In the following, we will be interested in an observable related to the Fourier transform of the correlator $G(t)$:

$$\rho(\omega) = \frac{1}{2\pi i} \int_{-\infty}^{+\infty} \mathrm{d}t\; e^{i\omega t}\; G(t)\,, \tag{173}$$

which is called the spectral function and, using the properties of the Fourier transform, one can show that is a real odd function.

In Eq. (146) we introduced the retarded correlator as the quantity of interest for the linear response formalism. It is easy to see that in momentum space it is related to the correlator in Eq. (168) via an integral transform over the positive half-axis:

$$G_R(\omega) = \int_0^\infty \frac{\mathrm{d}t}{2\pi}\, e^{i\omega t} G(t)\,, \tag{174}$$

and it is analytic for $\mathrm{Im}(\omega) > 0$. Using (169), one shows that

$$\rho(\omega) = \frac{1}{i}\left(G_R(\omega) - G_R(\omega)^*\right) = 2\,\mathrm{Im}\, G_R(\omega) \in \mathbb{R}\,. \tag{175}$$

as stated in the previous section in Eq. (163).

We want now to relate the Euclidean correlators obtained from lattice QCD to their real time counterparts. One way to tackle this problem is to switch to a spectral representation of the correlators. In order

to do that, we insert two complete sets of energy eigenstates of the Hamiltonian (in Fock space) $\{|\lambda\rangle\}$ in the definition of $G(t)$. The result is:

$$\begin{aligned} G(t) &= \frac{i}{Z}\sum_m \langle\lambda_m| e^{-\beta H}\left[e^{itH}Oe^{-itH}, O\right]|\lambda_m\rangle \\ &= \frac{i}{Z}\sum_{m,n}\Big[\langle\lambda_m| e^{-\beta H}e^{itH}Oe^{-itH}|\lambda_n\rangle\langle\lambda_n|O|\lambda_m\rangle \\ &\qquad - \langle\lambda_m| e^{-\beta H}O|\lambda_n\rangle\langle\lambda_n| e^{itH}Oe^{-itH}|\lambda_m\rangle\Big] \\ &= \frac{i}{Z}\sum_{m,n} O_{mn}O_{nm}\, e^{-\beta E_m}\left[e^{-it(E_n-E_m)} - e^{it(E_n-E_m)}\right] \\ &= \frac{2i}{Z}\sum_{m,n} O_{mn}O_{nm}\, e^{-\beta(E_n+E_m)/2}\sinh(\tfrac{\beta E_{nm}}{2})e^{-iE_{nm}t}, \end{aligned} \tag{176}$$

while for $G_E(t)$ we have instead:

$$\begin{aligned} G_E(\tau) &= \frac{1}{Z}\sum_m \langle\lambda_m| e^{-\beta H}e^{\tau H}Oe^{-\tau H}O|\lambda_m\rangle \\ &= \frac{1}{Z}\sum_{m,n} O_{mn}O_{nm}e^{-\beta E_m}e^{-\tau(E_n-E_m)} \\ &= \frac{1}{Z}\sum_{n,m} O_{mn}O_{nm}\, e^{-\beta E_m}e^{-E_{nm}\tau}, \end{aligned} \tag{177}$$

where we have used the shorthand notation:

$$E_{nm} = E_n - E_m, \qquad O_{nm} = \langle n|O(0)|m\rangle. \tag{178}$$

Using the formulas above, we can express the retarded correlator as[1]:

$$\begin{aligned} G_R(\omega) = -\frac{1}{Z}\sum_{n,m}\frac{O_{mn}O_{nm}}{\pi(\omega - E_{nm})}e^{-\beta(E_n+E_m)/2}\sinh(\tfrac{\beta E_{nm}}{2}) + \\ \frac{i}{Z}\sum_{n,m} O_{mn}O_{nm}e^{-\beta(E_n+E_m)/2}\sinh(\tfrac{\beta\omega}{2})\delta(\omega - E_{nm}), \end{aligned} \tag{179}$$

and similarly for the spectral function $\rho(\omega)$ with $\omega \in \mathbb{R}$, we obtain:

$$\frac{\rho(\omega)}{2\sinh\frac{\beta\omega}{2}} = \frac{1}{Z}\sum_{m,n} O_{mn}O_{nm}e^{-\beta(E_n+E_m)/2}\delta(\omega - E_{nm}). \tag{180}$$

Note that if we take the imaginary part of $G_R(\omega)$ we can recover formula (180).

1 Note the formula $\frac{i}{2\pi}\int_{-\infty}^{\infty}\exp(i\omega t)\exp(-iat)\,\theta(t) = \frac{i}{2}\delta(\omega - a) - \frac{1}{2\pi(\omega - a)}$.

Finally, it is easy to verify, using Eq. (177) and (180), that in configuration space, the Euclidean correlator is obtained from ρ via:

$$G_E(\tau) = \int_0^\infty \mathrm{d}\omega\, \rho(\omega) \frac{\cosh \omega(\frac{\beta}{2} - \tau)}{\sinh \beta\omega/2}. \tag{181}$$

In this equation we can see the Euclidean correlator expressed in terms of the spectral function. This relation will be the starting point for the analysis in the following chapter, where a Bayesian method will be used to reconstruct ρ from the Monte Carlo data on G_E. This will allow for an estimate for the conductivity σ using Eq. (164).

MAXIMUM ENTROPY METHOD

In this chapter, we present the numerical and statistical methods used to obtain the spectral function from the Euclidean correlator, available from lattice QCD. Firstly, we will give an introduction on the so-called inversion problems and what are the challenges involved. Then we will introduce the Bayesian probabilistic approach called Maximum Entropy Method (MEM), which is widely used in this thesis.

4.1 AN INTRODUCTION ON INVERSE PROBLEMS

When we study a physical process, a mathematical description is developed in order to be able to make useful predictions on other observables, described by the same laws of physics. This description often consists of a set of equations, e.g. ordinary and partial differential equations or integral equations, featuring a certain number of parameters. Depending on the nature of the process being analysed, this modelling procedure falls into three distinct classes [65, 66]:

1. Direct Problem: from the input and the parameters, find out the output of the model;
2. Reconstruction Problem: starting from the parameters and the output, recover the original input;
3. Identification Problem: knowing the input and the output, extract the parameters which best describe the relation between input and output.

The first case is called "direct" since it is oriented along a cause-effect sequence. For the opposite reason, the second and third type of problems are called "inverse" problems and they aim at reconstructing unknown causes from known consequences. A unified description for the modelling of the many inverse problems can be achieved by introducing the following notation. We call $\mathbb{X}$ the space of input, $\mathbb{Y}$ the space of output or data, $\mathbb{P}$ the space of system parameters and $\mathbb{A}_p$ the linear or non-linear space of operators from $\mathbb{X}$ to $\mathbb{Y}$ associated with $p \in \mathbb{P}$. Using this notation we can reformulate the problems above as:

1. given $x \in \mathbb{X}$ and $p \in \mathbb{P}$, find $y = A_p(x)$;
2. given $y \in \mathbb{Y}$ and $p \in \mathbb{P}$, find $x \in \mathbb{X}$ which solves $A_p(x) = y$;
3. given $y \in \mathbb{Y}$ and $x \in \mathbb{X}$, find $p \in \mathbb{P}$ such that $A_p(x) = y$.

Note that there are cases where the inverse problem can be formally cast into a direct one. For example, if the inverse of A_p is known and is a linear operator, then the problem is solved by $x = A_p^{-1}y$. However, the explicit determination of the inverse does not help if the output y is not in the domain of the definition of A_p^{-1}. This situation is typical in applications due to the fact that the output may be only imprecisely known and distorted by noise.

As one can imagine, depending on the number of parameters appearing in the model, different scenarios can open up. When this number is much greater than the data points, then it is either impossible to find a solution or many degenerate ones appear, making it difficult to find out what features of the solution follow from the data and which ones are just artefacts of the particular model. Even when the number of parameters is less than or equal to the data, but the problem is ill-posed, the inversion procedure can become unstable, preventing any sensible solution being found. In this regard, let us give a rigorous definition of an ill-posed problem, introduced by Jacques Hadamard [67]:

Definition Giving a mapping $A : \mathbb{X} \to \mathbb{Y}$, the equation

$$A(x) = y \tag{182}$$

is *well-posed* provided that

1. (existence) for each $y \in \mathbb{Y}$, $\exists\, x \in \mathbb{X}$ such that $A(x) = y$;
2. (uniqueness) $A(x_1) = A(x_2) \to x_1 = x_2$;
3. (stability) A^{-1} is continuous.

Equation Eq. (182) is ill-posed if it is not well-posed.

Frequently inverse problems are ill-posed because the forward operator A_p is smoothing, in the sense that details (small scale structures) are attenuated by the forward mapping. This means that the reconstruction must involve some sort of deregularization, whose main drawback is a loss of uniqueness: different causes can produce almost the same effects. Another case is when y is obtained from numerical simulations or from experiments, in which case it is inevitability discretised and affected by an error ϵ. Knowledge of the probability distribution function $\rho_\epsilon(y)$ is essential to estimate the error in the results. Typically, for a lattice QCD simulation we have a Gaussian distribution function, i.e.

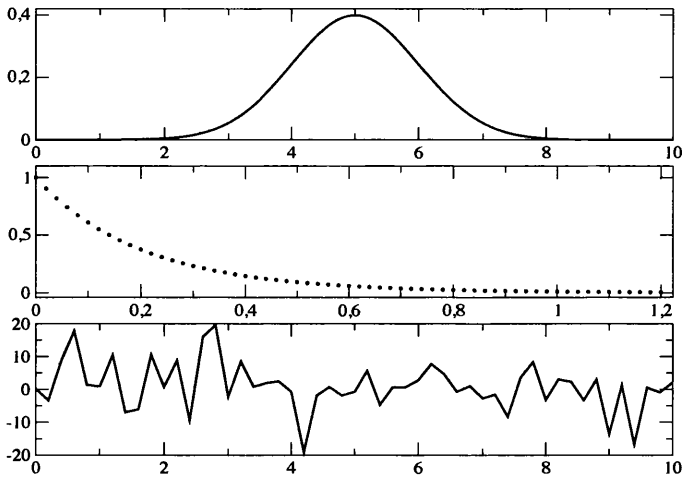

Figure 11: The original function (top), its Laplace transform (center), and the estimator obtained by solving the inverse problem (bottom). From this example, it is clear the meaning of ill-posedness. Picture from [66].

$\rho_\epsilon(y) \sim e^{-\left(\frac{y-\bar{y}}{\epsilon}\right)^2}$, where $\bar{y}$ is an estimation of the "exact" value. This difficulty is accentuated when the problem is unstable. In all the above cases, one should make use of any available a priori information on the space of models, e.g. some physical constraints.

In the following we will focus on one of the most important and widely known inverse problems. On a functional space of normalizable functions $x(\omega)$, the Fredholm integral equation of the first kind is defined as:

$$y(\tau) = \int_{-\infty}^{+\infty} d\omega K(\tau, \omega) x(\omega), \tag{183}$$

where $K(\tau, \omega)$ is the integral kernel of the aforementioned operator A.

Let us consider the inverse Laplace transform as a simple prototype for an ill-posed problem and show more concretely the difficulties mentioned above. It is defined as:

$$y(\tau) = \int_{0}^{+\infty} d\omega e^{-\tau\omega} x(\omega). \tag{184}$$

The latter can also be seen as a problem of analytical continuation. Let us instead consider the Fourier transform:

$$y(t) = \int_{-\infty}^{+\infty} d\omega e^{-it\omega} x(\omega). \tag{185}$$

Now, suppose that it can be analytically continued to define a function $y(z)$ of the complex variable $z = \tau + it$. If we restrict it to the real axis

$z = \tau$, the Laplace transform in Eq. (184) can be recovered. The function $x(\omega)$ can then be calculated by either an inverse Fourier transform from $y(t)$, which is known to be better behaved, or an inverse Laplace transform from $y(\tau)$, which is ill-defined. Since in most cases only $y(\tau)$ is available, we are forced to follow the second choice, where the kernel $K(\tau, \omega)$ has an exponential behaviour, the source of the numerical instability. In Fig. (11) is shown a naive attempt to make a numerical inverse Laplace transform of a Gaussian function knowing its Laplace transform at discretised points [66].

The example above shows the difficulties that the numerical analytical continuation to imaginary time poses. In order to make contact with the physics addressed in the previous chapter, let us rename $x \to \rho$ in Eq. (183) and consider a kernel of the form:

$$K(\tau, \omega) = \frac{\cosh \omega(\beta/2 - \tau)}{\sinh \beta\omega/2} . \tag{186}$$

If we also restrict the integral in Eq. (183) to positive frequencies, we recover Eq. (181), which we rewrite here for convenience:

$$G_E(\tau) = \int_0^\infty d\omega \, \rho(\omega) \frac{\cosh \omega(\frac{\beta}{2} - \tau)}{\sinh \beta\omega/2} . \tag{187}$$

The data is represented by the Euclidean correlator $G_E(\tau)$ obtained by a Monte Carlo simulation and thus affected by statistical error. $G_E(\tau)$ is provided for a discrete set of points, $\tau = \tau_i$, with $1 \leq \tau_i \leq N_\tau$, where N_τ is the number of the temporal lattice sites. Note that, during the analysis, a number of different subsets $\tau \in [\tau_{min}, \tau_{max}]$ might be considered. The aim will be the reconstruction of the spectral function ρ, which is in principle a continuous function. This falls into the class of ill-posed problems described above, where the number of data points is much smaller than the number of degrees of freedom to be reconstructed.

One possible approach is to perform a standard likelihood analysis based on strong assumptions on the shape of the spectral function, see e.g. [36, 39, 68]. Although reasonable in principle, this choice can present a few drawbacks, i.e. poor stability against a change in the number of parameters and the impossibility to study the fine structure of the spectral function.

The Maximum Entropy Method (MEM), discussed in the next section, represents another way to circumvent these problems. It is based on the method of statistical inference and reconstructs the most probable spectral function given some prior information on its properties and compatible with the available data.

4.2 BAYESIAN INFERENCE

In this section we review the Bayesian method used to reconstruct the spectral function ρ from Eq. (187). The starting point is the concept of Bayesian inference. Consider a probability space composed by a space of events Ω and a probability measure P. Given two possible events A, H, the conditional probability $P(A|H)$ is the probability that A happens, knowing that H has already happened. This is formally defined as:

$$P(A|H) \equiv \frac{P(A \cap H)}{P(H)}, \tag{188}$$

where $P(H)$ is the probability of H, $P(A \cap H)$ is the joint probability function for A and H. Since $P(A \cap H) = P(H \cap A)$, we can deduce that $P(A|H)$ and $P(H|A)$ are related as

$$P(H|A) = P(A|H)\frac{P(H)}{P(A)}, \tag{189}$$

which shows that the symbol $|$ is not symmetric in general. Consider a complete and mutually exclusive set[1] of events $\{A_i\}$, the probability of event H is:

$$P(H) = P(1 \cap H) = P((\cup_i A_i) \cap H) = \sum_i P(A_i \cap H), \tag{190}$$

and from the definition of conditional probability

$$P(H) = \sum_i P(A_i)P(H|A_i)\,. \tag{191}$$

Consider a specific set A_k. Then Bayes's formula is:

$$P(A_k|H) = \frac{P(A_k)P(H|A_k)}{Z}, \quad Z = \sum_i P(A_i)P(H|A_i)\,. \tag{192}$$

We will use the following notation:

- D will represent the data, affected by an error, as obtained from a Monte Carlo simulation of lattice QCD;
- H will summarize all the prior knowledge we have on the spectral function, e.g. $\rho(\omega \geq 0) \geq 0$.

1 Consider two events A and B such that $A \bigcap B = \varnothing$. They are two mutually exclusive events if $P(A \bigcap B) = P(\varnothing) = 0$. Thus, a complete and mutually exclusive set of events A_i with $i = 1, \ldots, n$ is such that $A_i \bigcap A_j = \varnothing$, $\forall i \neq j$ and $\bigcup_{i=1}^{n} A_i = \Omega$.

We can apply Bayes theorem in the context of statistical inference, by expressing the conditional probability of having a particular $\rho(\omega)$ as:

$$P[\rho|DH] = \frac{P[D|\rho H]P[\rho|H]}{P[D|H]}, \tag{193}$$

from which the most probable spectral function is obtained by maximization:

$$\frac{\delta P[\rho|DH]}{\delta \rho} = 0. \tag{194}$$

The meaning of the terms in Eq. (193) is:

- $P[D|\rho H]$ is the standard likelihood function,
- $P[D|H]$ is a normalization constant, which does not depend on the spectral function $\rho(\omega)$,
- $P[\rho|H]$ is called the prior probability and it is what differentiates the various algorithms based on Bayesian inference.

According to the central limit theorem, we expect the data obtained from a Monte Carlo simulation to follow the Gaussian distribution:

$$P[D|\rho H] = \frac{1}{Z_L} e^{-L}. \tag{195}$$

Here Z_L is a normalization constant and L is the likelihood function defined as

$$L = \frac{1}{2}\sum_{i,j}(G_E(\tau_i) - G_\rho(\tau_i))C_{ij}^{-1}(G_E(\tau_j) - G_\rho(\tau_j)), \tag{196}$$

where G_E is the average correlator from the Monte Carlo simulation, while G_ρ is the one obtained from the reconstructed spectral function using Eq. (187). The indices i and j run over the N Euclidean data points considered in the analysis:

$$N = \tau_{max} - \tau_{min}. \tag{197}$$

The $N \times N$ covariance matrix C, encodes the correlations in the data at different τ's and it is defined as:

$$C_{ij} = \frac{1}{N_{\text{CFG}}(N_{\text{CFG}}-1)} \sum_{m=1}^{N_{\text{CFG}}} (G_E^m(\tau_i) - G_E(\tau_i))(G_E^m(\tau_j) - G_E(\tau_j)), \tag{198}$$

where N_{CFG} is the number of available gauge configurations, and G_E^m is the correlator corresponding to the $m-$th configuration. The normalization constant Z_L is such that the integration of $P[D|\rho H]$ over D with the measure:

$$[dD] \equiv \prod_{i=\tau_{min}}^{\tau_{max}} dG_E(\tau_i), \tag{199}$$

is normalized to unity, yielding $Z_L = (2\pi)^{N/2}\sqrt{\det C}$. If only the term Eq. (195) appeared in Eq. (193), i.e. if $P[\rho|H]$ was constant, maximizing $P[\rho|DH]$ would be equivalent to maximizing Eq. (195) with respect to ρ, which is the standard χ^2-fitting.

4.3 SHANNON-JAYNES ENTROPY

In order to overcome the difficulties due to the ill-posedness of the problem, the prior probability must be taken into account. In the MEM, this is defined as:

$$P[\rho|H] = \frac{1}{Z_S} e^{\alpha S}, \tag{200}$$

where S is a functional called entropy, while α is a real parameter which balances the relative weight between the entropy and the likelihood function L of equation Eq. (195). This parameter will later be integrated out, so that the final result will not depend on it.

The entropy S assigns a real number $S[\rho]$ to each spectral function, which is here regarded as a positive semi-definite distribution. In order to explain the role of S, let us consider two different spectral functions ρ_1 and ρ_2. The entropy is such that if $S[\rho_1] > S[\rho_2]$, then ρ_1 has less information than ρ_2. The functional form of the entropy is justifiable by an axiomatic construction, extensively studied in [69], to which we refer for more details. Here we justify our choice for the entropy using an argument based on the law of large numbers (see the *monkey argument* in e.g. [70–72]).

Let us consider a discretised space of event composed of N cells. Suppose that M balls are thrown, where M is assumed to be large. As a result, there are now n_i balls in the i-th cell, which has probability p_i to receive a ball. We can write down the expectation value λ_i for the number of balls in the i-th cell as

$$\lambda_i = Mp_i \quad \text{with} \sum_{i=1}^{N} \lambda_i = M. \tag{201}$$

In the large M limit, the Poisson distribution $P_{\lambda_i}(n_i)$ describes the probability that the i-th cell receives n_i balls. A particular combination $\vec{n} = (n_1, n_2, \cdots, n_N)$ is then realized with probability:

$$P_{\vec{\lambda}}(\vec{n}) = \prod_{i=1}^{N} P_{\lambda_i}(n_i) = \prod_{i=1}^{N} \frac{\lambda_i^{n_i}\, e^{-\lambda_i}}{n_i!}, \tag{202}$$

where the normalization is given by $\sum_{n_i=0}^{\infty} P_{\lambda_i}(n_i) = 1$ $(i = 1, 2, \cdots, N)$. In order to make contact with physics, we reinterpret the number of balls n_i as the spectral function $\rho(\omega)$:

$$\rho_j \equiv \rho(\omega_j)\Delta\omega = q\, n_j, \quad \text{with } \omega_j \equiv j\Delta\omega, \tag{203}$$

where we allowed for a proportionality coefficient q and the frequency ω has been discretized into $N_\omega \equiv N$ bins of equal size $\Delta\omega$. We also introduce the so-called *default model* $m(\omega)$ as:

$$m_i \equiv m(\omega_i)\Delta\omega = q\lambda_i\,, \tag{204}$$

which then represents our expectations H on the spectral function. The probability to obtain a certain spectral function in a domain V is then:

$$P[\rho|H] = \sum_{\vec{n}\in V} P_{\vec{\lambda}}(\vec{n}) \simeq \int_V \frac{\prod_{i=1}^N \mathrm{d}\rho_i}{q^N} \prod_{i=1}^N \frac{\lambda_i^{n_i}\, e^{-\lambda_i}}{n_i!} \tag{205a}$$

$$\simeq \int_V \prod_{i=1}^N \frac{\mathrm{d}\rho_i}{\sqrt{\rho_i}} \frac{e^{S[\rho]/q}}{(2\pi q)^{N/2}}, \tag{205b}$$

where we have traded the sum for an integral and used the Stirling's formula, $n! \simeq \sqrt{2\pi n} e^{n\log n - n}$ to approximate the factorial. In Eq. (205b), $S[\rho]$ represents then the so-called *Shannon-Jaynes* entropy:

$$S[\rho] = \sum_{i=1}^{N_\omega} \left[\rho_i - m_i - \rho_i \log\left(\frac{\rho_i}{m_i}\right)\right]. \tag{206}$$

Comparing Eq. (200) with (205b), we set $q = \alpha^{-1}$ and the integration of $P[\rho|H]$ over ρ is done using the measure $[\mathrm{d}\rho]$ with the corresponding normalization factor Z_S:

$$[\mathrm{d}\rho] \equiv \prod_{l=1}^{N_\omega} \frac{\mathrm{d}\rho_l}{\sqrt{\rho_l}}, \quad Z_S \simeq \left(\frac{2\pi}{\alpha}\right)^{\frac{N_\omega}{2}}. \tag{207}$$

This concludes our derivation for the prior probability used in this work. In the next section, more details about the overall MEM procedure will be given.

4.4 MEM AND BRYAN'S METHOD

The MEM reconstruction is composed of three main steps, described as follows. We call ρ_α the most probable spectral function for a given α (and default model m) and it is obtained by maximizing $P[\rho|DH]$, which combining Eqs. (193), (195) and (200) becomes:

$$P[\rho|DH] \propto \frac{1}{Z_S Z_L} \exp Q[\rho]\,, \quad Q[\rho] \equiv \alpha S - L\,, \tag{208}$$

so that ρ_α satisfies:

$$\left.\frac{\delta Q}{\delta\rho(\omega)}\right|_{\rho=\rho_\alpha} = 0\,. \tag{209}$$

Note that, if the solution ρ_α exists, it can be proven to be unique [69]. As already mentioned above, the parameter α controls the relative weight of the entropy S (which tends to fit ρ to the default model m) and the likelihood function L (which tends to fit ρ to the lattice data D). In the absence of lattice data, the correct spectral function would be, by definition, the default model. In order to produce a result independent of α, we follow here Bryan's method [73]. Let us write explicitly the dependence on α, m in the prior knowledge H by rewriting $P[\ldots|H] \equiv P[\ldots|H\alpha m]$. Bryan's prescription is to express the final result as a weighted average over α:

$$\rho_{\text{out}}(\omega) = \int \mathrm{d}\alpha \; \rho_\alpha(\omega) \; P[\alpha|DHm] \; . \tag{210}$$

The posterior probability $P[\alpha|DHm]$ can be evaluated using Bayes' theorem iteratively. First we use it to rewrite $P[\alpha|DHm]$ as:

$$P[\alpha|DHm] = \frac{P[D|H\alpha m]P[\alpha|Hm]}{P[D|Hm]} \, , \tag{211}$$

and then we use it again to write the following identity:

$$P[\rho|DH\alpha m]P[D|H\alpha m] = P[D|\rho H\alpha m]P[\rho|H\alpha m] \, , \tag{212}$$

from which we can extract $P(D|H\alpha m)$ by integrating over ρ:

$$\begin{aligned} P[D|H\alpha m] &= \int [\mathrm{d}\rho] P[\rho|DH\alpha m]P[D|H\alpha m] \\ &= \int [\mathrm{d}\rho] P[D|\rho H\alpha m]P[\rho|H\alpha m] \, . \end{aligned} \tag{213}$$

Inserting Eq. (21

$$\begin{aligned} &= \int [\mathrm{d}\rho] P[D|\rho H\alpha m]P[\rho|H\alpha m] \, . \\ P[\alpha|DHm] &= \int [\mathrm{d}\rho] P[\alpha|Hm] \frac{P[D|\rho H\alpha m]P[\rho|H\alpha m]}{P[D|Hm]} \\ &\propto P[\alpha|Hm] \int [\mathrm{d}\rho] \, \frac{1}{Z_S Z_L} \exp Q[\rho] \, . \end{aligned} \tag{214}$$

Now if we assume that the integrand in Eq. (214) is sharply peaked around $\rho_\alpha(\omega)$, which should be satisfied for data with small errors, then the integral can be performed with a saddle point approximation. In Eq. (214) we make the change of variables $\rho' = \sqrt{\rho}$, so that we can reabsorb the measure $[\mathrm{d}\rho]$ defined in Eq. (207) as $\mathrm{d}\rho' = \mathrm{d}\rho/2\sqrt{\rho}$. Using the new variable ρ' the integral in Eq. (214) becomes:

$$\int [\mathrm{d}\rho] \exp Q[\rho] = \prod_{l=1}^{N_\omega} \int \mathrm{d}\rho'_l \exp Q[\rho_l(\rho'_l)] \, . \tag{215}$$

Now we can Taylor expand $Q[\rho]$ around ρ_α in the new variable ρ' and obtain (we suppress the suffix l for simplicity):

$$Q[\rho(\rho')] \simeq Q[\rho_\alpha] + \frac{1}{2}\rho'_1 \left.\frac{\delta^2 Q[\rho(\rho')]}{\delta\rho'_1\delta\rho'_2}\right|_{\rho_\alpha} \rho'_2, \tag{216}$$

with

$$\begin{aligned}
\left.\frac{\delta^2 Q[\rho(\rho')]}{\delta\rho'_1\delta\rho'_2}\right|_{\rho_\alpha} &= \left.\frac{\delta\rho'_1}{\delta\rho_1}\frac{\delta^2 Q[\rho]}{\delta\rho_1\delta\rho_2}\frac{\delta\rho'_2}{\delta\rho_2}\right|_{\rho_\alpha} \\
&= -\left.\left[4\sqrt{\rho_1}\left(\frac{\alpha\delta(\rho_1-\rho_2)}{\rho} + \frac{\delta^2 L}{\delta\rho_1\delta\rho_2}\right)\sqrt{\rho_2}\right]\right|_{\rho_\alpha} \\
&= -4\alpha\delta(\rho_1-\rho_2) - 4\left.\left(\sqrt{\rho_1}\frac{\delta^2 L}{\delta\rho_1\delta\rho_2}\sqrt{\rho_2}\right)\right|_{\rho_\alpha} \\
&= -4(\alpha+\Lambda),
\end{aligned} \tag{217}$$

where we have called Λ the real symmetric matrix:

$$\Lambda_{l,l'} \equiv \left.\left(\sqrt{\rho_l}\frac{\delta^2 L}{\delta\rho_l\delta\rho_{l'}}\sqrt{\rho_{l'}}\right)\right|_{\rho=\rho_\alpha}. \tag{218}$$

Finally, inserting Eq. (216) and Eq. (217) into Eq. (214) and performing the gaussian integral, we obtain the final result:

$$P[\alpha|DHm] \propto P[\alpha|Hm] \prod_k \sqrt{\frac{\alpha}{\alpha+\lambda_k}} \exp Q[\rho_\alpha], \tag{219}$$

where the λ_k's are the eigenvalues of the matrix Λ.

The prior probability for α can be chosen by either following Laplace rule ($P[\alpha|Hm] = \text{const.}$) or Jeffreys' rule ($P[\alpha|Hm] = 1/\alpha$) [74]. We choose the former, since it has been checked in [69] that the integral in Eq. (210) does not depend on this choice, as long as the probability is concentrated around its maximum at $\alpha = \hat{\alpha}$.

Numerically, in order to perform the average in Eq. (210), the integral is restricted to a region $[\alpha_{min}, \alpha_{max}]$, chosen to satisfy the criterion $P[\alpha|DHm] \geq 10^{-1} \times P[\hat{\alpha}|DHm]$. The integral is then carried out with a stepsize $\Delta\alpha$ and then normalized so that $\int_{\alpha_{min}}^{\alpha_{max}} d\alpha\, P[\alpha|DHm] = 1$.

In this thesis the error analysis is carried out in two steps. The statistical error is evaluated by producing jackknife ensembles of the final spectral function of Eq. (210), by systematically discarding each gauge configuration. Another source of uncertainty comes from the choice of default model m appearing in the entropy. This systematic error can be estimated by studying the sensitivity of the final results to the variation of m. This will be explained in greater detail later, when the results of this study will be presented in section 6.3.

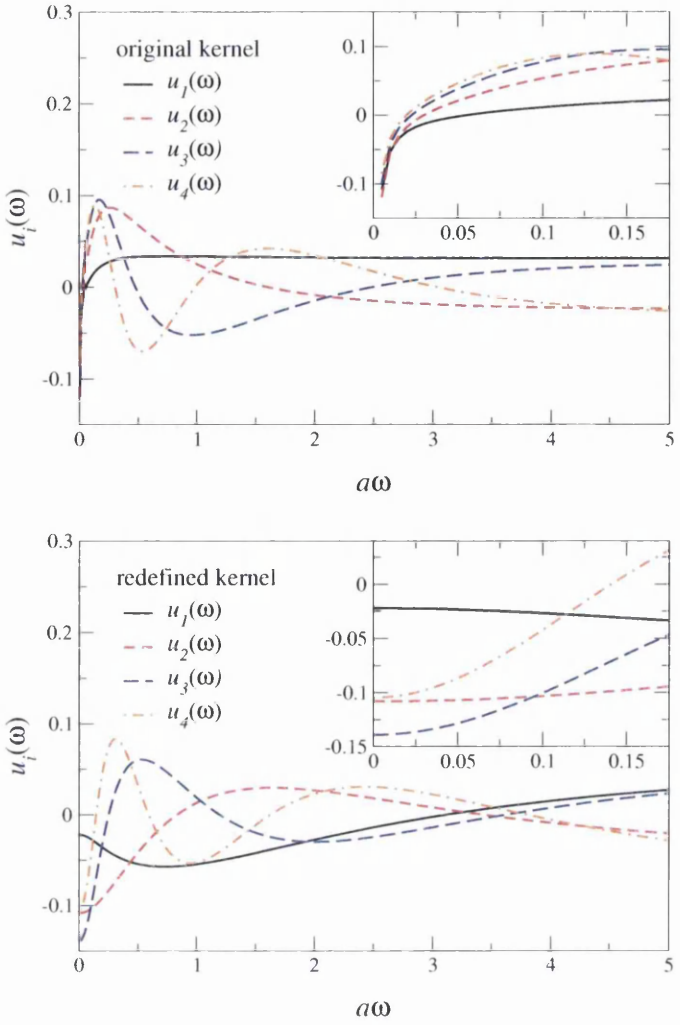

Figure 12: These plots from [40] show the first four basis functions $\vec{u}_i \equiv u_i(\omega)$ of Eq. (228) for $a\omega_{\max} = 5$, $N_\omega = 1000$ and the data comes from a simulation with staggered quarks on a lattice with $N_\tau = 24$. The inset shows a blow-up of the small energy region. On the left, the standard kernel of Eq. (186) is used, while on the right the redefined one of Eq. (235). In the latter case, the inset shows a non-singular behavior for the low-ω region.

4.5 SINGULAR VALUE DECOMPOSITION

The discretised spectral function ρ_l in Eq. (206) is represented by a vector with typically $N_\omega \sim O(10^3)$ degrees of freedom:

$$\omega_l = l\Delta\omega, \quad \rho_l = \rho(\omega_l)\Delta\omega, \qquad \text{with } l \in [0, N_\omega] \tag{220}$$

This makes the location of the global maximum of $Q[\rho]$ non-trivial. In [73] it is shown how this problem can be alleviated by performing

a singular value decomposition (SVD) of the kernel K, which restricts this search to a subspace of $O(10)$ degrees of freedom, compatible with the number N (defined in Eq. (197)) of data points in the correlators. Using Eq. (187), the extremum condition of Eq. (209)

$$\frac{\partial Q}{\partial \rho_l} = \alpha \frac{\partial S}{\partial \rho_l} - \frac{\partial L}{\partial \rho_l} = 0 \tag{221}$$

can be written as:

$$-\alpha \log \frac{\rho_l}{m_l} = \sum_{i=\tau_{min}}^{\tau_{max}} K_{il} \frac{\partial L}{\partial G_\rho^i}, \tag{222}$$

where the kernel is defined as $K_{il} = K(\tau_i, \omega_l)$ and $G_\rho^i = G_\rho(\tau_i)$ is the reconstructed correlator. Since the spectral function is positive semi-definite, it can be parametrized as:

$$\rho_l = m_l \exp a_l \quad \text{with } l \in [0, N_\omega]\,. \tag{223}$$

The solution of Eq. (222) is then represented by the vector $\vec{a}$ in the $N_\omega = O(10^3)$ dimensional space and reads

$$-\alpha \vec{a} = K^t \overrightarrow{\frac{\partial L}{\partial G_\rho}}, \tag{224}$$

where K^t is an $N_\omega \times N$ matrix and $\partial L / \partial G_\rho^i$ is an N dimensional column vector. The solution $\vec{a}$ in Eq. (224) turns out to be confined in a smaller subspace called the *singular subspace*, of dimension $N_s \leq N \ll N_\omega$. This can be shown by decomposing K^t into a product of three matrices with special properties. This procedure is called singular value decomposition and it is defined as

$$\begin{aligned} K^t &= U \,\Xi\, V^t \\ &= \begin{bmatrix} u_{11} & \cdots & u_{1N} \\ \vdots & \ddots & \vdots \\ u_{N_\omega 1} & \cdots & u_{N_w N} \end{bmatrix} \begin{bmatrix} \xi_1 & 0 & \cdots & 0 \\ 0 & \xi_2 & \ddots & \vdots \\ \vdots & \ddots & \ddots & 0 \\ 0 & \cdots & 0 & \xi_N \end{bmatrix} \begin{bmatrix} v_{11} & \cdots & v_{1N} \\ \vdots & \ddots & \vdots \\ v_{N1} & \cdots & v_{NN} \end{bmatrix} \end{aligned} \tag{225}$$

where

- U is an $N_\omega \times N$ matrix, with $U^t U = \mathbb{1}$,
- V is an $N \times N$ matrix, with $V^t V = \mathbb{1}$,
- Ξ is an $N \times N$ diagonal matrix.

The entries ξ_i of Ξ are called the singular values of K^t and they are also equivalently defined as the square root of the eigenvalues of the matrix $(K^t)^\dagger K^t$. They are positive semi-definite and can be ordered by their magnitude so that:

$$\xi_1 \geq \xi_2 \geq \ldots \geq \xi_{N_s} > \xi_{N_{s+1}} = \ldots = 0\,, \tag{226}$$

with

$$N_s \equiv \text{rank}[K^t] \leq N \leq N_\tau. \tag{227}$$

For the kernel appearing in Eq. (186), the singular values ξ_j are all non-zero but they are exponentially smaller as j increases. In this case the singular space can be defined as the space spanned by the first N_s columns of U. Then the SVD admits as a basis the collection of vectors $\{\vec{u}_1, \vec{u}_2, \ldots, \vec{u}_{N_s}\}$, where each entry is made up of N_ω components, i.e. $\vec{u}_i = (u_{i_1}, u_{i_2}, \ldots, u_{i_{N_\omega}})^t$. Since the vector $\vec{a}$ lies in the singular space, as one can read off from Eq. (224), it can be parametrized by the N_s coefficients $(b_1, \ldots, b_{N_s})$ as

$$\vec{a} = \sum_{i=1}^{N_s} b_i \vec{u}_i, \quad \text{or equivalently } a_l = \sum_{i=1}^{N_s} U_{li} b_i\,. \tag{228}$$

Since the matrix U is orthogonal, Eq. (224) can be simplified as

$$-\alpha\vec{b} = \vec{g} \equiv \Xi'\, V'^t \overrightarrow{\frac{\partial L}{\partial G_\rho}} = \Xi'\, V'^t C^{-1}(G_\rho - G_E)\,, \tag{229}$$

where Ξ' and V' are obtained by restricting Ξ and V respectively to the singular space, C is the covariance matrix of Eq. (198) and G_E is the Monte Carlo data.

A Newton search method is implemented to solve Eq. (229). The increment is given by

$$J\,\delta\vec{b} = -\alpha\vec{b} - \vec{g}, \quad \text{with} \quad J_{ij} = \alpha \mathbb{1}_{ij} + \frac{\partial g_i}{\partial b_j}\,. \tag{230}$$

By using the chain rule and the identity $\partial\rho/\partial b = \text{diag}[\rho]\, U$, we have

$$\frac{\partial g_i}{\partial b_j} = \Xi'\, V'^t C^{-1} \frac{\partial G_\rho}{\partial \rho} \frac{\partial \rho}{\partial b_j} = \Xi'\, V'^t C^{-1} K\, \text{diag}[\rho]\, U = MT\,, \tag{231}$$

with

$$M = \Xi'\, V'^t C^{-1} V' \Xi' \quad \text{and} \quad T = U^t\, \text{diag}[\rho]\, U\,, \tag{232}$$

so that Eq. (230) is rewritten as

$$[(\alpha + \mu)\, I + MT]\, \delta\vec{b} = -\alpha\vec{b} - \vec{g}\,. \tag{233}$$

In the last equation, an artificial parameter μ has been added, whose increase normally produces a decrease in $\delta\vec{b}$. This trick was introduced by Marquardt and Levenberg and it ensures that, at each iteration, $\delta\vec{b}$ remains small enough so that the lowest order approximation used in Eq. (230) remains valid.

4.6 MODIFICATION OF BRYAN'S ALGORITHM

In the analysis we will present in this thesis, the default model is represented by the function

$$m(\omega) = m_0\omega(b+\omega)\,, \tag{234}$$

where m_0 is a channel dependent constant and b is a parameter which allows for a non-zero value for $\rho(\omega)/\omega$ at small energies. Choosing different values for b will represent an important way to probe the systematics of the method. The funcional form in Eq. (234) is motivated by the large-ω behaviour of the mesonic spectral function, which can be evaluated in perturbation theory.

The kernel in Eq. (186) has a singular behaviour at small frequencies. This is shown in Fig. 12 from [40], where the first basis functions $\vec{u}_i$ of Eq. (228) are plotted. This leads to numerical instabilities when the Bryan method is adopted [40]. These can be cured by a redefinition of the integrands in Eq. (187) as

$$\overline{K}(\omega,\tau) = \frac{\omega}{2T}K(\omega,\tau), \qquad \overline{\rho}(\omega) = \frac{2T}{\omega}\rho(\omega), \tag{235}$$

such that $K(\omega,\tau)\rho(\omega) = \overline{K}(\omega,\tau)\overline{\rho}(\omega)$. This does not affect the identification of the dimension of the subspace for the SVD, but indeed the new basis functions $\vec{\overline{u}}_i$ are well behaved at small ω.

In chapter 6, a version of MEM, based on the code developed by J. Clowser and C. Allton [75], will be used to evaluate the conductivity of the quark-gluon plasma using Eq. (164) and data from lattice QCD simulations, which will be presented in chapter 5.

5

LATTICE QCD CALCULATIONS

In this chapter we will report on numerical lattice QCD calculations for the electromagnetic current introduced in Eq. (152). These will be done using gauge ensembles with different temperatures and volumes, which have been produced by a previous study [9, 10]. In the first part, we will give some details about the lattice action used for the generation of the gauge configurations. We will then describe the lattice operator used for the electromagnetic current and we will discuss the issues of renormalization and improvement. The measured Euclidean correlators are then presented and discussed.

In the following, we will refer to a site on the lattice by either using its positional vector x_μ, i.e. a tuple of 4 coordinates, or by labelling each site with an integer $n \in [1, N_V]$ which uniquely identifies it. When no ambiguity can occur, the two notations will be used interchangeably. Moreover, the 0-th component of a Lorentz vector x_0 will be the temporal one, while the spatial ones are usually indicated by a Latin subscript x_i with $i = 1, 2, 3$.

5.1 LATTICE ACTION

In section 1.5, we mentioned the possibility of having a different lattice spacing in the spatial and temporal directions. Using a finer temporal lattice spacing provides a better temporal resolution for the correlation functions without increasing too much the computational cost.

On a practical level, the anisotropy is achieved by assigning a different coefficient to the time-like and space-like terms in the action. This can be done by introducing new bare parameters in the action, which will be described later in this section. Tuning these parameters is a non-trivial task, which has been achieved in [9, 10], where a detailed explanation is provided.

The gauge dynamics is controlled by a Symanzik-improved action, which is defined by [76]:

$$S_G = \frac{6}{g^2}\left(\frac{1}{\gamma_g}\frac{5\Omega_{\text{sp}}}{3u_s^4} + \gamma_g\frac{4\Omega_{\text{tp}}}{3u_s^2u_t^2} - \frac{1}{\gamma_g}\frac{\Omega_{\text{sr}}}{12u_s^6} - \gamma_g\frac{\Omega_{\text{str}}}{12u_s^4u_t^2}\right), \qquad (236)$$

γ_g	4.3	a_s [fm]	0.1227(8)
γ_f	3.4	a_τ [fm]	0.03506(23)
c_t	0.9027	a_s^{-1} [GeV]	1.608(10)
c_s	1.5893	a_τ^{-1} [GeV]	5.63(4)
$m_{u,d}$	−0.0840	ξ	3.5
m_s	−0.0743	M_π/M_ρ	0.446(3)

Table 1: The parameters in the action (238).

where g is the gauge coupling of Eq. (81), u_s and u_t are the tadpole improvements and γ_g is the bare gauge anisotropy, which will be discussed later. The gluonic fields are represented by the variables

$$\Omega_C = \frac{1}{3}\sum_C \mathrm{Re\ Tr}(1 - W_C)\,, \tag{237}$$

where W_C denotes the path-ordered product of the gauge links along a closed contour C on the lattice. In particular, Ω_{sp} and Ω_{tp} are respectively the spatial and temporal plaquettes already introduced in section 1.5 (see Fig. 3). Additionally, we include planar 2×1 spatial rectangular loops denoted by Ω_{sr} and short temporal rectangles (one temporal link, two spatial), denoted by Ω_{str}. This action has a leading discretization error of $O(a_s^4, a_t^2, \alpha_s a_s^2)$ and it was used in [76] for a glueball study, to which we refer for more details.

Here we mention that the tadpole parameters $u_{s,t}$ are a mean-field improvement, which provides a better mapping of the lattice gauge fields to their analogues in the continuum. This has been introduced by Lepage and Mackenzie in [77] and it is achieved by separately renormalizing the spatial and temporal link variables $U_j(x) \to U_j(x)/u_s$ and $U_t(x) \to U_t(x)/u_t$. In our work u_t is fixed to 1 and u_s is tuned non-perturbatively. A gauge-invariant definition for u_s is given in terms of the mean spatial plaquette as $u_s = \langle \frac{1}{3}\mathrm{ReTr}U_{ss'}\rangle^{1/4}$. One starts with a guess $u_s = 1$ in the action, measures it in a simulation and then readjusts the input value accordingly, until the input value matches the measured one. This has been done in [9] with the result $u_s = 0.7336$.

In the fermion sector, we use a clover improved action with $N_f = 2 + 1$ flavors and stout-smeared links. The Dirac operator of Eq. (74) is defined as:

$$D[U] = m_0 + \gamma_0 \hat{W}_0 + \frac{1}{\gamma_f}\sum_i \gamma_i \hat{W}_i \tag{238a}$$

$$- \frac{c_t}{2}\sum_i \sigma_{0i}\hat{F}_{0i} - \frac{c_s}{2\gamma_g}\sum_{i<j}\sigma_{ij}\hat{F}_{ij}\,. \tag{238b}$$

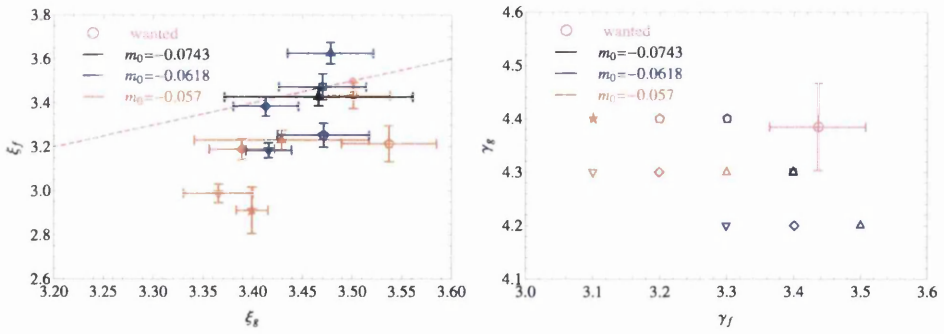

Figure 13: Plots from [9]. Renormalized gauge ξ_g and fermion ξ_f anisotropies (left) and the corresponding bare parameter $\gamma_{g,f}$ (right). These are tuned in order to obtain a target anisotropy of $\xi = \xi_f = \xi_g = 3.5$ (black symbols), which is achieved by using the bare parameters $\gamma_g = 4.3$ and $\gamma_f = 3.4$, with a bare mass of $m_0 = -0.0743$.

In the following, we will describe some its features. In Eq. (238a) we have the usual dimensionless Wilson operator

$$\hat{W}_\mu = \hat{\nabla}_\mu - \gamma_\mu \hat{\Delta}_\mu / 2 \,, \tag{239}$$

where

$$\hat{\nabla}_\mu f(x) = \frac{U_\mu(x) f(x+\mu) - U_\mu^\dagger(x-\mu) f(x-\mu)}{2} \tag{240a}$$

$$\hat{\Delta}_\mu f(x) = U_\mu(x) f(x+\mu) + U_\mu^\dagger(x-\mu) f(x-\mu) - 2 f(x) \,. \tag{240b}$$

The operators appearing in Eq. (238b) are the clover terms of Eq. (99) already described in section 1.5, with $\sigma_{\mu\nu} = \frac{i}{2}[\gamma_\mu, \gamma_\nu]$ and $\hat{F}_{\mu\nu}$ the lattice version of the field strength tensor. The parameters in front of the time-like and space-like clover terms c_t and c_s have been chosen with tree-level conditions as described in [78]. The numerical estimate used in the simulations is shown in Table 1.

In Eqs. (236), (238a) and (238b) we can see the appearance of the bare gauge (γ_g) and fermion (γ_f) anisotropies, which are the ones responsible for the lattice anisotropy. The strategy followed in [9, 10] is to tune them simultaneously in order to obtain a desired value for the renormalized anisotropy ξ. This is defined as the ratio of the lattice spacing in the spatial and temporal directions and it is a function of all the bare parameters of the action:

$$\xi(m_o, \gamma_f, \gamma_g) \equiv \frac{a_s}{a_\tau} \,. \tag{241}$$

They have been tuned non-perturbatively in [9] with a target value for the anisotropy of $\xi = 3.5$. In Fig. (13) taken from [9], we can see the results for the tuning of the anisotropy parameters. Since the anisotropy

is one of the novelties of this work, we will briefly outline the procedure in the following.

The bare fermion anisotropy γ_f, which gives a different weight to the spatial and temporal Wilson term, is tuned by restoring on the lattice the mesonic dispersion relation

$$E(\vec{p})^2 = m^2 + \frac{\vec{p}^2}{\xi_f^2}, \tag{242}$$

where the energy E and the mass m are in units of a_t, and $\vec{p} = 2\pi\vec{n}/L_s$, with L_s the spatial lattice size, is in units of a_s. The parameter ξ_f is the normalized fermion anisotropy, i.e. the anisotropy felt by the fermionic fields. It must be equal to the desired value for the lattice anisotropy $\xi \equiv a_s/a_\tau$. This has been done in [10], with a resulting bare fermion anisotropy of $\gamma_f = 3.4$.

The bare gauge anisotropy γ_g assigns a different gauge coupling to spatial and temporal Wilson loops in the gauge action of Eq. (236). It is tuned by imposing the equivalence between ratios of spatial R_{ss} and temporal R_{st} Wilson loops [79]:

$$R_{ss}(x,y) = \frac{W_{ss}(x,y)}{W_{ss}(x+1,y)} \longrightarrow e^{-a_s V_s(ya_s)}, \tag{243a}$$

$$R_{st}(x,t) = \frac{W_{st}(x,t)}{W_{st}(x+1,t)} \longrightarrow e^{-a_s V_s(ta_t)}. \tag{243b}$$

The renormalized gauge anisotropy ξ_g is obtained by minimizing

$$L(\xi_g) = \sum_{x,y} \frac{(R_{ss}(x,y) - R_{st}(x,\xi_g y))^2}{(\Delta R_s)^2 + (\Delta R_t)^2}, \tag{244}$$

where $\Delta R_{s,t}$ are the errors on $R_{ss,st}$. The parameter γ_g is then tuned to have $\xi_g = \xi = 3.5$. From [10] we use the value $\gamma_g = 4.3$.

In the action Eq. (238), the links U are stout-smeared in the three spatial directions, as described in [80]. The procedure of smearing greatly reduces the mixing with the high frequency modes of the theory and provides significant improvement over actions that explicitly break chiral symmetry [81]. An important property of stout smearing is that it is analytic everywhere and utilizes the exponential function in order to keep the links on the group manifold $SU(3)$ with no projection required. This makes it possible for it to be used in the HMC algorithm for the generation of configurations. Also the smearing does not involve the time direction, leaving the transfer matrix physical. The tuning of the smearing parameters has been done in [82] and the best choice was found to be smearing weight $\rho = 0.14$ and $n_\rho = 2$ iterations.

The strange quark mass parameter is chosen to reproduce the physical strange quark mass and our choice of light quark mass results in

N_s	N_τ	T [MeV]	T/T_c	N_{CFG}	N_{SRC}
24/32	16	352	1.90	1059	4
24	20	281	1.52	1001	4
24/32	24	235	1.27	500	4
24/32	28	201	1.09	502	4
24/32	32	176	0.95	501	4
24	36	156	0.84	501	4
24	40	141	0.76	523	4
32	48	117	0.63	601	4
24	128	43	0.24	401	1

Table 2: A summary of the gauge ensembles used in this work. They have lattice sizes of $N_s^3 \times N_\tau$, with N_{CFG} configurations available for each set and a number of N_{SRC} sources for the analysis. The critical temperature T_c is estimated from the normalized Polyakov loop inflection point, see [2] for details.

$M_\pi/M_\rho = 0.446(3)$ [10], while the physical value is ≈ 0.18. The numerical value of all the parameters appearing in Eq. (238) is summarized in Table 1.

We make use of a large number of non-zero temperature ensembles, which have been generated using a fixed lattice spacing approach. This has the advantage that results obtained at different temperatures will have the same discretization errors. Also, since the bare parameters are the same, results can be directly compared without any need for renormalization. In Table 2, the lattice ensembles used in this work are listed. The temporal lattice extension N_τ ranges from 128 down to 16 corresponding to temperatures in the range $0.24 < T/T_c < 1.90$. Spatial extents of $N_s = 24$ and 32 were used corresponding to $L_s = N_s a_s \sim 3$fm and 4fm respectively and both are available for 4 common values of T allowing for finite volume effects to be studied.

The critical temperature has been estimated in [2] by looking at the inflection point of the renormalized Polyakov loop, which is defined in Eq. (129). We impose a renormalization condition by fixing the value of L at a specific temperature T_R:

$$L_R(T_R) \equiv c\,. \tag{245}$$

This is necessary since the free energy $F = -T \log L(T)$ is only defined up to an additive constant. We choose 3 different renormalization schemes corresponding to different choices of T_R and c, see Fig. 14 for details. The result for the transition temperature is $T_c = 185(4)$ MeV,

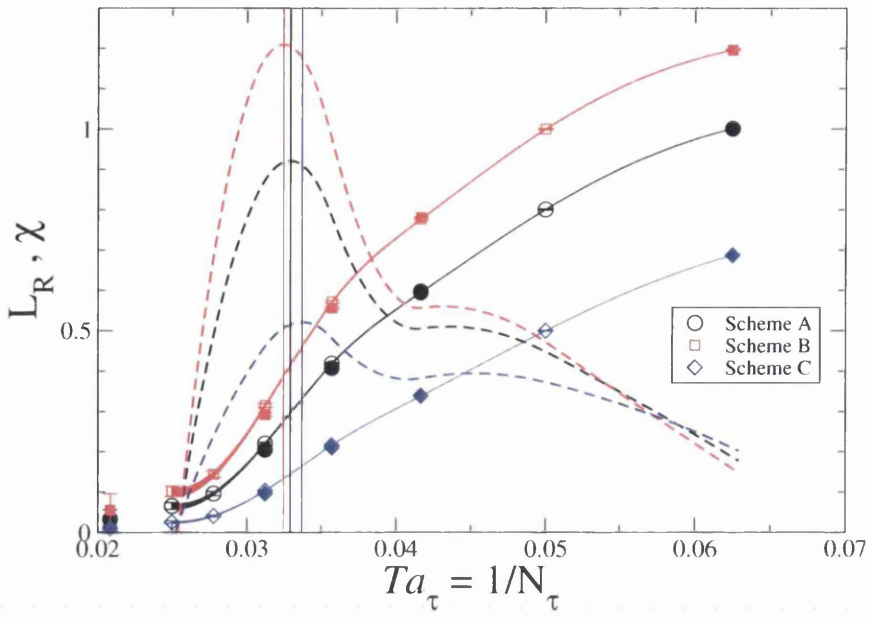

Figure 14: The normalized Polyakov loop L_R. The solid curves indicate a cubic splines interpolation of the data points, while the dashed curve represent their temperature derivatives χ. Three renormalization schemes are considered, Scheme A: $L_R(N_\tau = 16) = 1.0$, Scheme B: $L_R(N_\tau = 20) = 1.0$, Scheme C: $L_R(N_\tau = 20) = 0.5$.

where the error reflects the spread from the three renormalization schemes, while we found the statistical uncertainty negligible in this context.

This concludes the description of the technical details regarding lattice action used in this work. In the next section we will introduce the operators considered in the analysis.

5.2 CONSERVED CURRENT

In chapter 3, we showed how to obtain the electrical conductivity from Euclidean correlators of the electric current J_{em} (see Eq. (152)). In $N_f = 2 + 1$ QCD, the expression for the electromagnetic current is given by

$$J_{\text{em}} = \sum_{f=1}^{3} q_f j^f = \frac{2}{3} j^{\text{u}} - \frac{1}{3} j^{\text{d}} - \frac{1}{3} j^{\text{s}}, \tag{246}$$

where q_f is the fractional charge of the quarks and j^f is the vector current relative to the up, down and strange quark channels. In order to evaluate J_{em} on the lattice, we chose as an interpolator for j^f the exactly conserved vector current V^{C}.

In this section we will derive an expression for the conserved current for the fermion action (238) used in this work, which has been introduced in the previous section. In order to do so we must derive a Ward identity for the functional integral.

As we have seen in Eq. (72), the expectation value of an arbitrary operator O in QCD is expressed by

$$\langle O \rangle = \frac{1}{Z} \int \mathscr{D}[\psi, \bar{\psi}, U] \, O[\psi, \bar{\psi}, U] \, e^{-S[\psi, \bar{\psi}, U]} , \tag{247}$$

where S is the sum of the gauge and fermion actions described earlier. Let us now consider an infinitesimal symmetry transformation acting on the fermion fields in Eq. (247) and described by:

$$\psi \to \psi + \delta\psi , \quad \bar{\psi} \to \bar{\psi} + \delta\bar{\psi} . \tag{248}$$

If this transformation is a true symmetry of the action, then the expectation value of O ought not to change. In other words, in case of a non-anomalous transformation the integration measure is invariant and it is possible to derive Ward identities of the form

$$0 = \langle \delta O \rangle - \langle O \, \delta S \rangle , \tag{249}$$

where δO and δS denote the linear change of the operator O and the action S under the transformation of Eq. (248). In the simplest case for $O = 1$ we have $\langle \delta S \rangle = 0$, which leads to relations analogous to the classical Noether conservation laws.

Let us now consider a local transformation, acting on the Grassmann fields on lattice, defined as

$$\delta\psi(n) = i\epsilon(n)\lambda\psi(n), \quad \delta\bar{\psi}(n) = i\epsilon(n)\hat{\lambda}\bar{\psi}(n) , \tag{250}$$

where λ and $\hat{\lambda}$ are product of matrices which have both Dirac and flavour indices, e.g. $\lambda = \mathbb{1}, \tau^a, \gamma_5, \gamma_5\tau^a$ and $\hat{\lambda} = -\mathbb{1}, -\tau^a, \gamma_5, \gamma_5\tau^a$. Since the transformation does not involve the gauge fields, in the following we will only consider the fermion action. This is quadratic in the Grassman fields and, as shown in Eq. (73), it can be cast into the form

$$S = \sum_{n,m} \bar{\psi}(n) \, D(n,m) \, \psi(m) , \tag{251}$$

where D is the Dirac operator and we suppressed all the color and Dirac indices, leaving only the space-time ones n, m. Under the transformation in Eq. (250) the action changes and the linear term of the variation is given by:

$$\delta S = i \sum_{n,m} \bar{\psi}(n) \left[D(n,m) \, \lambda\epsilon(m) + \epsilon(n)\hat{\lambda} \, D(n,m) \right] \psi(m) \tag{252a}$$

$$\xrightarrow[\lambda=\mathbb{1}]{\hat{\lambda}=-\mathbb{1}} i \sum_{n,m} \left[\epsilon(m) - \epsilon(n) \right] \bar{\psi}(n) \, D(n,m) \, \psi(m) , \tag{252b}$$

where in the second line we have restricted ourselves to the case of the flavour singlet vector. We notice that in the sum of Eq. (252b), whenever $n = m$ the argument inside the parentheses vanishes, so we can neglect all the terms in the Dirac operator in Eq. (238) that contain $\delta_{m,n}$. Furthermore if m is not one of the nearest neighbours of n the Dirac operator vanishes, so we can trade the sum over m with a sum over the nearest neighbours of n.

$$\begin{aligned}\delta S &= i \sum_{n\neq m} [\epsilon(m) - \epsilon(n)]\, \bar{\psi}(n)\, D(n,m)\, \psi(m) \\ &= i \sum_{n,\mu} [\epsilon(n+\hat{\mu}) - \epsilon(n)]\, \bar{\psi}(n)\, D(n,n+\hat{\mu})\, \psi(n+\hat{\mu}) + \\ &\quad i \sum_{n,\mu} [\epsilon(n-\hat{\mu}) - \epsilon(n)]\, \bar{\psi}(n)\, D(n,n-\hat{\mu})\, \psi(n-\hat{\mu}). \end{aligned} \tag{253}$$

Selecting the right element in the Dirac operator and taking into account the anisotropy, we obtain:

$$\delta S = i \sum_n F_n\,, \tag{254}$$

with

$$\begin{aligned} F_n &= [\epsilon(n+\hat{0}) - \epsilon(n)]\, \bar{\psi}(n) \left[-\frac{1}{2}(1-\gamma_0) U_0(n)\right] \psi(n+\hat{0}) \\ &\quad + [\epsilon(n-\hat{0}) - \epsilon(n)]\, \bar{\psi}(n) \left[-\frac{1}{2}(1+\gamma_0) U_0^\dagger(n-\hat{0})\right] \psi(n-\hat{0}) \\ &+ \sum_i [\epsilon(n+\hat{i}) - \epsilon(n)]\, \bar{\psi}(n) \left[-\frac{1}{2\gamma_f}(1-\gamma_i) U_i(n)\right] \psi(n+\hat{i}) \\ &+ \sum_i [\epsilon(n-\hat{i}) - \epsilon(n)]\, \bar{\psi}(n) \left[-\frac{1}{2\gamma_f}(1+\gamma_i) U_i^\dagger(n-\hat{i})\right] \psi(n-\hat{i})\,. \end{aligned} \tag{255}$$

We define the conserved current as

$$\begin{aligned} V_\mu^{\mathrm{C}}(m) = c_\mu \Big[&\bar{\psi}(m+\hat{\mu})(1+\gamma_\mu)\, U_\mu^\dagger(m)\, \psi(m) \\ &-\bar{\psi}(m)(1-\gamma_\mu)\, U_\mu(m)\, \psi(m+\hat{\mu}) \Big]\,, \end{aligned} \tag{256}$$

$$\begin{aligned} V_\nu^{\mathrm{C}}(n)^\dagger = c_\nu \Big[&\bar{\psi}(n+\hat{v})(1-\widetilde{\gamma}_\nu)\, U_\nu^\dagger(n)\, \psi(n) \\ &-\bar{\psi}(n)(1+\widetilde{\gamma}_\nu)\, U_\nu(n)\, \psi(n+\hat{v}) \Big]\,, \end{aligned} \tag{257}$$

with $c_\mu = (\frac{1}{2}, \frac{\vec{1}}{2\gamma_f})$ and $\widetilde{\gamma}_\mu = \gamma_0\gamma_\mu\gamma_0 = (\gamma_0, -\vec{\gamma})$. In fact, using these definitions, we can rewrite the change in the action δS as:

$$\delta S = i \sum_{n,\mu} [a_\mu \nabla_\mu^+ \epsilon(n)]\, V_\mu^{\mathrm{C}}(n) = -i \sum_{n,\mu} \epsilon(n)\, [a_\mu \nabla_\mu^- V_\mu^{\mathrm{C}}(n)]\,, \tag{258}$$

where ∇^+_μ and ∇^-_μ are respectively the forward and backward dimensionless lattice derivatives:

$$\nabla^+_\mu f(x) = f(x + a\hat{\mu}) - f(x) \tag{259a}$$

$$\nabla^-_\mu f(x) = f(x) - f(x - a\hat{\mu}) . \tag{259b}$$

Since our choice of $\epsilon(n)$ is completely arbitrary, the relation (258) has to be valid for any n. This observation allows us to derive the following identity

$$\langle \nabla^-_\mu V^C_\mu(n) \rangle = 0 , \tag{260}$$

which proves that V^C_μ is the conserved vector current for the clover action. An important property of such an operator is that it is protected from renormalization, since the electromagnetic charge is conserved.

We now want to evaluate current-current correlator as a function of the Euclidean time separation:

$$\sum_{\vec{y},i} \langle\, V^C_i(\vec{x}, \tau_0)\, V^C_i(\vec{y}, \tau_0 + \tau)^\dagger \,\rangle . \tag{261}$$

Let us consider the quantity $\langle V^C_\mu(m)\, V^C_\nu(n)^\dagger \rangle$. If we plug in it the conserved current in Eq. (256) we obtain four pieces, which we evaluate by means of Wick contractions:

$$(c_\mu c_\nu)^{-1} \langle V^C_\mu(m)\, V^C_\nu(n)^\dagger \rangle =$$

$$+ \langle \bar{\psi}(m + \hat{\mu})(1 + \gamma_\mu)\, U^\dagger_\mu(m)\, \psi(m)\, \bar{\psi}(n + \hat{\nu})(1 - \tilde{\gamma}_\nu)\, U^\dagger_\nu(n)\, \psi(n) \rangle \tag{262a}$$

$$+ \langle \bar{\psi}(m)(1 - \gamma_\mu)\, U_\mu(m)\, \psi(m + \hat{\mu})\, \bar{\psi}(n)(1 + \tilde{\gamma}_\nu)\, U_\nu(n)\, \psi(n + \hat{\nu}) \rangle \tag{262b}$$

$$- \langle \bar{\psi}(m + \hat{\mu})(1 + \gamma_\mu)\, U^\dagger_\mu(m)\, \psi(m)\, \bar{\psi}(n)(1 + \tilde{\gamma}_\nu)\, U_\nu(n)\, \psi(n + \hat{\nu}) \rangle \tag{262c}$$

$$- \langle \bar{\psi}(m)(1 - \gamma_\mu)\, U_\mu(m)\, \psi(m + \hat{\mu})\, \bar{\psi}(n + \hat{\nu})(1 - \tilde{\gamma}_\nu)\, U^\dagger_\nu(n)\, \psi(n) \rangle , \tag{262d}$$

where the disconnected pieces have been neglected (see below for discussion). These four diagrams are not all independent from each other. In fact, one can show that (262a) is the complex conjugate of (262b) and (262c) is the complex conjugate of (262d), which leaves us with only two diagrams to deal with.

The expectation value of $\psi\bar{\psi}$ is called the fermion propagator S

$$S(x, y) \equiv \langle \psi(x) \bar{\psi}(y) \rangle . \tag{263}$$

$$\langle V_\mu^C(m)\, V_\nu^C(n)^\dagger \rangle = 2\mathrm{Re}\, Tr \Big[$$

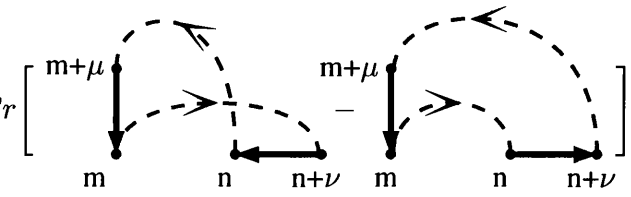

$$\Big]$$

Figure 15: The two diagrams that contributes to the current-current correlator. The dashed lines are the fermion propagators and the solid lines are the gauge links.

It can be evaluated, using Wick's theorem [15], by calculating the inverse of the Dirac operator D. More precisely, in the lattice computation, only one column of D^{-1} will be used. This can be understood by writing down all the indices in the definition of the fermion propagator, which gives us

$$\underset{\substack{ab\\mn}}{D_{\alpha\beta}}\ \underset{\substack{b\\n}}{S_\beta} = \delta(\alpha-\alpha^*)\delta(a-a^*)\delta(m-m^*)\,, \tag{264}$$

where $n,m \in [1,N_V]$ are space-time indices, $\alpha,\beta \in [1,4]$ are Dirac indices and $a,b \in [1,3]$ are the color ones. The r.h.s. of Eq. (264) is then a vector of dimensions $N_V \times 4 \times 3$ with zeros everywhere except at the source point (α^*,a^*,m^*) where there is a 1. If we multiply (264) on both sides by D^{-1} we obtain

$$\underset{\substack{ca\\lm}}{D^{-1}_{\gamma\alpha}}\ \underset{\substack{ab\\mn}}{D_{\alpha\beta}}\ \underset{\substack{b\\n}}{S_\beta} = \underset{\substack{ca\\lm}}{D^{-1}_{\gamma\alpha}}\ \delta(\alpha-\alpha^*)\delta(a-a^*)\delta(m-m^*) \tag{265a}$$

$$,\underset{\substack{c\\l}}{S_\gamma} = \underset{\substack{ca^*\\lm^*}}{D^{-1}_{\gamma\alpha^*}} \equiv S(l,m^*)\,, \tag{265b}$$

where it is shown that we selected in D^{-1} the column (α^*,a^*,m^*). Using the notation above for the fermion propagator, we can rewrite Eq. (262) as:

$$(c_\mu c_\nu)^{-1}\,\langle V_\mu^C(m)\, V_\nu^C(n)^\dagger\rangle =$$

$$-2\,\mathrm{Re\ Tr}\,\Big[S(n,m+\mu)U_\mu^\dagger(m)(1+\gamma_\mu)S(m,n+\hat{v})U_\nu^\dagger(n)(1-\tilde{\gamma}_\nu)\Big] \tag{266a}$$

$$+2\,\mathrm{Re\ Tr}\,\Big[S(n+\hat{v},m+\hat{\mu})U_\mu^\dagger(m)(1+\gamma_\mu)S(m,n)U_\nu(n)(1+\tilde{\gamma}_\nu)\Big]\,. \tag{266b}$$

In Fig.15 the two contributions are represented in a pictorial way.

The zero-momentum Euclidean correlator for a single flavour is then defined as

$$G_{\mu\nu}(\tau) = \frac{1}{V}\sum_{\vec{x}} \langle V_\mu^C(\vec{x},\tau)\, V_\nu^C(0,0)^\dagger\rangle\,, \tag{267}$$

and in particular we will study the diagonal spatial components

$$G(\tau) = \sum_{i=1}^{3} G_{ii}(\tau) = \frac{1}{V} \sum_{i=1}^{3} \sum_{\vec{x}} \langle V_i^{\mathrm{C}}(\vec{x}, \tau)\, V_i^{\mathrm{C}}(0,0)^{\dagger} \rangle \ , \tag{268}$$

as well as the temporal one

$$G_{00}(\tau) = \frac{1}{V} \sum_{\vec{x}} \langle V_0^{\mathrm{C}}(\vec{x}, \tau)\, V_0^{\mathrm{C}}(0,0)^{\dagger} \rangle \ . \tag{269}$$

The full electromagnetic current correlator is given by

$$G_{\mathrm{em}}(\tau) = \frac{1}{V} \sum_{i=1}^{3} \sum_{\vec{x}} \langle J_{\mathrm{em}}^{i}(\vec{x}, \tau)\, J_{\mathrm{em}}^{i}(0,0)^{\dagger} \rangle \ , \tag{270}$$

where J_{em} has been defined in Eq. (246). Following [83], at the flavour symmetric point $N_f = 3$ we can decompose Eq. (270) into a sum of disconnected M_{disc} and connected M_{conn} diagrams:

$$\langle J_{\mathrm{em}}(\vec{x}, \tau)\, J_{\mathrm{em}}(0,0)^{\dagger} \rangle \propto \Big[\Big(\sum_{f=1}^{N_f} q_f \Big)^2 M_{\mathrm{disc}} + \Big(\sum_{f=1}^{N_f} q_f^2 \Big) M_{\mathrm{conn}} \Big] , \tag{271}$$

where q_f denotes the electric charge of flavour f in units of the elementary charge e. Neglecting the disconnected pieces is then justified by the fact that their contribution is identically zero in the $N_f = 3$ case, since $\sum_{f=1}^{N_f} q_f \equiv 0$. We note that the same choice has been applied in all previous studies of the electrical conductivity, see e.g. [36, 39–41, 68]. Furthermore, we will show in section 6.4 that the disconnected diagrams for the charge susceptibility are compatible with zero.

5.3 IMPROVEMENT

In section 1.5, we introduced the discretised version of the continuum QCD action by trading first derivatives for symmetric differences on the lattice. This procedure gives rise to discretization effects, which, as we already pointed out, are of $O(a)$ for fermions and of $O(a^2)$ for the gauge fields. These artefacts would disappear in the continuum, where the lattice spacing vanishes, $a \to 0$. However, this limiting procedure is expensive.

We already mentioned that the discretization we chose in section 1.5 is not unique. It is then possible to add other terms in the action which do not spoil its continuum interpretation, but actually improve it. A systematic implementation of these ideas goes under the name of *Symanzik improvement*. In particular in section 1.5, we claimed that adding the clover term to the standard Wilson action S_w of Eq. (96) can

reduce the discretization errors from $O(a)$ to $O(a^2, \alpha_s a, \ldots)$ [24]. In principle, one should also take care of reducing the discretization errors in the observables used in the study.

Following an argument illustrated in [84], we can define a current which is both improved and conserved up to the precision we require. We call it V_μ^{CI}:

$$V_\mu^{\mathrm{CI}}(x) \equiv V_\mu^{\mathrm{C}}(x) + c_V \partial_\nu \bar{\psi}(x)\, \sigma_{\mu\nu}\, \psi(x) \tag{272a}$$

$$= V_\mu^{\mathrm{I}}(x) + O(a^2)\,. \tag{272b}$$

We see from (272a) that V_μ^{CI} differs from the conserved current V_μ^{C} by a term of $O(a)$ which is a total divergence. Thus, since $\partial_\mu \bar{\psi}\, \sigma_{\mu\nu}\, \psi$ has no power divergences in perturbation theory, one can conclude that the renormalization constant $Z_{V_\mu^{\mathrm{CI}}}$ is also equal to 1. On the other hand, from (272b) at tree level V_μ^{CI} differs from the improved current V_μ^{I} only by terms which are $O(a^2)$. This implies that $Z_{V_\mu^{\mathrm{CI}}} \neq Z_{V_\mu^{\mathrm{I}}}$, but they cannot give rise to any terms of $O(a)$ in V_μ^{CI}, which then is both conserved and improved.

In this work, we are interested in the zero-momentum limit of the Euclidean correlators, which is achieved by a summation over all the lattice points (see Eq. (5.2)). The spatial components of the improvement term in Eq. (272a), which is a total divergence, vanish in this limit. We are left with a term, which is highly suppressed in the massless limit. For this reason, we choose not to add the costly improvement term in the construction of the operator and use the form in Eq. (256) for the analysis.

5.4 RESULTS

In this section we present the results for the Euclidean correlators evaluated for temperatures in the range between 43 and 352 MeV (see Table 2 for details). These data appeared in [2–4], where they have been used to obtain the spectral functions in the vector channel, see chapter 6 for details.

The correlators were obtained using a modified version of the Chroma software suite [85, 86]. When possible, the bi-conjugate gradient stabilised method was used for the inversion of the Dirac operator of Eq. (264). The number of sources N_{SRC} used for each configuration is shown in Table 2, although in most ensembles $N_{\mathrm{SRC}} = 4$. The first source $s^{[0]} = (s_0^{[0]}, s_1^{[0]}, s_2^{[0]}, s_3^{[0]})$ was chosen randomly. The other $j = 1, 2, 3$ were picked at the locations:

$$s_i^{[j]} = s_i^{[0]} + \delta_{ij} L/2\,. \tag{273}$$

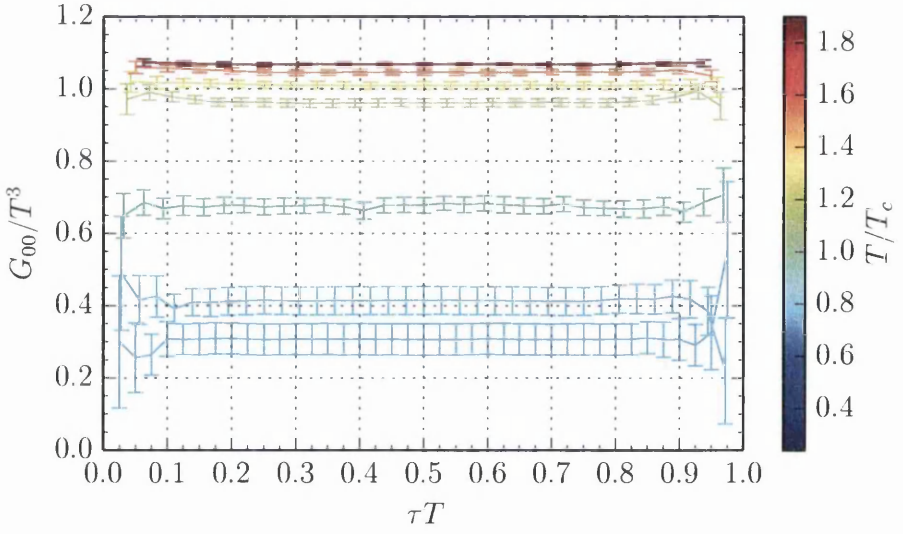

Figure 16: The time-time component of the conserved current in Eq. (269), for the light quark sector. The correlation function is rescaled by T^3 and it is calculated at different temperatures T as a function of the Euclidean time τT. Since it is related to the conservation of the electrical charge, the correlator relaxes to a constant, modulo some boundary effects, which are discussed in the text.

Data from different sources but from the same configuration were averaged together to reduce autocorrelation. The statistical error was estimated via data-blocking and the jackknife procedure.

The temporal correlator in Eq. (269) is connected to the conserved electrical charge and we expect it to be constant in Euclidean time. In Fig. (16) we show G_{00} normalized by T^3 for all the temperatures available, for the light quark channel. We observe some boundary effects, probably due to the presence of a singularity at the origin, as shown in [87] in the free case. One could argue that, due to the anisotropy the effect of the singularity is propagated to the neighbouring sites. We observe a clustering effect for correlators above T_c.

The lattice configurations at our disposal come with 2 different spatial extensions $N_s = 24, 32$. Both volumes are available for 4 different temperatures corresponding to $N_\tau = 16, 24, 28, 32$, as is shown in Table 2. This allows for a study of the volume effects for the conserved current. In Fig. (17) we plot the ratio between the correlators obtained in the $N_s = 32$ and $N_s = 24$ ensemble. We found no significant systematic volume effects in this context.

We show in Fig. 18 the diagonal spatial components of $G_{\mu\nu}(\tau)$. We note an important separation of scales separating the lowest temperature $T = 43\,\mathrm{MeV}$ from the other ones. In Fig. (19) we show the same

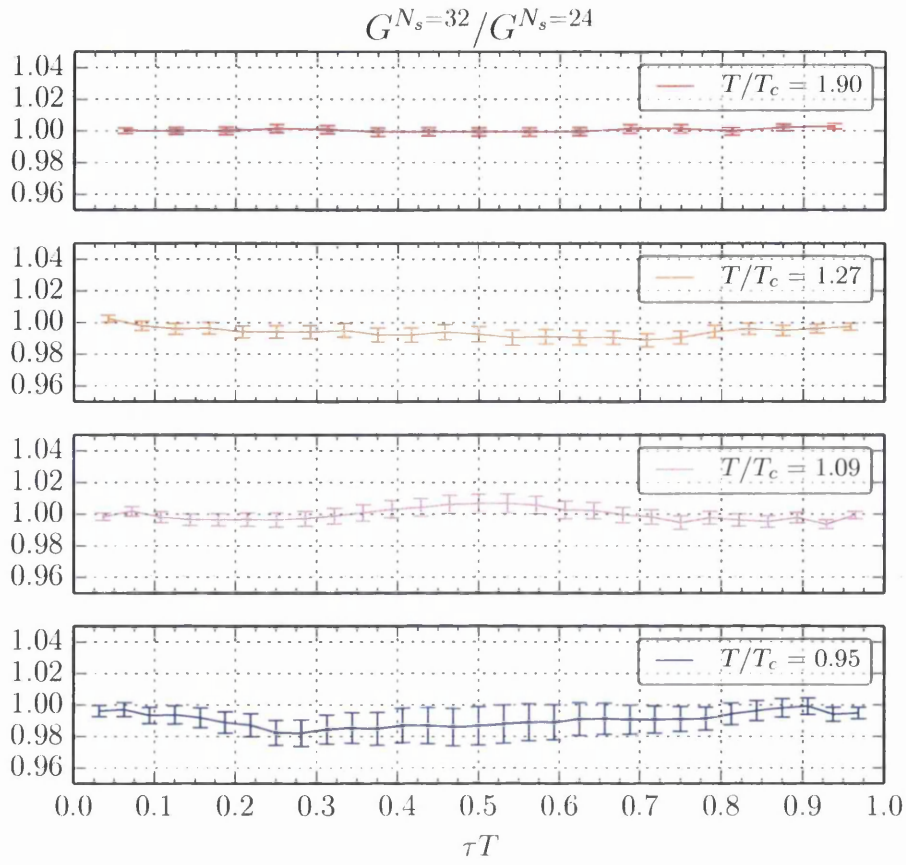

Figure 17: An estimate for the volume effects affecting the spatial-spatial correlator $G(\tau)$ in Eq. (268) in the light quark channel. The ratio of $G(\tau)$ in the $N_s = 32$ and $N_s = 24$ is evaluated for 4 temperatures corresponding to $N_\tau = 16, 24, 28, 32$.

correlators normalized by their value in the free massless case. The latter can be achieved by setting all the links to unity in the simulation. As we noted for G_{00}, correlators above T_c, measured in ensembles of increasing temperature, show little differences between each other, while below T_c their behaviour rapidly changes with T. The deviation we observe from the expected free behaviour at high temperatures might come from different sources of systematics. One of these is related to the difficulty of defining the anisotropy in a free theory. Moreover, our determination $\xi = a_s/a_t$ carries an uncertainty as well as one can see from the plot in Fig. (13).

In Fig. (20) we instead normalize the spatial correlator with the one at the lowest temperature available. This has been achieved by fitting the $N_\tau = 128$ correlator with a spline and then using its functional form for

the normalization of correlators at higher temperatures. Remarkably, the clustering effect noted above disappears.

In the next chapter, we will use the Euclidean correlators presented here as a source for the MEM reconstruction (see chapter 4) of the spectral functions.

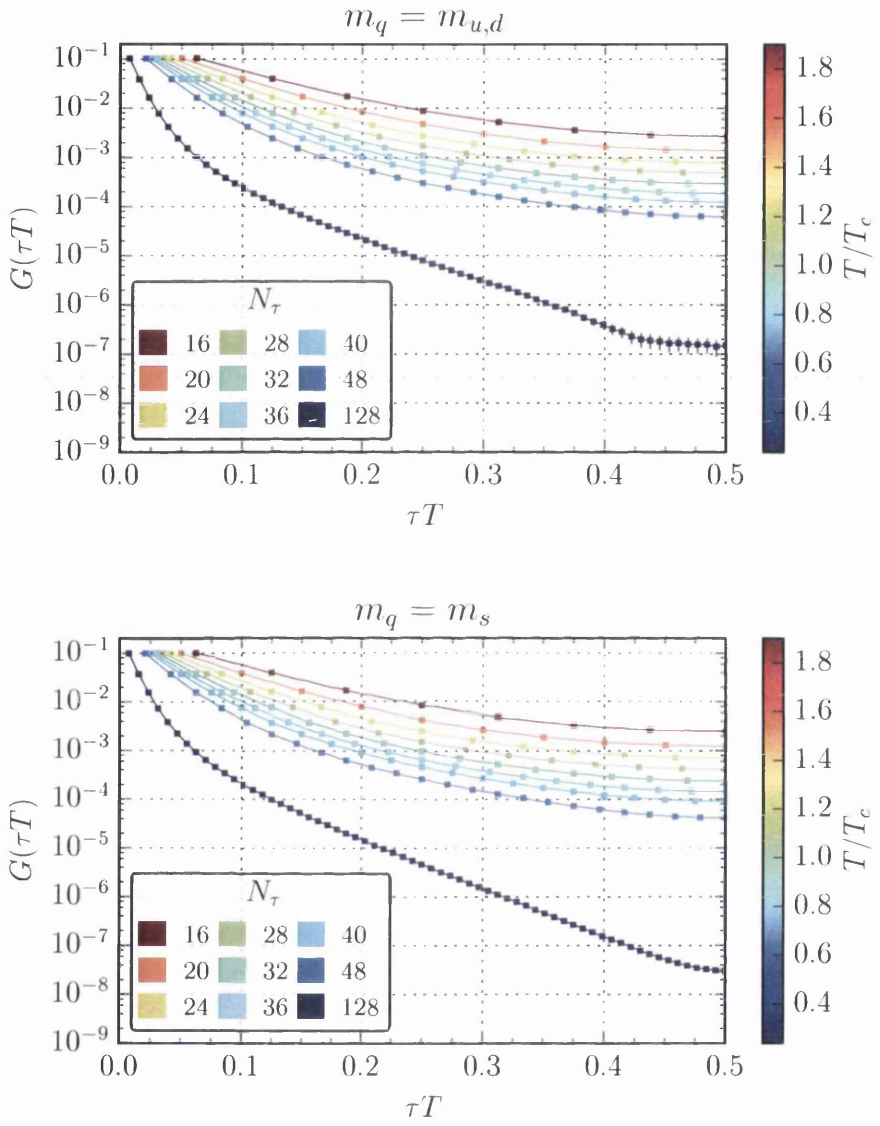

Figure 18: The spatial-spatial correlator $G(\tau) = \sum_i G_{ii}$ of Eq. (268) in lattice units for the light (top) and strange (bottom) quark channels, see Table 1. Its behaviour is shown for different temperatures T.

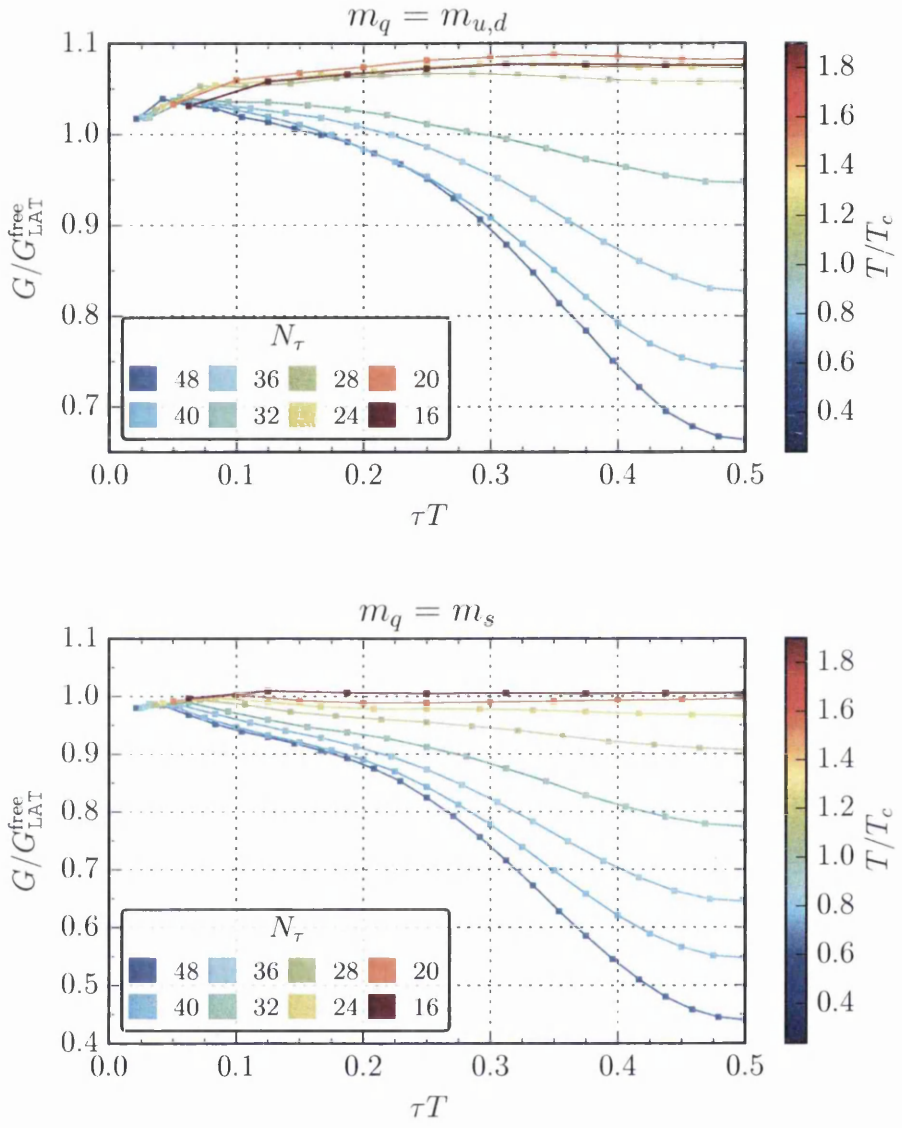

Figure 19: Euclidean correlator $G(\tau)$ of Eq. (268), normalised by its value in the free massless case (on the lattice), for the light quark (top) and for the strange quark (bottom) channels. See section 5.4 for more details.

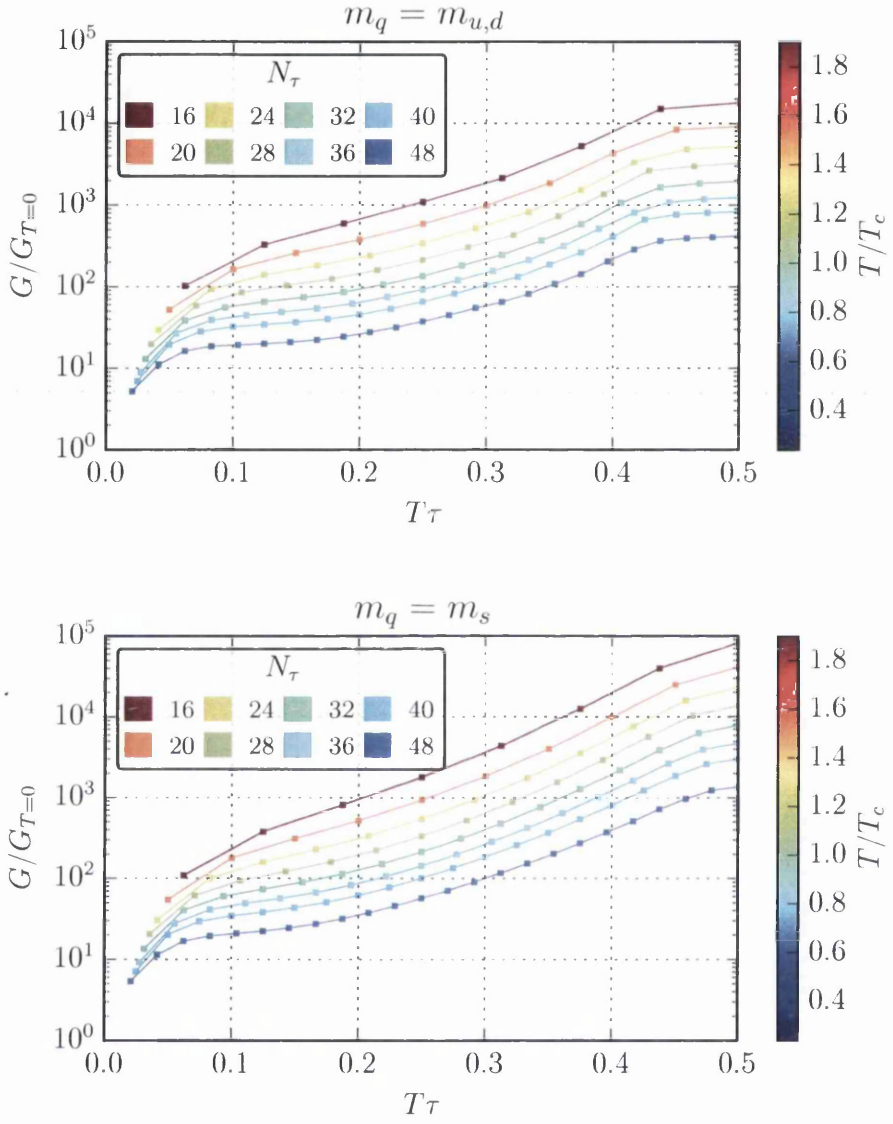

Figure 20: Euclidean correlator $G(\tau)$ of Eq. (268), normalised by its value in the zero temperature ensemble with $N_\tau = 128$, for the light (top) and strange (bottom) quark channels. See section 5.4 for more details.

6

RESULTS

In the first part of this chapter, we will show the spectral functions relative to the vector channel obtained with the MEM method (see chapter 4). The results for the temperature dependence of the electrical conductivity in QCD will then be presented, along with a detailed discussion of the systematics involved. The susceptibilities of conserved charges are then analysed. In particular, the electrical charge susceptibility χ_Q will allow for a determination of the diffusion coefficient. We will then compare our findings with those obtained by other groups.

6.1 SPECTRAL FUNCTIONS

Spectral functions represent one of the most important diagnostic tools of the medium created in heavy-ion collisions (see section 2.6). In particular, we can use them to study the transport coefficients of the quark-gluon plasma, as well as its in-medium properties, such as dissolution of quarkonia states at high temperature, see e.g. [88–90].

In this thesis, we are interested in the spectral functions relative to the electromagnetic channel ρ_{em}, which yield information about vector mesons, such as the ρ and ϕ particles, and the electrical conductivity σ, which will be discussed later. They are related to the Euclidean correlators G_{em} presented in section 5.4 by[1]:

$$G_{\mathrm{em}}(\tau) = \int_0^\infty \mathrm{d}\omega\, \rho_{\mathrm{em}}(\omega) \frac{\cosh\left[\omega(N_\tau/2 - \tau)\right]}{\sinh\left(N_\tau\, \omega/2\right)}, \tag{274}$$

where τ is the Euclidean time and N_τ is the extent of the lattice in the temporal direction. In the following, it will be useful to normalise the electromagnetic observables of interest by the sum of the square of the individual quark charges contributing to the electromagnetic current[2]:

$$C_{\mathrm{em}} = e^2 \sum_{f=1}^{N_f} q_f^2 . \tag{275}$$

1 See section 3.4 for a detailed derivation.

2 See Eq. (271) and discussion therein.

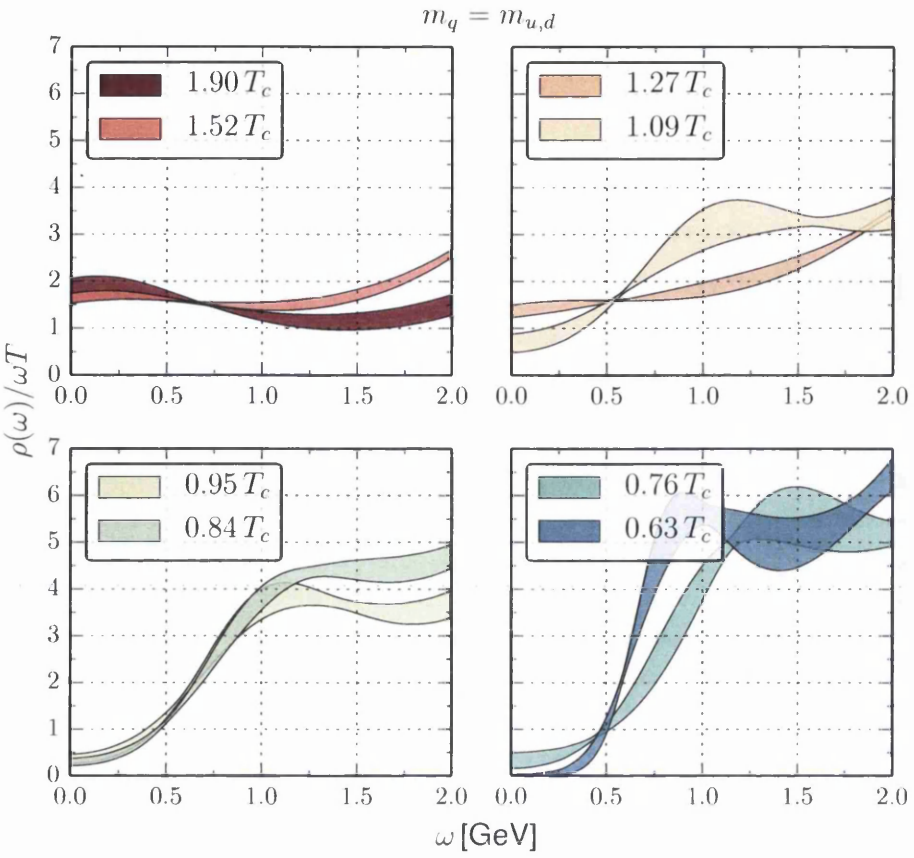

Figure 21: Spectral functions in the light quark channel normalized by ωT for different values of the temperature T. The intercept is proportional to σ/T, see Eq. (164).

When only light quarks are considered $C_{\rm em} = 5/9\,e^2$; otherwise, when the strange quark is included $C_{\rm em} = 2/3\,e^2$. We can then define

$$\rho(\omega) = C_{\rm em}^{-1}\,\rho_{\rm em}(\omega)\,, \qquad \sigma = C_{\rm em}^{-1}\,\sigma_{\rm em}\,. \tag{276}$$

Spectral functions extracted using the MEM procedure are shown in Figs. 21-24 for all the available temperatures, which are listed in Table 2. In Appendix A.2, we show that the physical dimension of ρ expressed in units of the lattice spacing is $(a_s\,a_t)^{-1}$. We plot the spectral function through a dimensionless ratio, either dividing by ωT or by ω^2, which both carry a dimension of a_t^{-2}. Because of this, we need to add a factor of the anisotropy $\xi = a_s/a_t$, which is implied in all the plots. Note that we considered $\xi = 3.5$ without error, which might affect the results for no more than $2 - 3\%$, while the area of the filled curves is a jackknife estimate of the statistical error on the MEM reconstruction.

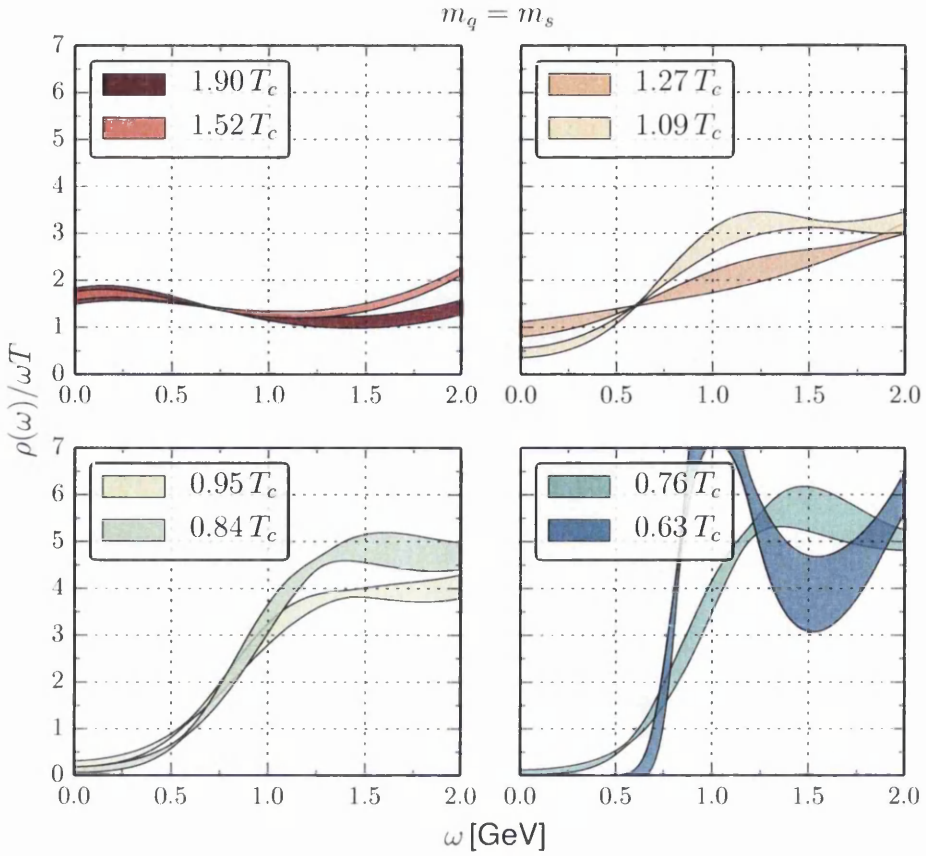

Figure 22: Spectral functions in the strange quark channel normalized by ωT for different values of the temperature T. The intercept is proportional to σ/T, see Eq. (164).

In the free theory and for massless quarks, the spectral function assumes the form [87]:

$$\rho_{\text{free}}(\omega) = 2\pi T^2 \omega \delta(\omega) + \frac{3}{2\pi}\,\omega^2\,\tanh(\omega/4T)\,, \tag{277}$$

which increases quadratically for large values of ω, as one would expect from naive dimensional analysis (see Appendix A.2). In the regime of large frequencies, perturbation theory is applicable because of asymptotic freedom and can be used to evaluate the radiative corrections to the coefficient of ω^2 [91, 92].

At small energies, the spectral function is dominated by a transport peak. In the free case, this is represented by a δ-function, as we can see from Eq. (277), but when interactions are turned on, this singular behaviour is smoothed out.

For example, if we consider heavy quarks with $M \gg T$, they will have a typical thermal momentum p and velocity v of

$$p \sim \sqrt{MT}, \qquad v \sim \sqrt{T/M} \ll 1\,. \tag{278}$$

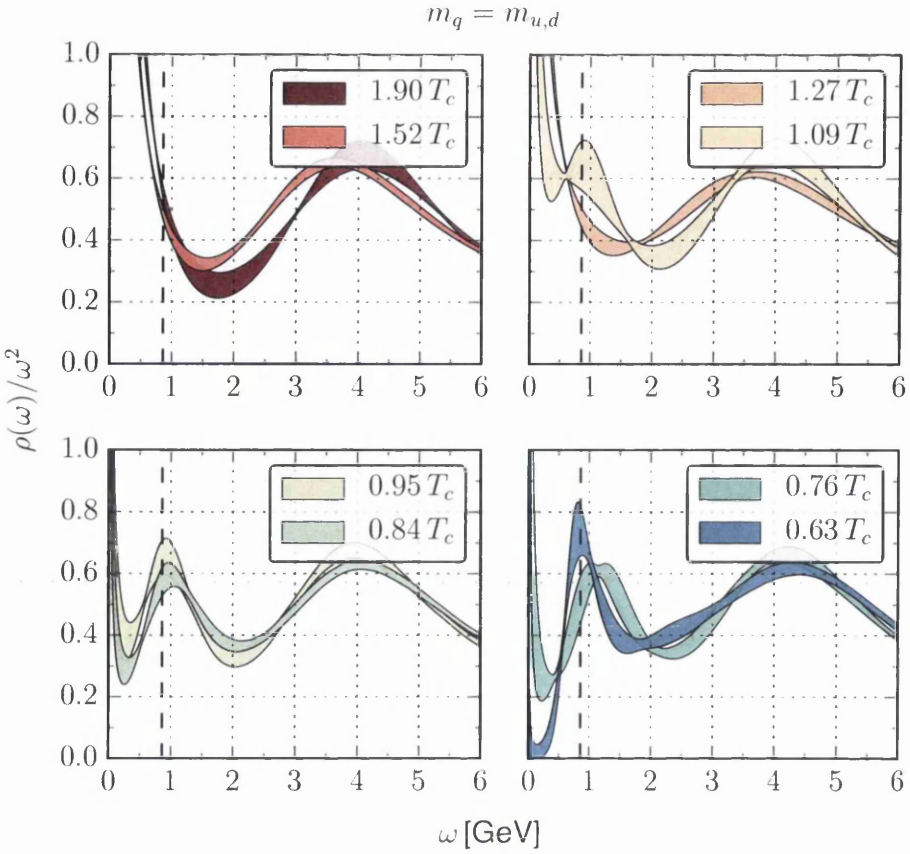

Figure 23: Spectral functions in the light quark channel divided by squared frequency to enhance the peak close to the origin. The vertical dashed line indicates the mass of the ρ meson from [9].

The system is then considered non-relativistic. Since $p \gg T$ it takes many collisions to change the momentum substantially. It is then a good approximation to model the interaction of the heavy quark with the medium as uncorrelated momentum kicks. This is done by the Langevin effective theory [93–95]:

$$\frac{dp_i}{dt} = \xi_i(t) - \varsigma p_i \,, \qquad \langle \xi_i(t)\xi_j(t')\rangle = \varsigma(2MT)\delta_{ij}\,\delta(t-t') \,. \tag{279}$$

Here ς is a momentum drag coefficient and $\xi_i(t)$ delivers random momentum kicks. Following [93–95], this theory predicts a Lorentzian form for the transfer peak:

$$\rho_{HQ}(\omega, T) \propto \frac{\varsigma\,\omega}{\omega^2 + \varsigma^2}, \qquad m \gg T \,. \tag{280}$$

Note how the delta function is recovered in the limit $\varsigma \to 0$, which supports the fact that, in a free theory, the mean free path is infinite

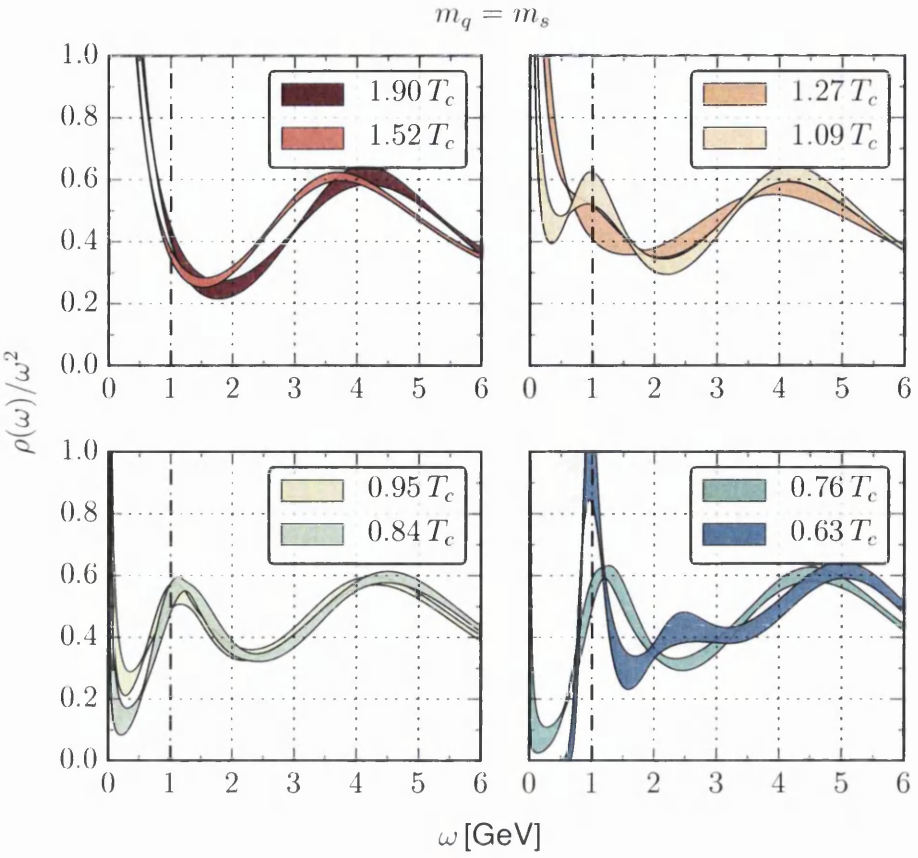

Figure 24: Spectral functions in the strange quark channel divided by squared frequency to enhance the peak close to the origin. The vertical dashed line indicates the mass of the ϕ meson from [9].

and transport coefficients diverge. The case of massless quarks can be treated with perturbation theory and the Boltzmann equation [7, 94, 96] and results in a spectral function which has the same functional form of Eq. (280).

These theoretical expectations are qualitatively present in our data. In Fig. 21 and Fig. 22 we plot the ratio $\rho(\omega)/\omega T$, where, according to Eq. (164), the conductivity σ/T is proportional to the intercept. This is manifestly dependent on the temperature: it vanishes at low T and it is non-zero when $T \gtrsim 0.76\,T_c$. This will be investigated further in section 6.2.

From Eq. (180), we know that a stable meson state contributes with a δ function peak to the spectral function:

$$\rho(\omega) \sim |\langle 0|J_H|H\rangle|^2\,\delta(p^2 - M^2)\,, \tag{281}$$

where M is the mass of the state. When the system is heated up, the thermal effects change the delta function into a smeared peak, with

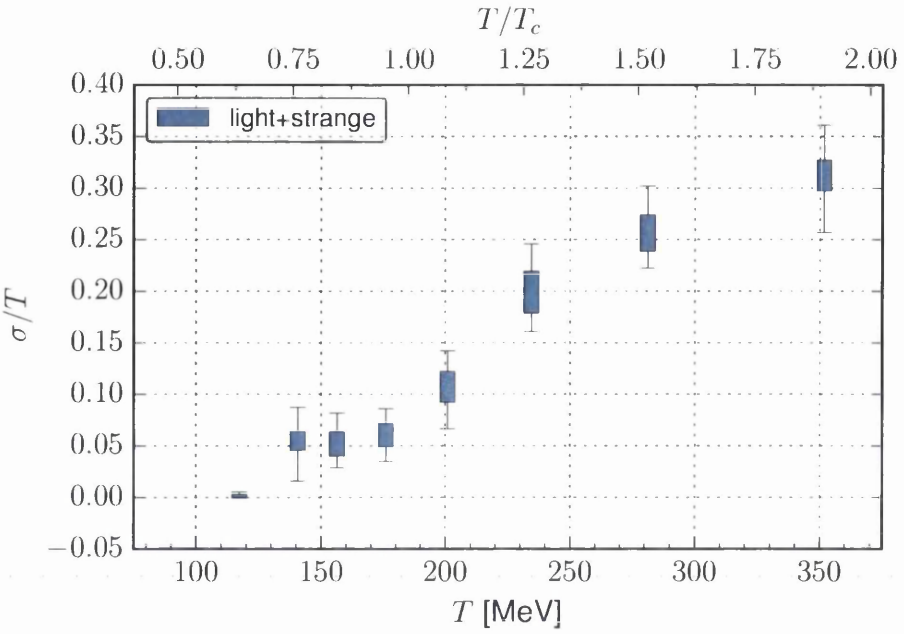

Figure 25: Temperature dependence of $C_{\text{em}}^{-1}\sigma/T$, including the contributions from the up, down and strange channels as in Eq. (246). The vertical size of the rectangles reflects the systematic uncertainty due to changes in the default model, when varying $0.4 < b < 1$. The error bars instead include the statistical jackknife error as well.

a definite thermal width, which increases with temperature. The contribution from the mesonic state in the spectral function becomes, at sufficiently high temperatures, very broad and eventually disappears. This is often referred to as *melting* of a hadronic state.

This effects are shown in Figs. (23) and (24), where the spectral function $\rho(\omega)$ is divided by the squared frequency ω^2 in order to enhance the bound state peak. The vertical dashed line is a zero temperature estimate from [9] of the mass of the bound state. This is represented by the ρ particle, in case of the light quark channel (Fig. 23) and by the ϕ meson for the strange one (Fig. 24). At temperatures $T \lesssim T_c$, i.e. below the deconfinement transition, the spectral function shows a clear peak at the position of the bound state mass $\omega \sim M$. As the temperature is increased, the peak becomes broader and broader until it is no longer distinguishable at $T \gtrsim 1.27\, T_c$.

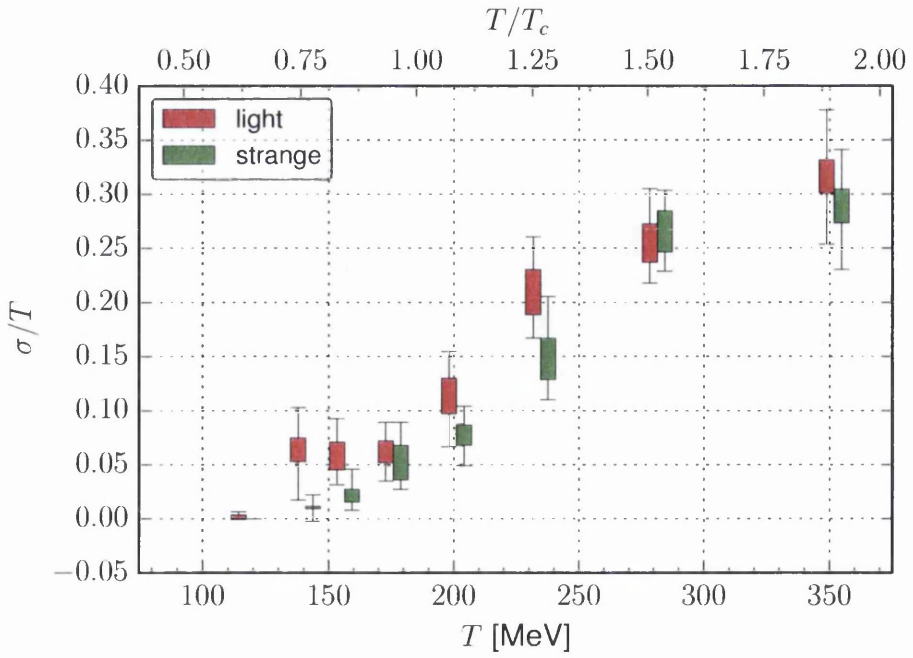

Figure 26: Comparison between light and strange quark conductivities.

6.2 CONDUCTIVITY

The electrical conductivity σ is extracted from the spectral functions shown above by taking the low frequency limit[3]:

$$\sigma = \frac{1}{6} \lim_{\omega \to 0} \frac{\rho(\omega)}{\omega} \qquad \text{with} \quad \sigma = C_{\text{em}}^{-1} \sigma_{\text{em}} \,, \tag{282}$$

where C_{em} has been introduced in Eq. (276). The results for the temperature dependence of σ/T are shown in Fig. 25 for all the available temperatures straddling the QGP transition.

We observe an increase in σ/T as the transition to the deconfined phase is made, with the rise starting already below T_c. For temperatures lying deep in the confined region, i.e. $T \lesssim 0.75\, T_c$, the conductivity is compatible with zero. Around T_c it rises up to ≈ 0.05 and then keeps increasing. When the temperature reaches $T = 352$ MeV its value is almost 5 times bigger, with $\sigma/T \approx 0.3$. We note that since the transition is a crossover (see section 2.5), a smooth behaviour between the cold and hot regimes may be expected. The conductivity might be underestimated below T_c, where the transport of charged hadrons must contribute. These might lead to a narrow transport peak, whose details cannot be resolved by the Euclidean correlator [95].

3 See section 3.3 for more details.

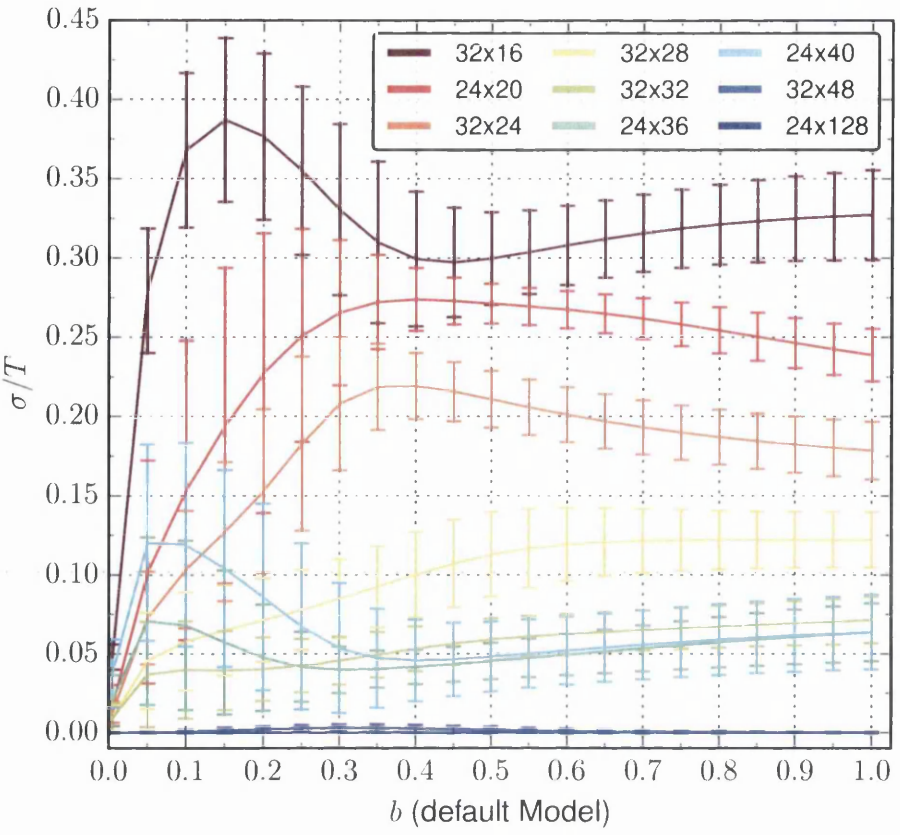

Figure 27: Dependence of the conductivity $C_{\mathrm{em}}^{-1}\sigma/T$ on the parameter b in the default model. Stability is achieved for $b \gtrsim 0.4$.

In Fig. 26 we can see how σ/T depends on the quark mass used in the inversion of the Dirac operator. Results for the strange sector show a smaller conductivity than the light one, especially below the crossover region.

6.3 STABILIITY TESTS

In chapter 4, we discussed how the inversion of Eq. (274) to obtain the spectral function ρ represents an ill-posed problem. This means that, independently from the tool adopted to perform the task, the results are bound to suffer from systematic uncertainties and it is important to keep them under control. The MEM method was introduced in the context of QCD around 10 years ago, but few groups have used it since [40, 69, 97–99]. It is then highly desirable to rely on a series of tests, which will be shown in this section, to check the robustness of the results obtained.

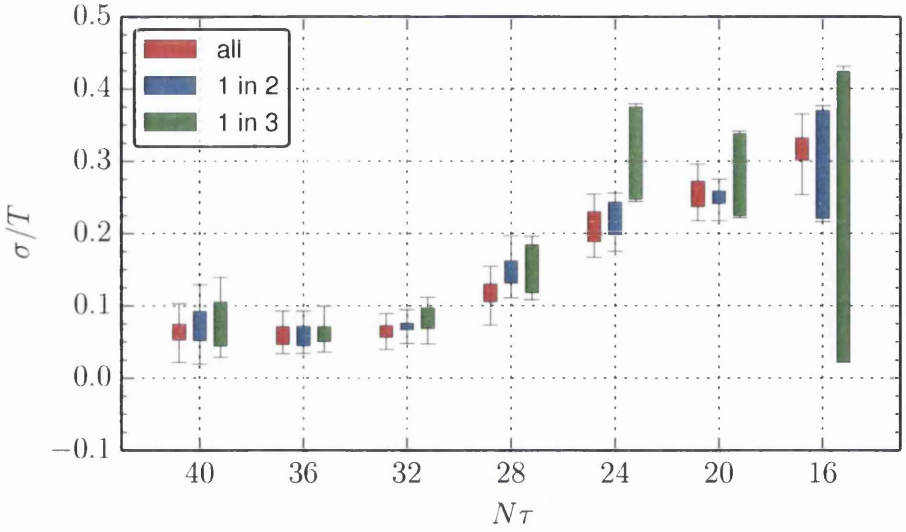

Figure 28: Stability tests for the MEM reconstruction. The conductivity $C_{em}^{-1}\sigma/T$ is plotted when only a subset of the available time slices is used.

As we anticipated in section 4.2, we can vary the interval of Euclidean points used in the process:

$$\Delta\tau = \tau_{max} - \tau_{min}\,. \tag{283}$$

We kept $\tau_{max} = N_\tau/2$, but explored the effect of changing $\tau_{min} = 1,\ldots,4$. We found that stability was achieved when $\tau_{min} \gtrsim 3$. The results shown for the conductivity σ in Figs. 25-26 were obtained with $\tau_{min} = 4$. Similarly, we varied the ω range with $0 \leq \omega \leq \omega_{max}$ and found stability provided $\omega_{max} \sim 3-5$; here we used $\omega_{max} = 3$. Also, we discretised the frequency interval (see Eq. 220) with $N_\omega = 1000$ points. Increasing it to $N_\omega = 2000$ produced no difference in the results.

In section 4.6, we introduced the default model $m(\omega)$ used in our analysis. It is quadratic in ω, in order to match the theoretical expectations listed in section 6.1 and we choose it to have a minimal number of parameters:

$$m(\omega) = m_0(b+\omega)\omega\,. \tag{284}$$

The normalization coefficient m_0 is determined by a χ^2 fit to the correlator. In absence of data, the default model $m(\omega)$ becomes the most probable spectral function, so that the parameter b permits a non-zero value of the intercepts of $m(\omega)/\omega$, i.e. a non-zero conductivity. Varying b effectively changes the default model and it provides a crucial

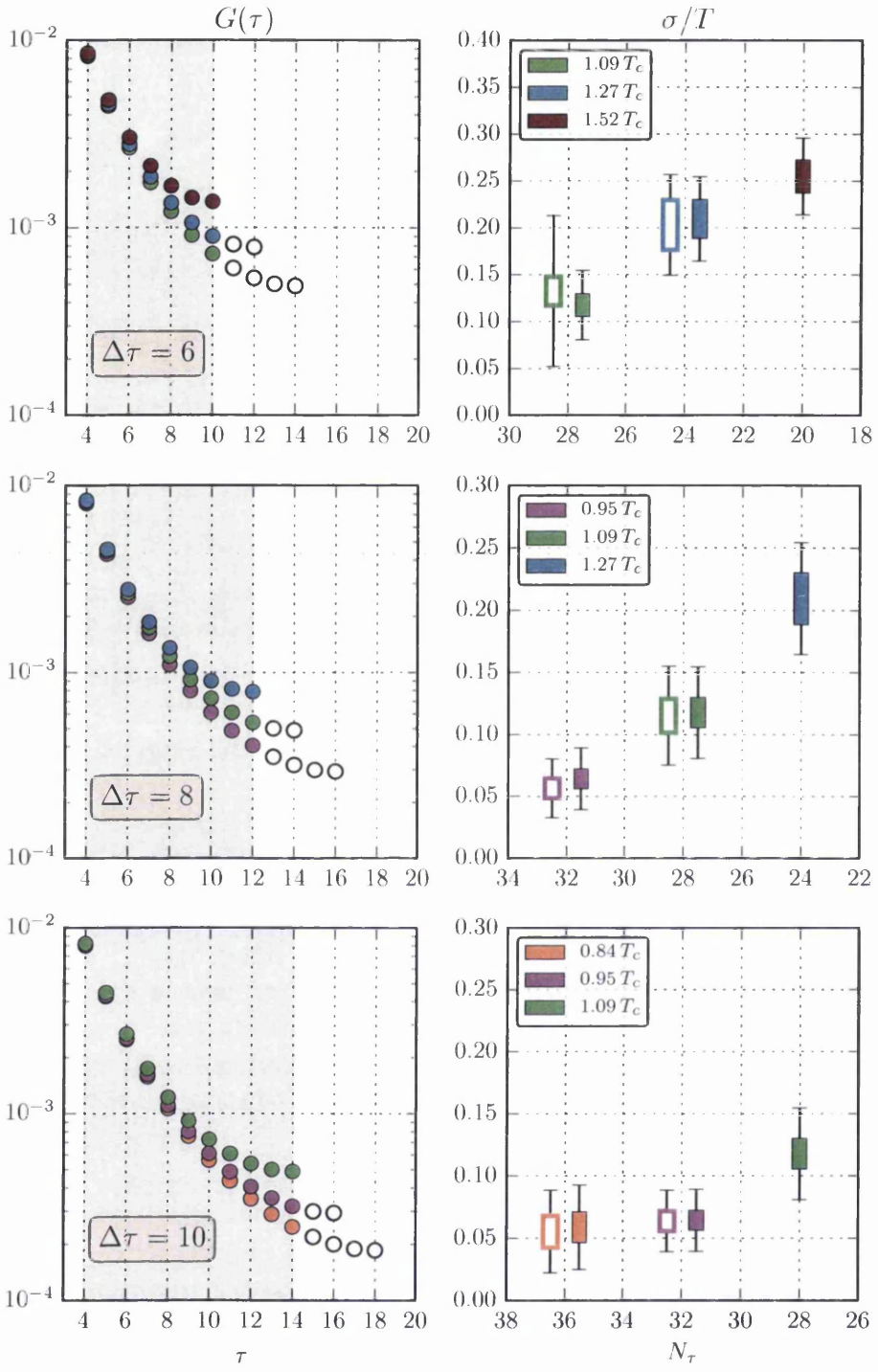

Figure 29: Stability tests discarding the last time slices in the correlator. Left: correlators with used time slices indicated. Right: corresponding MEM results for $C_{\mathrm{em}}^{-1}\sigma/T$. Open symbols use the restricted time range $\Delta\tau$ shown in the left pane, full symbols use the entire time range available.

test to verify the robustness of our results. The dependence on b of the conductivity is shown in Fig. 27. It is clear how setting $b = 0$ should be avoided, since it unnaturally pushes the conductivity to zero. Instead, when $b \gtrsim 0.4$ the value for σ stabilises, forming clear plateaux. A larger sensitivity to b at the highest temperature is to be expected, since a smaller number of time slices is available to perform the MEM analysis.

From the point of view of the MEM algorithm, it is clear how a higher resolution in the correlator $G(\tau)$ is more desirable. In our case, this was achieved by the introduction of the anisotropy. In order to justify this choice a posteriori, we run MEM using only a subset of the available time slices in the correlator, and check whether the result is stable. This is shown in Fig. 28, where the red symbols use all the available points $4 \leq \tau \leq N_\tau/2$, the blue ones use only the even times slices $\tau = 4, 6, 8, \ldots, N_\tau/2$, while the green ones use one every three $\tau = 4, 7, 10, \ldots$ which is roughly the number of points available without the anisotropy. It is clear that for high temperatures, the anisotropy is crucial to extract a signal for the conductivity. For colder ensembles the result is instead stable.

The number of Euclidean points available in the correlator will decrease as the temperature is raised. One might think that this difference in the extent of $G(\tau)$ is responsible for the T-dependence of the conductivity, rather than a genuine thermal effect. To show that this is not the case, we run the MEM analysis on correlators at different temperatures, but constrained to have the same number of time slices, which is achieved by systematically discarding the last points in colder ensembles. A graphical representation of the procedure is shown in Fig. 29. We observe excellent stability as the Euclidean time range is varied.

6.4 SUSCEPTIBILITIES

An estimate of the fluctuations of a conserved charge in an excited medium can provide useful physical information. In fact, these fluctuations can be measured [100] in heavy-ion collision experiments (discussed in section 2.6), so that a combination with a first principles lattice QCD calculation is possible, which can then provide a reliable thermometer for such experiments.

The fluctuations are quantified by the susceptibilities, which are the second order derivatives of the free energy with respect to the chemical potential associated with the investigated charge. In particular, the

quark number density n_i and the quark number susceptibilities χ_i are defined as:

$$n_i = \frac{T}{V}\frac{\partial}{\partial \mu_i} \ln Z\,, \qquad \chi_{ij} = \frac{T}{V}\frac{\partial^2}{\partial \mu_i \partial \mu_j} \ln Z\,. \tag{285}$$

Here Z is the partition function of QCD, introduced in chapter 1 (see Eq. 101) and μ_i are the quark chemical potentials for each flavour, with $i \in \{l, s\}$, where l stands for "light", as we are considering degenerate up and down quarks, and s for strange.

We now proceed with some technical remarks. It is useful to introduce the following terms:

$$T_1^i = \langle \frac{T}{V} \mathrm{Tr}\left[D^{-1}\frac{\partial D}{\partial \mu_i}\right]\rangle\,, \quad T_2^i = \langle \frac{T}{V} \mathrm{Tr}\left[D^{-1}\frac{\partial^2 D}{\partial \mu_i^2}\right]\rangle\,, \tag{286a}$$

$$T_3^{ij} = \langle \frac{T}{V} \mathrm{Tr}\left[D^{-1}\frac{\partial D}{\partial \mu_i}\right] \mathrm{Tr}\left[D^{-1}\frac{\partial D}{\partial \mu_j}\right]\rangle\,, \tag{286b}$$

$$T_4^i = \langle \frac{T}{V} \mathrm{Tr}\left[D^{-1}\frac{\partial D}{\partial \mu_i} D^{-1}\frac{\partial D}{\partial \mu_i}\right]\rangle\,, \tag{286c}$$

where D is the Dirac operator defined in Eq. (238), T is the temperature and V is the physical volume. The terms T_1, T_2, T_4 are called *connected* since they only contain one trace, while T_3 is called *disconnected.* In Appendix A.3 we will see that, from a numerical point of view, it is the most expensive to evaluate.

The quantities defined in Eq. (285) can then be rewritten using the definitions above. We obtain:

$$n_i = T_1^i\,, \tag{287a}$$

$$\chi_{ii} = -(T_1^i)^2 + T_2^i + T_3^{ii} - T_4^i\,, \tag{287b}$$

$$\chi_{ij} = -T_1^i T_1^j + T_3^{ij} \quad (\text{here } i \neq j)\,. \tag{287c}$$

The lattice evaluation of the different T terms of Eq. (286) has been done in collaboration with P. Giudice [5] and the results are shown in Fig. 30. Note that we only used lattices with spatial extent $N_s = 24$, see Table 2 for more details. The numerical evaluation has been carried out using noisy estimator techniques, which are described in Appendix A.3. In particular, we used $N_v = 9$ noise vectors ξ_i for the connected terms T_2, T_4 and $N_v = 100$ for the disconnected term T_3. For the $N_\tau = 40$ ensemble, this was increased to $N_v = 200$.

We can see that only the connected terms T_2 and T_4 contribute significantly to the susceptibilities in Eq. (287). Note how the terms relative to the light quark channel are considerably bigger than the strange ones. In [101], a hopping parameter expansion predicted a negative

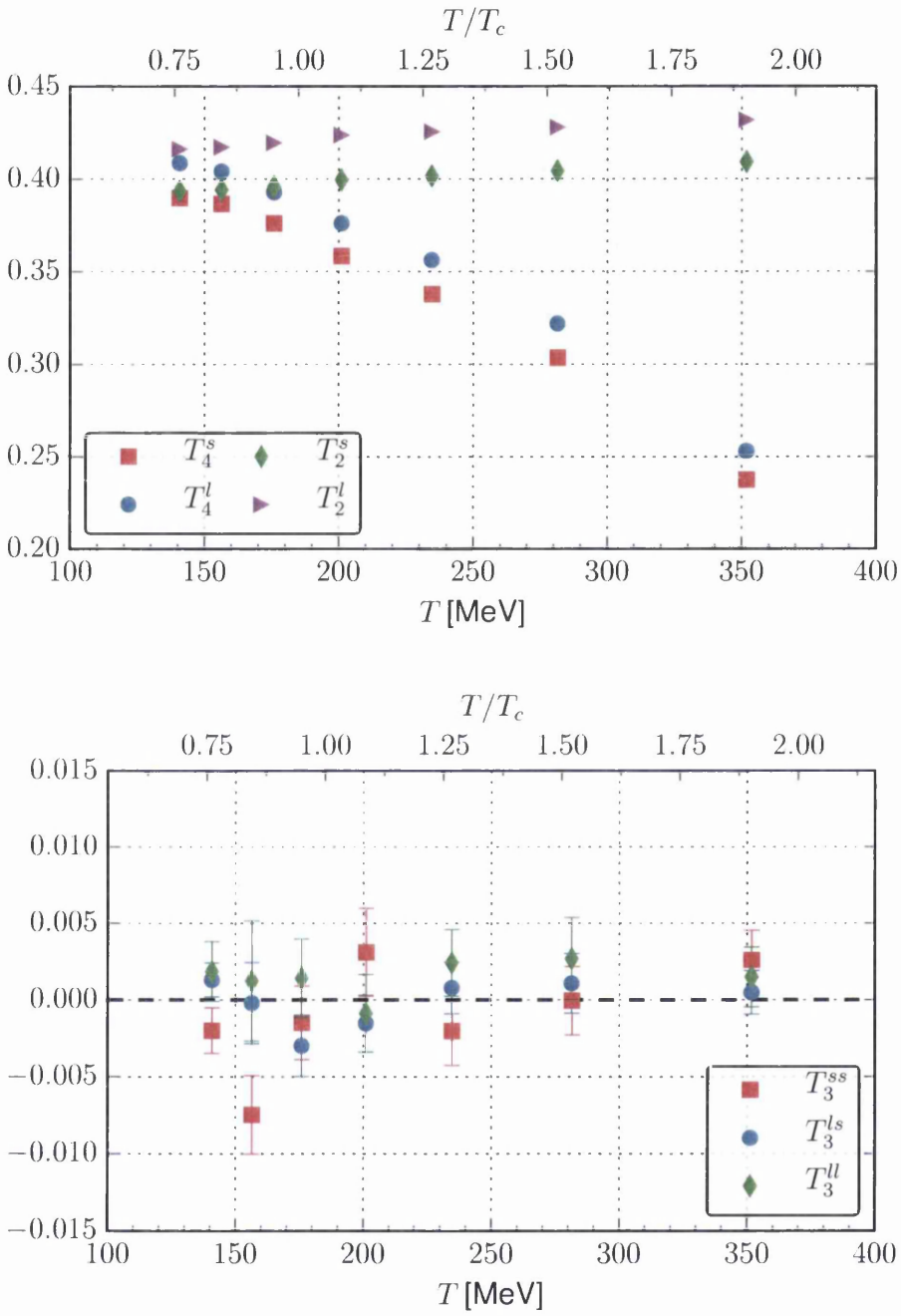

Figure 30: Terms T_2, T_4 and T_3.

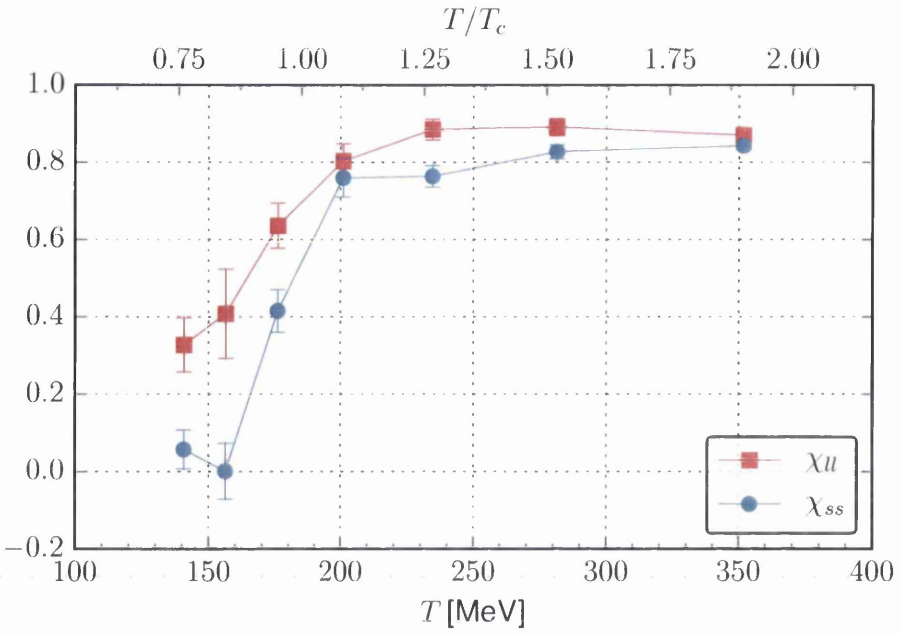

Figure 31: Quark number susceptibilities for light χ_{ll} and strange χ_{ss} quarks. All the quantities are normalised with respect to the value obtained for free massless Wilson fermions on the lattice.

value for the term T_3. This is, within errors, consistent with our results in Fig. 30 (Bottom). The off-diagonal term T_3^{ls}, representing the correlation between different flavors, is expected to be different from zero, as shown in the context of Hard thermal loop (HTL) perturbation theory [102]. More recent lattice calculations [103] have shown that T_3^{ls} has a clear dip in the crossover region. Our results are consistent with this, but also compatible with zero, both at low and high temperature, which might be a consequence of our rather large pion mass. The only negative non-zero value is achieved for T_3^{ss} at the temperature of 156 MeV.

In Fig. 31 the quark number susceptibilities of Eq. (285) are shown separately for light and strange quarks. They exhibit a rapid rise in the crossover region; at low temperature they are small due to quark confinement, but at high temperature they are large and approach the ideal gas limit. We note that fluctuations have also been used to probe quark deconfinement [104] by studying event-by-event fluctuations of charged particle ratios [105].

We also consider the second order susceptibilities of baryon number, electrical charge and isospin, which have been studied by many groups in the past [103, 106–108]. These are defined as:

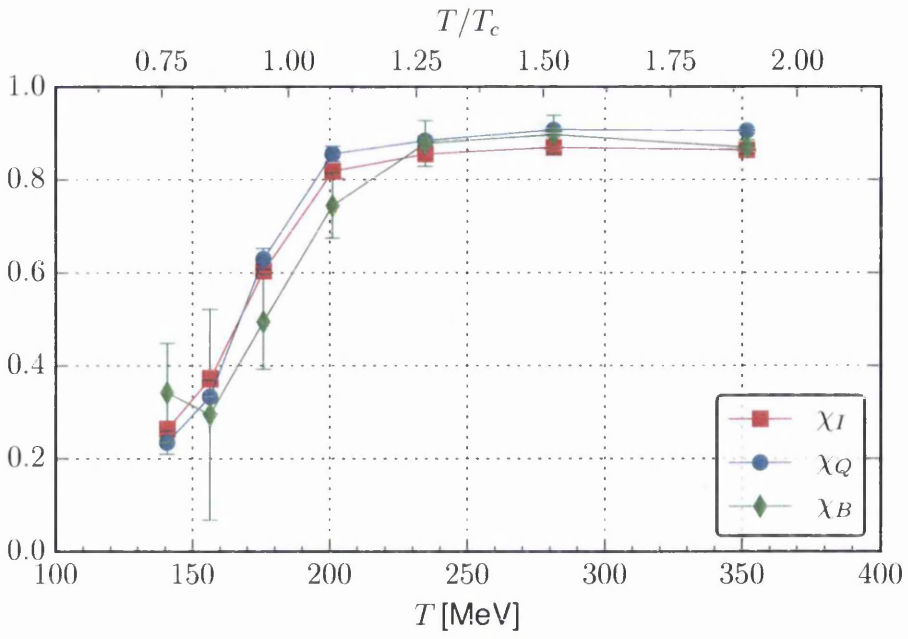

Figure 32: Electrical χ_Q, Isospin χ_I and Baryonic susceptibilities are shown for different values of the temperature T. All the quantities are normalised with respect to the value obtained for free massless Wilson fermions.

- Electrical charge:

$$Q = \frac{T}{V}\frac{\partial \ln Z}{\partial \mu_Q} = \sum_{i=1}^{3} q^i n_i \,, \qquad \chi_Q = \frac{\partial Q}{\partial \mu_Q} = \sum_{i=1}^{3} (q^i)^2 \chi_{ii} + \sum_{i \neq j}^{3} q^i q^j \chi_{ij} \,. \tag{288}$$

- Baryon number:

$$B = \frac{T}{V}\frac{\partial \ln Z}{\partial \mu_B} = \sum_{i=1}^{3} n_i \,, \qquad \chi_B = \frac{\partial B}{\partial \mu_B} = \sum_{i=1}^{3} \chi_{ii} + \sum_{i \neq j}^{3} \chi_{ij} \,. \tag{289}$$

- Isospin (with $\mu_I = \mu_d - \mu_u$):

$$\begin{aligned} \chi_I = \frac{T}{V}\frac{\partial^2 \ln Z}{\partial \mu_I^2} &= \frac{1}{4}\frac{T}{V}\left[\frac{\partial^2 \ln Z}{\partial \mu_u^2} + \frac{\partial^2 \ln Z}{\partial \mu_d^2} - 2\frac{\partial^2 \ln Z}{\partial \mu_u \partial \mu_d}\right] \\ &= \frac{1}{4}\sum_{i=1}^{2}\left[T_2^i - T_4^i\right] . \end{aligned} \tag{290}$$

Note how χ_I depends only on the terms T_2 and T_4 but not T_3 which, from a numerical point of view, is the most expensive quantity to determine since it comes from a disconnected diagram. The results for these

quantities are shown in Fig. 32, where they have been normalised by their value in the free massless Wilson case.

For χ_I and χ_Q, a steep increase is observed above 150 MeV and for $T \gtrsim 250$ MeV the value of χ_I is above 85% of the Stefan-Boltzmann value. As we discussed in section 5.4 regarding the Euclidean correlators, this might be considered as a systematic error due to the uncertainty affecting the lattice anisotropy and the difficulty of defining the latter in the free theory.

The value of the electrical charge susceptibility reaches an apparent saturation value above 250 MeV. This result will be used in Section 6.5 to determine the diffusion coefficient.

The data for the baryon number susceptibility present larger errorbars due to the different combination of the terms in Eq. (286). The result clearly shows the release of baryon degrees of freedom when the system undergoes the transition from confined to QGP matter.

6.5 DIFFUSION

In the long wavelength limit, the correlator Eq. (181) can be described by the diffusion equation. This can be seen as a low energy effective theory which can be solved by coupling the equation for the current conservation to some constitutive equation. These are expressed in terms of a derivative expansion with unknown parameters, which are determined by a matching procedure with QCD. We follow here the treatment of [35, 96] and write down the constitutive equation for the electrical current J_{em} in presence of an external electric field $\mathbf{E}$ as:

$$\mathbf{J}_{\mathrm{em}} = -D\boldsymbol{\nabla}Q + \sigma \boldsymbol{E} + \text{higher order terms}\ldots \tag{291}$$

where D is the diffusion coefficient, and Q is the electrical charge of Eq. (288).

In the Hamiltonian describing the evolution of this system, both μ_Q and A_0 couple to the charge density, which implies that a perturbation of the form $\mu_Q(x) + A_0(x) = 0$ leaves the system unaffected. The consequence is that in Eq. (291) the coefficients in front of these quantities are not independent, so that we have:

$$D = \frac{\sigma}{\chi_Q}, \tag{292}$$

where χ_Q is the electrical charge susceptibility defined in Eq. (288). The conservation law for the current $\partial_\mu j^\mu_{\mathrm{em}}(x) = 0$ can then be solved in the presence of an electric field in the long wavelength limit [96, 109], yielding a result for the electromagnetic spectral function similar to that of Eq. (280). In fact, the drag coefficient ς appearing in Eq. (280) is directly related to D by $D = T/(m\varsigma)$ [110].

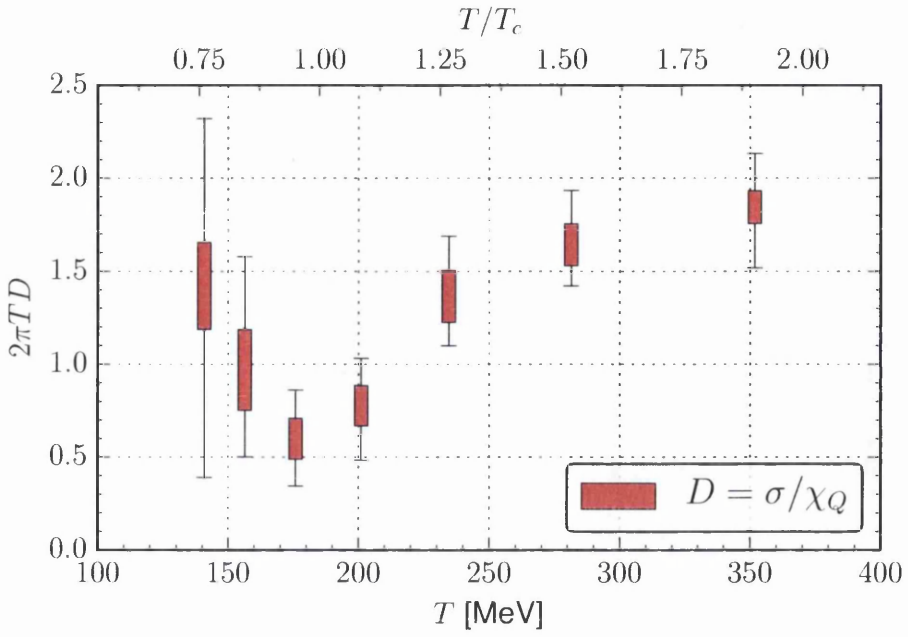

Figure 33: The diffusion coefficient D of Eq. (292) as a function of the temperature. The vertical size of the rectangles reflects the systematics from the estimate of the conductivity (see Fig. 25), while the error bars include the statistical jackknife error from both σ and χ_Q. A noisier value for the latter is responsible for the larger uncertainty at low T.

In Fig. 33, we plot our result for the diffusion coefficient, obtained by taking the ratio between our lattice evaluation of σ and χ_Q. Despite the large error bars, one can see that D is of the order $(2\pi T)^{-1}$ and shows a dip in the crossover region. Similar conclusions were found in [111], where the authors combined our data for the light quarks conductivity with the results for the susceptibility from [103]. The results for D were then used to study the charge density fluctuations with stochastic hydrodynamics in QCD matter undergoing Bjorken expansion.

6.6 DISCUSSION

The electrical conductivity of the quark-gluon plasma has been the subject of many studies in the past [8, 34, 36–41, 68, 112–120].

Many attempts have been made to describe the temperature dependence of σ by either some effective QCD models or semi-analytical tools [8, 34, 37, 38, 112, 114–120]. A detailed analysis of them is out of the scope of this thesis, here instead we list them for the interested reader: the calculation in perturbation theory [8, 34]; the conductivity

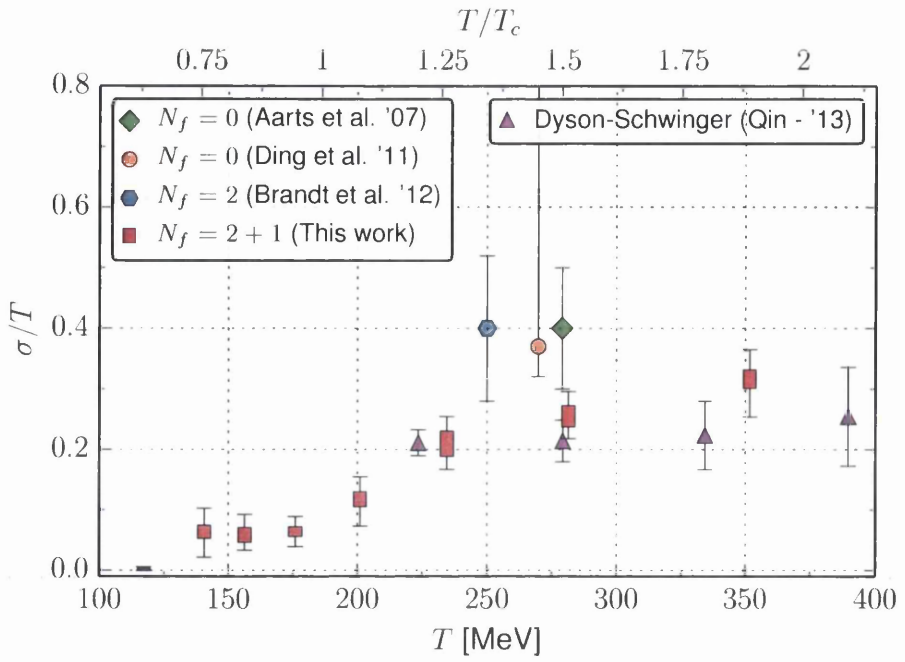

Figure 34: Temperature dependence of the electrical conductivity σ/T in the light sector compared with previously obtained results: diamonds [40], circle [39], hexagon [68], triangle [112]. Note that the $N_f = 0$ results are inserted matching the values of T/T_c.

of a gas of pions [114, 115]; the dilute instanton-liquid model [116]; a calculation using the Dyson-Schwinger method [112] (also shown in Fig. 34); an approach involving the off-shell Parton-Hadron-String Dynamics (PHSD) [117]; results obtained via the relativistic Boltzmann equation [118, 119] and a holographic calculation [38].

Now we discuss results in the context of lattice QCD, obtained by other groups [36, 39–41, 68, 113]. An early study of the conductivity was performed in 2004 by Gupta [41], using a quenched calculation with staggered fermions. Note that matching the physical degrees of freedom in the staggered formulation is troublesome and the Euclidean correlator G_{em} receives a signal from an opposite parity partner, which effectively reduces the number of usable points in the temporal direction. Results were obtained by fitting the Fourier transform of the electromagnetic correlator, which gave $\sigma/T = 7$ at $1.5 \leq T/T_c \leq 3.0$, where the critical temperature in pure $SU(3)$ gauge theory is around 290 MeV.

In 2007, another lattice study with staggered fermions was performed by Aarts et al. [40] using the same MEM method as in this thesis. They found a value $\sigma/T = 0.4(1)$ corresponding to $T/T_c = 1.5$, represented by a green diamond in Fig. 34.

A quenched study using Wilson-Clover fermions with a continuum limit extrapolation, was performed in 2011 by Ding et al. [39]. The conductivity was obtained as a result of fitting the correlator using a simple ansatz for the spectral function, featuring a Breit-Wigner term and a free spectral function. The result was $0.33 \leq \sigma/T \leq 1$ at a temperature of $T = 1.45\,T_c$ [39] and it is represented by the orange circle in Fig. 34. This work was then extended in [36, 113] by Kaczmarek et al. to the temperatures $1.1\,T_c$, $1.2\,T_c$ and $1.4\,T_c$, for which the authors found no temperature dependence for σ within the systematic errors.

In [68], Brandt et al. produced a $N_f = 2$ lattice calculation with Wilson-Clover fermions. The difference of the thermal and zero temperature spectral functions was constrained using an exact sum rule. This was then fitted using an ansatz with many coefficients to parametrize the transport and bound state peak and the deviation from the free theory of the spectral function. They obtained $\sigma/T = 0.40(12)$ at $T = 250$ MeV as shown in Fig. 34.

Our results, shown as well in Fig. 34, are the first $N_f = 2 + 1$ calculation of σ over a wide range of temperatures across T_c. Inside the QGP, they are comparable with the ones described above, but we have for the first time observed an increase of σ, which starts already in the confined phase.

7

CONCLUSIONS

In this thesis, we studied the temperature dependence of the electrical conductivity and the charge diffusion coefficient, in the framework of lattice QCD.

We used a clover-improved fermion action with $N_f = 2+1$ flavors on anisotropic lattices [9, 10]. In particular we worked with an anisotropy of $\xi = a_s/a_t = 3.5$ with $a_t = 0.03506(23)$ fm on lattices with spatial extension $N_s = 24, 32$ and a temporal extension varying between $N_\tau = 16 \div 128$. We scanned a temperature range between 43 MeV and 352 MeV with a critical temperature of $T_c = 185(4)$ MeV, which is estimated by looking at the inflection point of renormalized Polyakov loops.

We studied the conserved vector current, which though more expensive to compute, does not require any renormalization. We analysed the ratio of the correlators between the interacting and the free theory and noticed that they tend to cluster together in the QGP phase, where they approach clear plateaux. The numerical value of the latter is different from 1, which might be due either to the influence of the uncertainty on the anisotropy or discretization artefacts. A definite answer can be given only by taking the continuum limit. We also compared thermal correlators with their vacuum value at $T \approx 0$, and found out that they differ by many orders of magnitude. The volume effects have been estimated by inspecting the ratio between correlators obtained in the $N_s = 32$ and in the $N_s = 24$ ensembles and appeared to be negligible.

Spectral functions $\rho(\omega)$ in the electromagnetic channel were extracted from the correlators using the Maximum Entropy Method (MEM) with a modified version of the Bryan algorithm [40, 69, 73]. At low temperature we found evidence for a bound state peak corresponding to the mass of the vector meson (ρ or ϕ), which matches hadron spectroscopy calculations carried out at zero temperature [10]. The peak survives until $T \approx T_c$ and is then no longer distinguishable at higher temperatures. When plotting $\rho(\omega)/\omega T$ we see a transport peak at the origin, whose intercept depends on the temperature. It is absent at low temperatures and appears when $T \gtrsim 0.76\, T_c$.

The conductivity is obtained from the low-frequency limit of $\rho(\omega)/\omega$ by using the Kubo relations for all the available temperatures. It is non-zero in the crossover region and rises smoothly until it reaches $\sigma/T \approx 0.3$ at the highest temperature. Inside the QGP its value is compatible with previously obtained results [36, 39, 40, 68, 113], while for the first time its temperature dependence is evaluated from lattice QCD.

The MEM reconstruction has been subject to several tests to ensure the robustness of the results. First, we check the independence from the default model $m(\omega) = m_0\omega(b+\omega)$ by varying the value of b between 0 and 1. We found that for values of $b \gtrsim 0.4$ the conductivity stabilises into a plateau, while for small b it is unnaturally forced to 0. This systematic effect is taken into account in the final error by considering all the values with $b \gtrsim 0.4$.

The impact of the anisotropy, i.e. having more time slices available in the correlator, is checked by performing the MEM reconstruction using only a subset of the available points. This leads to high instabilities at high temperatures where N_τ is small, which shows how the anisotropy pays off in this regime.

The susceptibilities χ of the baryon, electrical and isospin charge have been evaluated. These are expressed as a linear combination of the diagonal and cross terms for the quark number susceptibilities, which are then numerically evaluated using stochastic estimators. The disconnected piece are small and, in most cases, compatible with zero. All the susceptibilities experience a steep increase at the crossover point, at the lowest temperature of 141 MeV are different from zero and at high temperature they reach 85% of the Stefan-Boltzmann value.

Finally, we calculated the charge diffusion coefficient by taking the ratio between the electrical conductivity and the electrical charge susceptibility. This is affected by rather large error bars and it varies between $0.5 \div 2 \times (2\pi T)^{-1}$, showing the signs of a dip in the crossover region.

The analysis presented in this thesis is based on data at non-zero lattice spacing. It would be interesting to repeat the analysis in the continuum limit, as has been done in the quenched theory [36, 39, 113]. In this respect the results obtained here should be regarded as preliminary.

APPENDIX

A.1 GAMMA MATRICES

The Euclidean gamma matrices γ_μ with $\mu = 0,1,2,3$ satisfy the anti-commutation relations:

$$\{\gamma_\mu, \gamma_\nu\} = 2\delta_{\mu\nu}\,. \tag{293}$$

In this work, we choose the so-called chiral representation [14], where $\gamma_5 = \gamma_0\gamma_1\gamma_2\gamma_3$ is diagonal. They are defined as:

$$\gamma_0 = \begin{pmatrix} 0 & 0 & -1 & 0 \\ 0 & 0 & 0 & -1 \\ -1 & 0 & 0 & 0 \\ 0 & -1 & 0 & 0 \end{pmatrix} \qquad \gamma_1 = \begin{pmatrix} 0 & 0 & 0 & -\mathrm{i} \\ 0 & 0 & -\mathrm{i} & 0 \\ 0 & \mathrm{i} & 0 & 0 \\ \mathrm{i} & 0 & 0 & 0 \end{pmatrix}$$

$$\gamma_2 = \begin{pmatrix} 0 & 0 & 0 & -1 \\ 0 & 0 & 1 & 0 \\ 0 & 1 & 0 & 0 \\ -1 & 0 & 0 & 0 \end{pmatrix} \qquad \gamma_3 = \begin{pmatrix} 0 & 0 & -\mathrm{i} & 0 \\ 0 & 0 & 0 & \mathrm{i} \\ \mathrm{i} & 0 & 0 & 0 \\ 0 & -\mathrm{i} & 0 & 0 \end{pmatrix}$$

$$\gamma_5 = \begin{pmatrix} 1 & 0 & 0 & 0 \\ 0 & 1 & 0 & 0 \\ 0 & 0 & -1 & 0 \\ 0 & 0 & 0 & -1 \end{pmatrix}\,. \tag{294}$$

A.2 DIMENSIONAL ANALYSIS

In this appendix we want to derive the dimension of the spectral function $\rho(\omega)$ in terms of the temporal a_t and spatial a_s lattice spacing. In this context, we will label with "phys" quantities which carry a dimension O^{phys}. Dimensionless quantities, like the ones obtained from the

lattice, do not carry any label instead. Let us consider the dimensionless Dirac operator we use in our study (see Eq. 238). Neglecting its mass, it has the form:

$$D = \not{D}_0 + \frac{1}{\xi_f}\sum_i \not{D}_i + \text{clover}\,. \tag{295}$$

We can consider the free case without any loss of generality so that:

$$D_0\psi(x) = \frac{\psi(x+\hat{0}) - \psi(x-\hat{0})}{2}\,, \tag{296}$$

$$D_i\psi(x) = \frac{\psi(x+\hat{\imath}) - \psi(x-\hat{\imath})}{2}\,, \tag{297}$$

The action then assumes the form (neglecting the clover term):

$$\begin{aligned} S =& a_s^3\, a_t \sum_x \bar{\psi}^{\text{phys}}(x) M^{\text{phys}} \psi^{\text{phys}}(x) \\ =& a_s^3\, a_t \sum_x \left[\frac{1}{a_t}\bar{\psi}^{\text{phys}}(x)\not{D}_0\psi^{\text{phys}}(x) + \frac{1}{a_t\,\xi_f}\sum_i \bar{\psi}^{\text{phys}}(x)\not{D}_i\psi^{\text{phys}}(x)\right]. \end{aligned} \tag{298}$$

We remind that the anisotropy is defined as

$$a_s = \xi\, a_t\,, \tag{299}$$

so the spatial Dirac term has effectively a a_s^{-1} in front of it. In Eq. (238) the factor a_t then drops out and we are left with:

$$S = a_s^3 \sum_x \left[\bar{\psi}^{\text{phys}}(x)\not{D}_0\psi^{\text{phys}}(x) + \frac{1}{\xi_f}\sum_i \bar{\psi}^{\text{phys}}(x)\not{D}_i\psi^{\text{phys}}(x)\right]. \tag{300}$$

If we apply the substitution

$$\psi^{\text{phys}} = a_s^{-\frac{3}{2}}\psi\,, \tag{301}$$

we obtain

$$S = \sum_x \left[\bar{\psi}(x)\not{D}_0\psi(x) + \frac{1}{\xi_f}\sum_i \bar{\psi}(x)\not{D}_i\psi(x)\right], \tag{302}$$

where all the quantities are dimensionless. The conserved current, defined in section 5.2, is:

$$\begin{aligned} V_i(m) = \frac{1}{2\xi_f}\Big[& \bar{\psi}(m+\hat{\imath})(1+\gamma_i)\,\psi(m) \\ & -\bar{\psi}(m)(1-\gamma_i)\,\psi(m+\hat{\imath})\Big]. \end{aligned} \tag{303}$$

Physically, the current is the amount of charge that flows in a unit surface per unit time, so that:

$$V_i^{\text{phys}} \equiv a_s^{-2} a_t^{-1} V_i \,. \tag{304}$$

In fact, we have

$$\begin{aligned} V_i^{\text{phys}}(m) &= \frac{a_s^{-2} a_t^{-1}}{2\xi_f} \bar{\psi}(m+\hat{\imath})(1+\gamma_i)\,\psi(m) + \dots \\ &= \frac{a_s^{-3}}{2} \bar{\psi}(m+\hat{\imath})(1+\gamma_i)\,\psi(m) + \dots \\ &= \frac{1}{2} \bar{\psi}^{\text{phys}}(m+\hat{\imath})(1+\gamma_i)\,\psi^{\text{phys}}(m) + \dots \,, \end{aligned} \tag{305}$$

where in the second line we used Eq. (299). Let us consider the current-current correlator. The vacuum $|0\rangle$ is normalized as $\langle 0|0\rangle = 1$ and the only object that carries a dimension is the current. We want to compute the zero momentum limit of the correlator:

$$G(t)^{\text{phys}} \equiv a_s^3 \sum_{\vec{y},i} \langle\, V_i^{\text{phys}}(\vec{x}, x_0)\, V_i^{\text{phys}}(\vec{y}, t+x_0)^\dagger \,\rangle \tag{306}$$

$$= a_s^3\, a_s^{-4}\, a_t^{-2} \sum_{\vec{y},i} \langle\, V_i(\vec{x}, x_0)\, V_i(\vec{y}, t+x_0)^\dagger \,\rangle \tag{307}$$

$$= a_s^{-1} a_t^{-2} G(t) \,. \tag{308}$$

Now the relation to the spectral function is (see Eq. 181):

$$G(t) = \int_0^\infty \mathrm{d}\omega \rho(\omega) K(\omega, t) \,, \tag{309}$$

where the frequency scales with the temporal lattice spacing as

$$\omega^{\text{phys}} = \omega a_t^{-1} \,. \tag{310}$$

Multiplying Eq. (309) by $a_s^{-1} a_t^{-2}$ on both sides and using (310) we have:

$$\begin{aligned} a_s^{-1} a_t^{-2} G(t) = G(t)^{\text{phys}} &= \int \mathrm{d}\omega\, a_s^{-1} a_t^{-2} \rho(\omega) K(\omega, t) \\ &= \int \mathrm{d}\omega^{\text{phys}}\, a_s^{-1} a_t^{-1} \rho(\omega) K(\omega, t) \end{aligned} \tag{311}$$

So it must be that:

$$\rho^{\text{phys}} = a_t^{-1}\, a_s^{-1} \rho \,. \tag{312}$$

Introducing the temperature as usual

$$T = (a_t N_t)^{-1} \,, \tag{313}$$

and taking the dimensionless ratio between $\rho(\omega)$ and T, we have:

$$\frac{1}{T} \frac{\rho^{\text{phys}}}{\omega^{\text{phys}}} = (a_t N_t) \frac{a_t^{-1} a_s^{-1} \rho}{\omega a_t^{-1}} = a_t^1 a_s^{-1} \frac{\rho N_t}{\omega} = \frac{\rho N_t}{\omega \xi} \,, \tag{314}$$

where we can see that a factor of the anisotropy has to be introduced in order to get the right result.

A.3 NOISY ESTIMATORS

Here we will describe the stochastic method used to evaluate the trace of an $N \times N$ matrix, where N is very large. These are widely used in the context of lattice QCD for the calculation of flavor singlet quantities, also referred to as disconnected diagrams. In particular, we will employ them in the calculation of the susceptibilities discussed in section 6.4, where in the case of Eq. (286), $N \equiv N_c \times N_D \times N_V$ with color $N_c = 3$, Dirac $N_D = 4$ and space-time N_V indices.

In this method, one generates an ensemble of random, independent $N-$dimensional complex vectors $\vec{\xi}$, where each component ξ_i is drawn from a Gaussian distribution of unit variance. The identity

$$\frac{1}{2}\int \prod_{k=1}^{N} \frac{\mathrm{d}^2\xi_k}{2\pi}\, \xi_i^*\, \xi_j\, \exp^{-|\vec{\xi}|^2/2} = \delta_{ij}\,, \tag{315}$$

follows from the properties of the Gaussian integral and can be symbolically rewritten in the form

$$\langle \xi_i^*\, \xi_j \rangle = \delta_{ij}\,, \tag{316}$$

where the average $\langle\rangle$ is intended over the set $\{\,\vec{\xi}\,\}$ of the N_v generated noisy vectors. These are then used as a source for the inversion of the Dirac operator (cfg. Eq. (264))

$$D_{ij} S_j = \xi_i\,. \tag{317}$$

A stochastic estimate of the inverse D^{-1} can then be obtained on each gauge configuration by an average over the noise vectors using the formula:

$$\langle \xi_j^*\, S_i \rangle = D^{-1}_{ik}\, \langle \xi_j^*\, \xi_k \rangle = D^{-1}_{ij}\,, \tag{318}$$

from which the trace $\mathrm{Tr}\, D^{-1}$ can be obtained by setting $i = j$.

In the case one has to evaluate the square of a trace $(\mathrm{Tr}\, A)^2$, it is more efficient to use L sets of independent noisy vectors [121, 122]:

$$(\mathrm{Tr}\, A)^2 = \frac{2}{L(L-1)} \sum_{i>j=1}^{L} \langle \vec{\xi}^{\dagger} A\, \vec{\xi} \rangle_i\; \langle \vec{\xi}^{\dagger} A\, \vec{\xi} \rangle_j\,, \tag{319}$$

where $\langle\rangle_i$ represent the estimate from the $i-$th ensemble. The diagonal terms are then not taken into account, as they would introduce a bias in the final result given by a term whose relative significance is $O(1/N_v)$. This is the reason why the disconnected term T_3 in Eq. (286) is numerically expensive to obtain.

LIST OF FIGURES

LIST OF TABLES

BIBLIOGRAPHY

[1] C. Allton, G. Aarts, A. Amato, W. Evans, P. Giudice, et al., *Quark-gluon plasma phenomenology from the lattice*, arXiv:1310.5135.

[2] C. Allton, G. Aarts, A. Amato, W. Evans, P. Giudice, et al., *2+1 flavour thermal studies on an anisotropic lattice*, *PoS* LATTICE2013 (2014) 151.

[3] A. Amato, G. Aarts, C. Allton, P. Giudice, S. Hands, et al., *Electrical conductivity of the quark-gluon plasma across the deconfinement transition*, *Phys.Rev.Lett.* 111 (2013) 172001.

[4] A. Amato, G. Aarts, C. Allton, P. Giudice, S. Hands, et al., *Transport coefficients of the QGP*, arXiv:1310.7466.

[5] P. Giudice, G. Aarts, C. Allton, A. Amato, S. Hands, et al., *Electric charge susceptibility in 2+1 flavour QCD on an anisotropic lattice*, arXiv:1309.6253.

[6] G. Aarts, C. Allton, A. Amato, P. Giudice, S. Hands, and J.-I. Skullerud *In preparation.*

[7] P. B. Arnold, G. D. Moore, and L. G. Yaffe, *Photon emission from quark gluon plasma: Complete leading order results*, *JHEP* 0112 (2001) 009.

[8] P. B. Arnold, G. D. Moore, and L. G. Yaffe, *Transport coefficients in high temperature gauge theories. 2. Beyond leading log*, *JHEP* 0305 (2003) 051.

[9] H.-W. Lin et al., *First results from 2+1 dynamical quark flavors on an anisotropic lattice: Light-hadron spectroscopy and setting the strange-quark mass*, *Phys.Rev.* D79 (2009) 034502.

[10] R. G. Edwards, B. Joo, and H.-W. Lin, *Tuning for Three-flavors of Anisotropic Clover Fermions with Stout-link Smearing*, *Phys.Rev.* D78 (2008) 054501.

[11] M. Creutz, *Quarks, Gluons and Lattices.* Cambridge Monographs on Mathematical Physics. Cambridge University Press, 1983.

[12] T. DeGrand and C. DeTar, *Lattice Methods for Quantum Chromodynamics.* World Scientific, 2006.

[13] J. Smit, *Introduction to Quantum Fields on a Lattice.* Cambridge Lecture Notes in Physics. Cambridge University Press, 2002.

[14] C. Gattringer and C. Lang, *Quantum Chromodynamics on the Lattice: An Introductory Presentation.* Lecture Notes in Physics. Springer, 2009.

[15] I. Montvay and G. Münster, *Quantum Fields on a Lattice.* Cambridge Monographs on Mathematical Physics. Cambridge University Press, 1997.

[16] M. Peskin and D. Schroeder, *An Introduction To Quantum Field Theory.* Frontiers in physics. Westview Press, 1995.

[17] M. Bellac, *Thermal Field Theory.* Cambridge Monographs on Mathematical Physics. Cambridge University Press, 2000.

[18] L. Ryder, *Quantum Field Theory.* Cambridge University Press, 1996.

[19] I. Aitchison and A. Hey, *Gauge Theories in Particle Physics: QCD and the Electroweak Theory, Third Edition.* Graduate Student Series in Physics. Taylor & Francis, 2003.

[20] J. I. Kapusta and C. Gale, *Finite-Temperature Field Theory: Principles and Applications.* Cambridge monographs on mathematical physics. Cambridge University Press, 2006.

[21] K. G. Wilson, *Confinement of quarks, Phys. Rev. D* 10 (Oct, 1974) 2445–2459.

[22] K. Symanzik, *Continuum limit and improved action in lattice theories:(I). Principles and ϕ^4 theory, Nuclear Physics B* 226 (1983) 187–204.

[23] K. Symanzik, *Continuum limit and improved action in lattice theories:(II). O(N) non-linear sigma model in perturbation theory, Nuclear Physics B* 226 (1983) 205–227.

[24] B. Sheikholeslami and R. Wohlert, *Improved continuum limit lattice action for QCD with wilson fermions, Nuclear Physics B* 259 (1985) 572–596.

[25] S. Musberg, G. Münster, and S. Piemonte, *Perturbative calculation of the clover term for Wilson fermions in any representation of the gauge group SU(N), JHEP* 1305 (2013) 143.

[26] S. Duane, A. D. Kennedy, B. J. Pendleton, and D. Roweth, *Hybrd Monte Carlo, Physics Letters B* 195 (1987) 216–222.

[27] J. W. Tukey, *Bias and confidence in not quite large samples.*, *Annls. Math. Stat. 29* (1958).

[28] U. Wolff, *Monte Carlo errors with less errors*, *Arxiv preprint hep-lat/0306017* (2003).

[29] M. H. Quenouille, *Notes on bias in estimation*, *Biometrika 43* (1956).

[30] K. Dusling and D. Teaney, *Simulating elliptic flow with viscous hydrodynamics*, *Phys.Rev.* C77 (2008) 034905.

[31] M. Luzum and P. Romatschke, *Conformal Relativistic Viscous Hydrodynamics: Applications to RHIC results at s(NN)**(1/2) = 200-GeV*, *Phys.Rev.* C78 (2008) 034915.

[32] D. A. Teaney, *Viscous Hydrodynamics and the Quark Gluon Plasma*, arXiv:0905.2433.

[33] C. Gale, S. Jeon, and B. Schenke, *Hydrodynamic Modeling of Heavy-Ion Collisions*, *Int.J.Mod.Phys.* A28 (2013) 1340011.

[34] P. B. Arnold, G. D. Moore, and L. G. Yaffe, *Transport coefficients in high temperature gauge theories. 1. Leading log results*, *JHEP* 0011 (2000) 001.

[35] H. B. Meyer, *Transport Properties of the Quark-Gluon Plasma: A Lattice QCD Perspective*, *Eur.Phys.J.* A47 (2011) 86.

[36] O. Kaczmarek and M. Müller, *Temperature dependence of electrical conductivity and dilepton rates from hot quenched lattice QCD*, arXiv:1312.5609.

[37] Y. Yin, *Electrical conductivity of the quark-gluon plasma and soft photon spectrum in heavy-ion collisions*, arXiv:1312.4434.

[38] S. I. Finazzo and J. Noronha, *A holographic calculation of the electric conductivity of the strongly coupled quark-gluon plasma near the deconfinement transition*, *Phys.Rev.* D89 (2014) 106008.

[39] H.-T. Ding, A. Francis, O. Kaczmarek, F. Karsch, E. Laermann, et al., *Thermal dilepton rate and electrical conductivity: An analysis of vector current correlation functions in quenched lattice QCD*, *Phys.Rev.* D83 (2011) 034504.

[40] G. Aarts, C. Allton, J. Foley, S. Hands, and S. Kim, *Spectral functions at small energies and the electrical conductivity in hot, quenched lattice QCD*, *Phys.Rev.Lett.* 99 (2007) 022002.

[41] S. Gupta, *The Electrical conductivity and soft photon emissivity of the QCD plasma*, *Phys.Lett.* B597 (2004) 57–62.

[42] H. B. Nielsen and M. Ninomiya, *A no-go theorem for regularizing chiral fermions*, *Physics Letters B* 105 (1981) 219–223.

[43] J. C. Collins and M. J. Perry, *Superdense Matter: Neutrons or Asymptotically Free Quarks?*, *Phys. Rev. Lett.* 34 (May, 1975) 1353–1356.

[44] E. V. Shuryak, *Theory of Hadronic Plasma*, *Sov.Phys.JETP* 47 (1978) 212–219.

[45] M. Shifman, A. Vainshtein, and V. Zakharov, *QCD and resonance physics. theoretical foundations*, *Nuclear Physics B* 147 (1979) 385–447.

[46] Y. Aoki, Z. Fodor, S. Katz, and K. Szabo, *The QCD transition temperature: Results with physical masses in the continuum limit*, *Phys.Lett.* B643 (2006) 46–54.

[47] Y. Aoki, G. Endrodi, Z. Fodor, S. Katz, and K. Szabo, *The Order of the quantum chromodynamics transition predicted by the standard model of particle physics*, *Nature* 443 (2006) 675–678.

[48] S. Borsanyi et al., *Is there still any T_c mystery in lattice QCD? Results with physical masses in the continuum limit III*, *JHEP* 1009 (2010) 073.

[49] S. Borsanyi, G. Endrodi, Z. Fodor, A. Jakovac, S. D. Katz, et al., *The QCD equation of state with dynamical quarks*, *JHEP* 1011 (2010) 077.

[50] F. R. Brown, F. P. Butler, H. Chen, N. H. Christ, Z.-h. Dong, et al., *On the existence of a phase transition for QCD with three light quarks*, *Phys.Rev.Lett.* 65 (1990) 2491–2494.

[51] M. Cheng, S. Ejiri, P. Hegde, F. Karsch, O. Kaczmarek, et al., *Equation of State for physical quark masses*, *Phys.Rev.* D81 (2010) 054504.

[52] R. D. Pisarski and F. Wilczek, *Remarks on the chiral phase transition in chromodynamics*, *Phys. Rev. D* 29 (Jan, 1984) 338–341.

[53] B. Svetitsky and L. G. Yaffe, *Critical Behavior at Finite Temperature Confinement Transitions*, *Nucl.Phys.* B210 (1982) 423.

[54] L. Yaffe and B. Svetitsky, *First Order Phase Transition in the SU(3) Gauge Theory at Finite Temperature*, *Phys.Rev.* D26 (1982) 963.

[55] K. A. Olive, *The Violent Universe: The Big Bang*, arXiv:1005.3955.

[56] K. Yagi, T. Hatsuda, and Y. Miake, *Quark-gluon plasma: From big bang to little bang*, *Camb.Monogr.Part.Phys.Nucl.Phys.Cosmol.* 23 (2005) 1–446.

[57] T. Schäfer and D. Teaney, *Nearly Perfect Fluidity: From Cold Atomic Gases to Hot Quark Gluon Plasmas*, *Rept.Prog.Phys.* 72 (2009) 126001.

[58] P. Romatschke and U. Romatschke, *Viscosity Information from Relativistic Nuclear Collisions: How Perfect is the Fluid Observed at RHIC?*, *Phys.Rev.Lett.* 99 (2007) 172301.

[59] H. Song and U. W. Heinz, *Suppression of elliptic flow in a minimally viscous quark-gluon plasma*, *Phys.Lett.* B658 (2008) 279–283.

[60] P. Kovtun, D. T. Son, and A. O. Starinets, *Viscosity in strongly interacting quantum field theories from black hole physics*, *Phys.Rev.Lett.* 94 (2005) 111601.

[61] G. Policastro, D. T. Son, and A. O. Starinets, *The Shear viscosity of strongly coupled N=4 supersymmetric Yang-Mills plasma*, *Phys.Rev.Lett.* 87 (2001) 081601.

[62] K. Tuchin, *Particle production in strong electromagnetic fields in relativistic heavy-ion collisions*, *Adv.High Energy Phys.* 2013 (2013) 490495.

[63] L. McLerran and V. Skokov, *Comments About the Electromagnetic Field in Heavy-Ion Collisions*, arXiv:1305.0774.

[64] L.D.Landau and E.M.Lifshitz, *Statistical Physics.* Vol 5, Part 1.

[65] *1. The General Discrete Inverse Problem*, ch. 1, pp. 1–40. http://epubs.siam.org/doi/pdf/10.1137/1.9780898717921.ch1.

[66] A. Tarantola, *Inverse Problem Theory and Methods for Model Parameter Estimation.* Society for Industrial and Applied Mathematics, 2005.

[67] J. Hadamard, *Sur les problèmes aux dérivés partielles et leur signification physique*, *Princeton University Bulletin* 13 (1902) 49–52.

[68] B. B. Brandt, A. Francis, H. B. Meyer, and H. Wittig, *Thermal Correlators in the ρ channel of two-flavor QCD*, *JHEP* 1303 (2013) 100.

[69] M. Asakawa, T. Hatsuda, and Y. Nakahara, *Maximum entropy analysis of the spectral functions in lattice QCD*, *Prog.Part.Nucl.Phys.* 46 (2001) 459–508.

[70] J. Skilling and S. Sibisi, *Maximum entropy and Bayesian methods: proceedings of the Fourteenth International Workshop on Maximum Entropy and Bayesian Methods : Cambridge, England, 1994*. Fundamental theories of physics. Kluwer Academic Publishers, 1996.

[71] Gull S.F. and Daniell G.J., *Image reconstruction from incomplete and noisy data*, *Nature* 272 (apr, 1978) 686–690. 10.1038/272686a0.

[72] E. T. Jaynes and J. H. Justice, *Maximum Entropy and Bayesian Methods in Applied Statistics*.

[73] R. Bryan, *Maximum entropy analysis of oversampled data problems*, *European Biophysics Journal* 18 165–174.

[74] H. Jeffreys, *Theory of Probability (Third Edition)*.

[75] J. Clowser, *Application of the Maximum Entropy Method to Dynamical Fermion simulations*. PhD thesis, Swansea University, 2002.

[76] C. J. Morningstar and M. J. Peardon, *The Glueball spectrum from an anisotropic lattice study*, *Phys.Rev.* D60 (1999) 034509.

[77] G. P. Lepage and P. B. Mackenzie, *On the viability of lattice perturbation theory*, *Phys.Rev.* D48 (1993) 2250–2264.

[78] P. Chen, *Heavy quarks on anisotropic lattices: The Charmonium spectrum*, *Phys.Rev.* D64 (2001) 034509.

[79] T. R. Klassen, *The Anisotropic Wilson gauge action*, *Nucl.Phys.* B533 (1998) 557–575.

[80] C. Morningstar and M. J. Peardon, *Analytic smearing of SU(3) link variables in lattice QCD*, *Phys.Rev.* D69 (2004) 054501.

[81] T. A. DeGrand, A. Hasenfratz, and T. G. Kovacs, *Optimizing the chiral properties of lattice fermion actions*, `hep-lat/9807002`.

[82] R. Morrin, A. O. Cais, M. Peardon, S. M. Ryan, and J.-I. Skullerud, *Dynamical QCD simulations on anisotropic lattices*, *Phys.Rev.* D74 (2006) 014505.

[83] Y. Burnier and M. Laine, *Towards flavour diffusion coefficient and electrical conductivity without ultraviolet contamination*, *Eur.Phys.J.* C72 (2012) 1902.

[84] G. Martinelli, C. Sachrajda, and A. Vladikas, *A study of improvement in lattice QCD*, *Nuclear Physics B* 358 (1991) 212–227.

[85] P. A. Boyle, *The BAGEL assembler generation library*, *Computer Physics Communications* 180 (2009) 2739–2748.

[86] R. G. Edwards and B. Joo, *The Chroma software system for lattice QCD*, *Nucl.Phys.Proc.Suppl.* 140 (2005) 832.

[87] G. Aarts and J. M. Martinez Resco, *Continuum and lattice meson spectral functions at nonzero momentum and high temperature*, *Nucl.Phys.* B726 (2005) 93–108.

[88] A. Mocsy, P. Petreczky, and M. Strickland, *Quarkonia in the Quark Gluon Plasma*, *Int.J.Mod.Phys.* A28 (2013) 1340012.

[89] G. Aarts, C. Allton, S. Kim, M. P. Lombardo, M. B. Oktay, et al., *S wave bottomonium states moving in a quark-gluon plasma from lattice NRQCD*, *JHEP* 1303 (2013) 084.

[90] G. Aarts, C. Allton, T. Harris, S. Kim, M. P. Lombardo, et al., *The bottomonium spectrum at finite temperature from $N_f = 2 + 1$ lattice QCD*, *JHEP* 1407 (2014) 097.

[91] Y. Burnier and M. Laine, *Massive vector current correlator in thermal QCD*, *JHEP* 1211 (2012) 086.

[92] P. Baikov, K. Chetyrkin, J. Kuhn, and J. Rittinger, *Vector Correlator in Massless QCD at Order $O(alpha_s^4)$ and the QED beta-function at Five Loop*, *JHEP* 1207 (2012) 017.

[93] P. Petreczky and D. Teaney, *Heavy quark diffusion from the lattice*, *Phys.Rev.* D73 (2006) 014508.

[94] G. D. Moore and J.-M. Robert, *Dileptons, spectral weights, and conductivity in the quark-gluon plasma*, `hep-ph/0607172`.

[95] G. Aarts and J. M. Martinez Resco, *Transport coefficients, spectral functions and the lattice*, *JHEP* 0204 (2002) 053.

[96] J. Hong and D. Teaney, *Spectral densities for hot QCD plasmas in a leading log approximation*, *Phys.Rev.* C82 (2010) 044908.

[97] I. Wetzorke, F. Karsch, E. Laermann, P. Petreczky, and S. Stickan, *Meson spectral functions at finite temperature*, *Nucl.Phys.Proc.Suppl.* 106 (2002) 510–512.

[98] F. Karsch, E. Laermann, P. Petreczky, S. Stickan, and I. Wetzorke, *A Lattice calculation of thermal dilepton rates*, *Phys.Lett.* B530 (2002) 147–152.

[99] F. Karsch, S. Datta, E. Laermann, P. Petreczky, S. Stickan, et al., *Hadron correlators, spectral functions and thermal dilepton rates from lattice QCD*, *Nucl.Phys.* A715 (2003) 701–704.

[100] B. Abelev et al., *Net-Charge Fluctuations in Pb-Pb collisions at $\sqrt{s_{NN}} = 2.76$ TeV*, *Phys.Rev.Lett.* 110 (2013) 152301.

[101] S. A. Gottlieb, W. Liu, D. Toussaint, R. Renken, and R. Sugar, *The Quark Number Susceptibility of High Temperature QCD*, *Phys.Rev.Lett.* 59 (1987) 2247.

[102] J. Blaizot, E. Iancu, and A. Rebhan, *Quark number susceptibilities from HTL resummed thermodynamics*, *Phys.Lett.* B523 (2001) 143–150.

[103] S. Borsanyi, Z. Fodor, S. D. Katz, S. Krieg, C. Ratti, et al., *Fluctuations of conserved charges at finite temperature from lattice QCD*, *JHEP* 1201 (2012) 138.

[104] M. Asakawa, U. W. Heinz, and B. Muller, *Fluctuation probes of quark deconfinement*, *Phys.Rev.Lett.* 85 (2000) 2072–2075.

[105] M. Bleicher, S. Jeon, and V. Koch, *Event-by-event fluctuations of the charged particle ratio from nonequilibrium transport theory*, *Phys.Rev.* C62 (2000) 061902.

[106] R. Gavai and S. Gupta, *Simple patterns for non-linear susceptibilities near T(c)*, *Phys.Rev.* D72 (2005) 054006.

[107] C. Bernard, C. E. DeTar, L. Levkova, S. Gottlieb, U. Heller, et al., *QCD thermodynamics with 2+1 flavors at nonzero chemical potential*, *Phys.Rev.* D77 (2008) 014503.

[108] A. Bazavov, H. T. Ding, P. Hegde, F. Karsch, C. Miao, et al., *Quark number susceptibilities at high temperatures*, `arXiv:1309.2317`.

[109] L. P. Kadanoff and P. C. Martin, *Hydrodynamic equations and correlation functions*, *Annals of Physics* 24 (1963) 419–469.

[110] G. D. Moore and D. Teaney, *How much do heavy quarks thermalize in a heavy ion collision?*, *Phys.Rev.* C71 (2005) 064904.

[111] B. Ling, T. Springer, and M. Stephanov, *Hydrodynamics of charge fluctuations and balance functions*, *Phys.Rev.* C89 (2014) 064901.

[112] S.-x. Qin, *A Divergence-Free Method to Extract Observables from Meson Correlation Functions*, `arXiv:1307.4587`.

[113] A. Francis and O. Kaczmarek, *On the temperature dependence of the electrical conductivity in hot quenched lattice QCD*, *Prog.Part.Nucl.Phys.* 67 (2012) 212–217.

[114] D. Fernandez-Fraile and A. Gomez Nicola, *The Electrical conductivity of a pion gas*, *Phys.Rev.* D73 (2006) 045025.

[115] D. Fernandez-Fraile and A. Gomez Nicola, *Transport coefficients and resonances for a meson gas in Chiral Perturbation Theory*, *Eur.Phys.J.* C62 (2009) 37–54.

[116] S.-i. Nam, *Electrical conductivity of quark matter at finite T under external magnetic field*, *Phys. Rev. D* 86 (Aug, 2012) 033014.

[117] T. Steinert and W. Cassing, *Electric and magnetic response of hot QCD matter*, *Phys.Rev.* C89 (2014) 035203.

[118] M. Greif, I. Bouras, Z. Xu, and C. Greiner, *Electric Conductivity of the Quark-Gluon Plasma investigated using a pQCD based parton cascade*, arXiv:1408.7049.

[119] A. Puglisi, S. Plumari, and V. Greco, *Electric Conductivity from the solution of the Relativistic Boltzmann Equation*, arXiv:1408.7043.

[120] S.-x. Qin and D. H. Rischke, *Charmonium Spectral Functions and Transport Properties of Quark-Gluon Plasma*, *Phys.Lett.* B734 (2014) 157.

[121] S. Gottlieb, W. Liu, D. Toussaint, R. L. Renken, and R. L. Sugar, *Quark-number susceptibility of high-temperature QCD*, *Phys. Rev. Lett.* 59 (Nov, 1987) 2247–2250.

[122] R. V. Gavai, S. Gupta, and P. Majumdar, *Susceptibilities and screening masses in two flavor QCD*, *Phys.Rev.* D65 (2002) 054506.